DIGITALCOMMONS
@WAYNESTATE

Wayne State University

Wayne State University Dissertations

January 2019

Solvent Effects And Charge Transfer States In Organic Photovoltaics

Kangmin Liu
Wayne State University, liukangmin@gmail.com

Follow this and additional works at: https://digitalcommons.wayne.edu/oa_dissertations

 Part of the Physical Chemistry Commons

Recommended Citation

Liu, Kangmin, "Solvent Effects And Charge Transfer States In Organic Photovoltaics" (2019). *Wayne State University Dissertations*. 2174.
https://digitalcommons.wayne.edu/oa_dissertations/2174

This Open Access Dissertation is brought to you for free and open access by DigitalCommons@WayneState. It has been accepted for inclusion in Wayne State University Dissertations by an authorized administrator of DigitalCommons@WayneState.

المنارة للاستشارات

www.manaraa.com

SOLVENT EFFECTS AND CHARGE TRANSFER STATES IN ORGANIC PHOTOVOLTAICS

by

KANGMIN LIU

DISSERTATION

Submitted to the Graduate School

of Wayne State University,

Detroit, Michigan

in partial fulfillment of the requirements

for the degree of

DOCTOR OF PHILOSOPHY

2018

MAJOR: CHEMISTRY (Physical)

Approved By:

_____

Advisor Date

_____

_____

_____

_____

www.manaraa.com

DEDICATION

This dissertation is dedicated to my parents.

www.manaraa.com

ACKNOWLEDGMENTS

First and foremost, I would like to thank my research advisor Vladimir Chernyak for all the support and guidance throughout the program. He is not only a great scientist, but also an excellent teacher who can show the greatness of physics and mathematics with merely a piece of chalk and a blackboard. Every discussion with him gives me some inspirations.

Besides Vladimir, I am also indebted to other members of the Chernyak group. Dr. Hao Li helped me run various calculations, and he also revised my manuscript for publication. Dr. Tian Shi guided me to start my research project and assisted me to understand many difficult concepts. Dr. Micheal Catanzaro helped me on a lot of mathematical topics. Ruixi has always been a great companion in the lab. Austin has given me valuable suggestions for my defense preparation and dissertation revision. Thank for all their quality time, understanding and help.

I also want to thank Dr. Sergei Tretiak for accepting me as a graduate student to work in Los Alamos National Laboratory during summer 2014. Dr. Kirill Velizhanin also gave valuable advice and guidance during my visit. The group meetings, seminars, and discussions at LANL were invaluable to my development as a Ph.D.

I really appreciate the opportunity for attending the joined group meetings of Prof. Schlegel's, Prof. Cisneros's, Prof. Wen Li's and Prof. Zhenfei Liu's labs. The presentations and discussions are extremely useful for enriching my knowledge. I also gave a couple of talks in the meeting and received priceless advice from the professors, students, and post-docs. Especially the members of the Schlegel group, including Bishnu Thapa, Xuetao Shi, Tu Yijung, Mikyung Lee, they not only have given me valuable suggestions but also indispensable emotional support. Thank you all so much!

I am also thankful for the opportunity for working as a teaching assistant for Dr. Barbara Munk, Pof. Wen Li and Dr. Maryfrances Barber. I learned priceless lessons from them about how to improve my teaching and communication skills.

Graduate school is a mixture of ups and downs. I am so grateful to have a group of friends to share the joyful moments as well as the hardship I had to go through. The memories I

www.manaraa.com

had with all my friends, including Bishnu Thapa, Vimukthi Senevirathne, Fangchao Liu, Peng Wen, Xiaoxiao Liao, Ruixi Wang, and Pradip Adhikari, will always be a precious part of my life.

I appreciate the financial support provided by Wayne State University, Department of Chemistry for the six years of my graduate school study.

I would like to thank the Wayne State Chemistry Department staff, especially Melissa Rochon, Nestor Ocampo, Jackie Baldyga, and Tenecia Smith. Melissa helped me numerous times from my application for the graduate school to the end of the program. Nestor also helped me a lot on technical problems.

Special thanks go to the Wayne State Computing Grid staff. They have been providing impressive computing services to the whole university. My work could not have been accomplished without their technical support.

Last but not least, I would like to thank my parents for their love and support over the years. They always give me the greatest comfort deep in my heart. My deepest gratitude goes to my late grandfather, who had been my mentor since the beginning of my life.

www.manaraa.com

TABLE OF CONTENTS

DEDICATION ii

ACKNOWLEDGMENTS iii

LIST OF TABLES vii

LIST OF FIGURES ix

CHAPTER 1 INTRODUCTION 1

1.1 Organic Solar Cells 5

1.1.1 Development of OPV Materials 5

1.1.2 Advantages/Disadvantages of OPV Materials 7

1.1.3 Power Conversion Process 8

1.2 Charge Transfer State 11

1.3 Solvent Effects 13

CHAPTER 2 COMPUTATIONAL BACKGROUND 16

2.1 Overview 16

2.2 Analysis of Excitonic and Charge Transfer Interactions 18

2.2.1 Transition Density Matrix 18

2.2.2 Real Space Representation of Transition Density Matrix 19

2.2.3 Charge Transfer Character 20

2.3 Solvation Models: Linear-Response and State-Specific Methods 25

2.3.1 Basic Continuum Solvation Model 26

2.3.2 Electronic Excitations in QM-PCM Formulation 28

CHAPTER 3 A TDDFT STUDY ON THE PCPDTBT:PCBM LOW BAND GAP SYSTEM 35

3.1 Introduction 35

3.2 Methods 36

3.2.1 Optimization of Geometries 37

3.2.2 Excited State Calculation 38

3.2.3 Applying Dielectric Environment 39

www.manaraa.com

3.2.4 Calculation of Charge Transfer Character 41
3.3 Results and Discussion 44
3.3.1 Electronic Excitations in Vacuo 45
3.3.2 Electronic Excitations in Solvent 49
3.3.3 Comparison of Excited State Calculations in Solvent Based on *Vacuum* Geometry and *Solvated* Geometry 52
3.4 Summary 54
CHAPTER 4 CONCLUSION AND FUTURE DIRECTIONS 56
4.1 Conclusion 56
4.2 Future Directions 57
APPENDIX A SUPPLEMENTARY INFORMATION 60
A.1 Excited State Calculations in Vacuo 61
A.1.1 CAM-B3LYP/6-31G(d) with Grimmes D3 Dispersion 61
A.1.2 CAM-B3LYP/6-31G(d) with Grimmes D2 Dispersion 62
A.1.3 ωB97XD/6-31G(d) 63
A.2 Excited State Calculations in Solvent Based on *Vacuum* Geometries 64
A.2.1 CAM-B3LYP/6-31G(d) with Grimmes D3 Dispersion 64
A.2.2 CAM-B3LYP/6-31G(d) with Grimmes D2 Dispersion 65
A.2.3 ωB97XD/6-31G(d) 66
A.3 Excited State Calculations in Solvent Based on *Solvated* Geometries 67
A.3.1 CAM-B3LYP/6-31G(d) with Grimmes D3 Dispersion 67
A.3.2 CAM-B3LYP/6-31G(d) with Grimmes D2 Dispersion 68
A.3.3 ωB97XD/6-31G(d) 69
BIBLIOGRAPHY 70
ABSTRACT 86
AUTOBIOGRAPHICAL STATEMENT 88

www.manaraa.com

LIST OF TABLES

Table 1.1 Three generations of solar cells, with their main materials, PCE, advantages, disadvantages and main usage. 2

Table 3.1 Number of basis functions for each atom. 42

Table 3.2 Representation of Charge transfer and excitonic character by the elements of Transition Density Matrix. 43

Table A.1 Excitation energies Ω and oscillator strengths f of PCPDTBT, PCBM, and PCPDTBT: PCBM in vacuo. Charge transfer characters for PCPDTBT: PCBM are listed. D stands for Donor and A for Acceptor, DA-charge transfer from Donor to Acceptor, AD-charge transfer from Acceptor to Donor, DD-charge localization within Donor, AA-charge localization in Acceptor. Computed by CAM-B3LYP/6-31G(d) on the ground state geometry optimized by the same functional with the empirical dispersion correction GD3. 61

Table A.2 Excitation energies Ω and oscillator strengths f of PCPDTBT, PCBM, and PCPDTBT: PCBM in vacuo. Charge transfer characters for PCPDTBT: PCBM are listed. Computed by CAM-B3LYP/6-31G(d) on the ground state geometry optimized by the same functional with the empirical dispersion correction GD2. 62

Table A.3 Excitation energies Ω and oscillator strengths f of PCPDTBT, PCBM, and PCPDTBT: PCBM in vacuo. Charge transfer characters for PCPDTBT: PCBM are listed. Computed by ωB97XD/6-31G(d) on the ground state geometry optimized by the same functional. 63

Table A.4 Excitation energies Ω, oscillator strengths f, and CT characters of the molecular pair of PCPDTBT: PCBM in solvent with varying static dielectric constant, ε. Three modes are of the main concern, including the first two excitonic states (EX-1,2) and the charge transfer state (CT-1). Computed by CAM-B3LYP/6-31G(d) using the LR and the SS approaches on the *vacuum* geometry optimized by the same functional with the empirical dispersion correction GD3. 64

Table A.5 Excitation energies Ω, oscillator strengths f, and CT characters of the molecular pair of PCPDTBT: PCBM in solvent with varying static dielectric constant, ε. Computed by CAM-B3LYP/6-31G(d) using the LR and the SS approaches on the *vacuum* geometry optimized by the same functional with the empirical dispersion correction GD2. 65

Table A.6 Excitation energies Ω, oscillator strengths f, and CT characters of the molecular pair of PCPDTBT: PCBM in solvent with varying static dielectric constant, ε. Computed by ωB97XD/6-31G(d) using the LR and the SS approaches on the *vacuum* geometry optimized by the same functional. 66

www.manaraa.com

Table A.7 Excitation energies Ω, oscillator strengths f, and CT characters of PCPDTBT: PCBM in solvent with varying dielectric constant, ε. The first two excitonic states (EX-1,2) and the charge transfer state (CT-1) are of the main concern. Computed by CAM-B3LYP/6-31G(d) using the LR and the SS approaches on the *solvated* geometry optimized by the same functional with the empirical dispersion correction GD3. 67

Table A.8 Excitation energies Ω, oscillator strengths f, and CT characters of the molecular pair of PCPDTBT: PCBM in solvent with varying static dielectric constant, ε. Computed by CAM-B3LYP/6-31G(d) using the LR and the SS approaches on the *solvated* geometry optimized by the same functional with the empirical dispersion correction GD2. 68

Table A.9 Excitation energies Ω, oscillator strengths f, and CT characters of the molecular pair of PCPDTBT: PCBM in solvent with varying static dielectric constant, ε. Computed by ωB97XD/6-31G(d) using the LR and the SS approaches on the *solvated* geometry optimized by the same functional. 69

www.manaraa.com

LIST OF FIGURES

Figure 1.1 Conversion efficiencies of best research solar cells worldwide from 1976 through 2018 for various photovoltaic technologies. Efficiencies determined by certified agencies/laboratories [7]. 3

Figure 1.2 Molecular structures of some important 1^{st}, 2^{nd} and 3^{rd} Generation organic solar cell materials as donor ((a)-(g)) and acceptor ((h)-(j)). 1^{st} GEN.: (a) PA; 2^{nd} GEN.: (b) PPV, (c) PEDOT, (d) P3HT and (e) MEH-PPV; 3^{rd} GEN.: (f) PCPDTBT, (g) PCDTBT. Fullerene derivative as electron acceptors: (h) C_{60}, (i) PCBM and (j) $PC_{70}BM$. 6

Figure 1.3 Illustration of the photoinduced charge transfer from the polymer (donor) to PCBM (acceptor) on the left, and a schematic of the power conversion process on the right. 9

Figure 2.1 Schematic illustrations of one-electron excitation in a dimer molecular system, with two monomers A and B. (0) for ground state, (1) for local excitation (excitonic state), (2) for charge transfer state, (1) and (2) are represented with localized orbitals. The linear combinations of (1) and (2) provide the delocalized states as (3) and (4). 21

Figure 2.2 Molecular orbitals of a dimer (monomer A and B) system represented in the localized and delocalized orbital space. 23

Figure 3.1 Chemical structures of (a) Poly[2,6-(4,4-dimethyl-4H-cyclopenta[2,1-b:3,4-b′]-dithiophene)-alt-4,7-(2,1,3-benzothiadiazole)] (PCPDTBT) and (b) [6,6]-Phenyl-C61-butyric acid methyl ester ($PC_{61}BM$ or PCBM) 36

Figure 3.2 Optimized geometries of the polymer molecule PCPDTBT 38

Figure 3.3 The energy of the ground state geometry optimized in vacuo and in solvent with various dielectric constant, $\varepsilon_0 = 1$ represents vacuo, $\Delta\Omega$ is the energy difference between the geometries optimized in solvent and in vacuo. 40

Figure 3.4 A schematic representation of the structure of the transition density matrix. 43

Figure 3.5 Contour plots of the transition density matrices for three excited states with one charge transfer number assigned to each block. The axis labels represent indices of non-hydrogen atoms from PCBM to PCPDTBT (PCBM: 1-74, PCPDTBT: 75-162). The inset of each plot shows the character of the electronic mode. D stands for Donor and A represents Acceptor, DA-charge transfer from Donor to Acceptor, AD-charge transfer from Acceptor to Donor, DD-charge localization within Donor, AA-charge localization in Acceptor. 44

www.manaraa.com

Figure 3.6 Stick absorption spectra of PCPDTBT, PCBM, and PCPDTBT: PCBM complex (from left to right) in vacuo computed at CAM-B3LYP/GD3 (top row), CAM-B3LYP/GD2 (middle row), and ωB97XD (bottom row). The x-axis denotes transition energies Ω, the y-axis denotes $\mathrm{Log}_{10}(f)$, f being unitless oscillator strength of a given transition. States are color-coded according to the CT character, i.e., blue for EX states with $CT \leq 0.1$, green for hybrid states with $0.1 < CT < 0.9$, and red for CT states with $CT \geq 0.9$. 45

Figure 3.7 Density of states of PCPDTBT: PCBM complex in vacuo computed at (a) CAM-B3LYP/GD3, (b) CAM-B3LYP/GD2, and (c) ωB97XD. The x-axis denotes transition energies Ω; the y-axis denotes density of states with arbitrary units. 46

Figure 3.8 Visualization of natural transition orbitals (NTOs) of the lowest CT state with the highest occupied transition orbital (HOTO) on the left and the lowest unoccupied transition orbital (LUTO) on the right computed at (a) CAM-B3LYP/GD3, (b) CAM-B3LYP/GD2, (c) ωB97XD. The associated eigenvalues λ are 0.91, 0.92, and 0.97, respectively, which represent the weights of the particle-hole pairs contribution to the excitation. . . 48

Figure 3.9 The lowest two excited states EX-1,2 and the lowest charge transfer state CT-1 of PCPDTBT: PCBM in vacuo given by contour plots of the transition density matrices from the ground state to excited states, obtained by CAM-B3LYP/GD3/6-31G(d) (top), CAM-B3LYP/GD2/6-31G(d) (middle), ωB97XD/6-31G(d) (bottom). The axis labels represent indices of non-hydrogen atoms from PCBM to PCPDTBT (PCBM: 1-74, PCPDTBT: 75-162). The inset of each plot shows the character of the electronic mode, excitation energy Ω, oscillator strength f, and the CT character. 49

Figure 3.10 Transition energies of states with respect to the dielectric constant of the solvent. Solid and dashed curves represent SS and LR approaches, respectively. Computed at (a) CAM-B3LYP/GD3, (b) CAM-B3LYP/GD2, (c) ωB97XD based on the ground geometries optimized in vacuo. 51

Figure 3.11 Comparison of excited state calculations in solvent based on *vacuum* geometry (1^{st} row) and *solvated* geometry (2^{nd} row). For the solvated calculations, each PCPDTBT: PCBM ground state geometry is optimized in the presence of solvent with the corresponding dielectric constant. Computed at (a) CAM-B3LYP/GD3, (b) CAM-B3LYP/GD2, (c) ωB97XD level of theory. 52

www.manaraa.com

Figure 3.12 CT character of excited states with respect to the dielectric constant of the solvent. Solid and dashed curves represent SS and LR approaches, respectively. Computed at (a) CAM-B3LYP/GD3, (b) CAM-B3LYP/GD2, (c) ωB97XD based on the ground geometries optimized in vacuo (1^{st} row) and in solvent (2^{nd} row). 53

Figure A.1 Natural transition orbitals of (a) EX-1 and (b) EX-2 states, both have two major contributing pairs, λ is the associated eigenvalue which represents the weight of the particle-hole pair contribution to the excitation. The highest occupied transition orbital (HOTO) and the lowest unoccupied transition orbital (LUTO) are labeled. 61

Figure A.2 Natural transition orbitals of (a) EX-1 and (b) EX-2 states, both have two major contributing pairs, λ is the associated eigenvalue which represents the weight of the particle-hole pair contribution to the excitation. The highest occupied transition orbital (HOTO) and the lowest unoccupied transition orbital (LUTO) are labeled. 62

Figure A.3 Natural transition orbitals of (a) EX-1 and (b) EX-2 states, both have two major contributing pairs, λ is the associated eigenvalue which represents the weight of the particle-hole pair contribution to the excitation. The highest occupied transition orbital (HOTO) and the lowest unoccupied transition orbital (LUTO) are labeled. 63

www.manaraa.com

CHAPTER 1 INTRODUCTION

The improvements of living standard around the world, especially in the developing countries, calls for more energy resources. Meanwhile, severe environmental issues (extreme weather, air, and water pollution) urge researchers to improve energy utilization efficiency and to find alternative/renewable energy sources. The International Energy Agency (IEA) predicts the global energy needs will increase by 30% between today and 2040 [1]. According to the IEA's Renewables 2018 market analysis and forecast report [2], 40% of global energy consumption growth will come from renewable sources in the next five years. In 2017, renewable energy accounted for an estimated 70% of net additions to global power capacity [3]. Among available renewable energy options, solar photovoltaics (PV) is taking the lead, providing a promising future for clean energy.

However, despite the rapid growth, the application of solar PV still only accounts for less than 2% of the total energy consumption in 2016 [3]. This is due to the higher cost compared to traditional resources such as coal and oil, as well as the growing price of renewable subsidies and grid integration. Envisioning a bright PV future, in 2010 the Department of Energy (DOE) set up a goal that by reaching the price of $1/watt, at the same cost of coal-based energy, the U.S. and the rest of the world would be able to enjoy a clean and unlimited electricity generated from the sunlight [4]. In 2016, the DOE set the following Levelized Cost of Electricity (LCOE) goals for PV to achieve by 2030 in order to enable significantly greater PV adoption: $0.03 per kilowatt-hour (kWh) for utility-scale, $4 per kWh for commercial, and $0.05 per kWh for residential systems [5]. The achievement of these goals requires the collaboration of multiple parties including the government, the private sector, and the scientists. Policy, finance, and market mechanisms have to be applied to support the development and application of PV. More importantly, the researchers should aspire to improve the efficiency of the PV modules so that these materials can match and even surpass their traditional energy counterparts. There are three major areas which demand attention: (1) increasing efficiency and energy yield; (2) reducing material and process costs,

www.manaraa.com

and (3) understanding reliability and mitigating degradation [6].

Over the past four decades, solar cell materials have evolved into the third generation. Many new types of solar cells have been invented and existing cell efficiencies have increased by various degrees. Table 1.1 lists all the three generations of solar cells with their main material, power conversion efficiency (PCE), advantages/disadvantages and primary usage. The high-performance experimental multi-junction cell is a special type of photovoltaic material. Although it holds the world record in solar cell performance (reached more than 45% in 2015) [7], it has limited commercial applications due to its high production price. Considering the variety of cells, the emerging PV research is very promising. For example, the performance of perovskite cells almost doubled in five years, from 12% in 2013 to 23% in 2018 [7]. The extensive study on organic semiconductors is also fruitful: their PCE has increased by more than five times in twenty years, from merely 3% to 17% [8].

Table 1.1: Three generations of solar cells, with their main materials, PCE, advantages, disadvantages and main usage.

GEN.	**Materials**	**PCE**	**Advantages**	**Disadvantages**	**Usage**
1^{st}	crystalline silicon	21-28%	good PCE, high stability	rigid, high energy in production	rooftops
2^{nd}	thin film amorphous silicon, CIGS & CdTe	22-23%	low production costs, flexible	scarce elements, high energy in production	utility-scale photovoltaic power stations
3^{rd}	polymers, organometallic, inorganic substances	11-17%	low-cost, flexible, easy production	low PCE	still in R&D phase

Forty years ago Heeger, MacDiarmid, Shirakawa, and coworkers discovered that the organic conjugated polymers can be doped to form metallic-like conducting materials [9], the research on conjugated oligomers and polymers has gained monumental advancement. The organic photovoltaic (OPV) cells have many advantages including lightweight, flexible, and

www.manaraa.com

cheap manufacturing. However, they are still less competitive in terms of performance compared to other photovoltaic platforms. More work is needed to improve the PCE so that the organic semiconductor can compete with other materials.

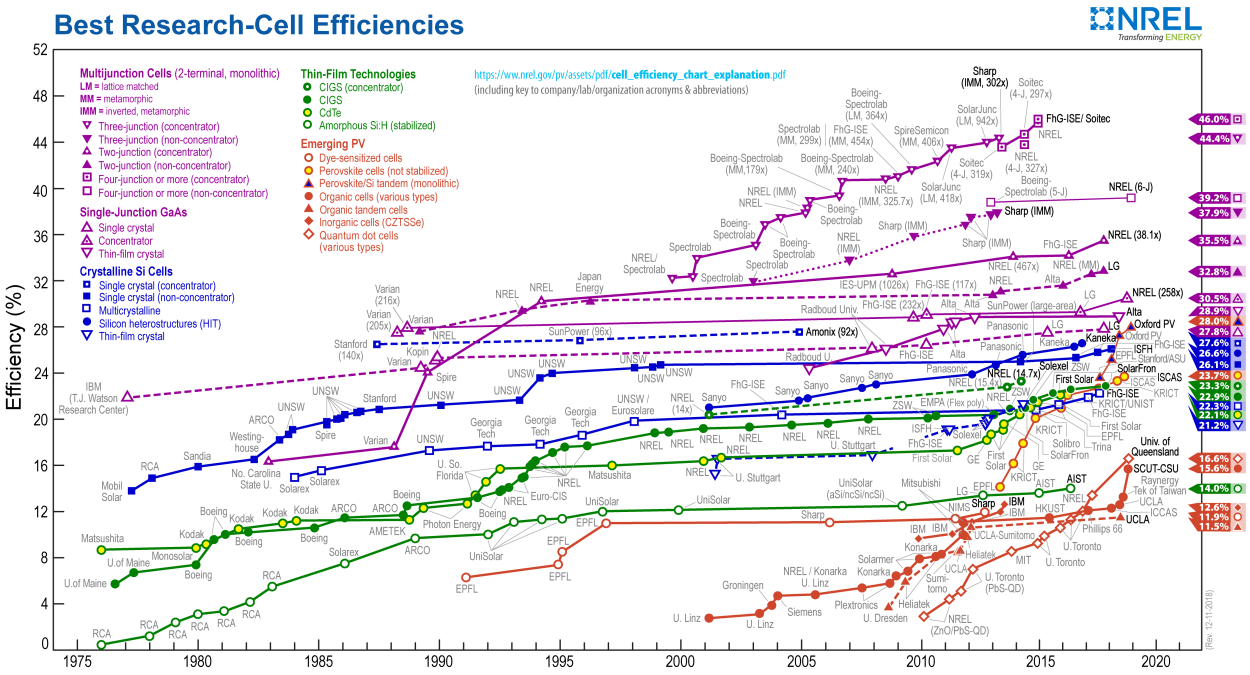

Figure 1.1: Conversion efficiencies of best research solar cells worldwide from 1976 through 2018 for various photovoltaic technologies. Efficiencies determined by certified agencies/laboratories [7].

The light-to-electricity power conversion in OPV devices can be modeled by a four-step process. Each step includes multiple factors which can impact the overall efficiency in various degrees. As a result, the detailed mechanisms of each step play a crucial role in the optimization of the whole performance. Therefore improvements require a deeper understanding of the basic chemistry and physics behind all aspects of the process. In next section the detailed conversion process and all relevant terms will be analyzed. In particular, charge transfer states (CTSs) exist as a dispensable part of the overall solar cell function. The exact role of CTSs is still under debate [10–14], but there is a consensus that they are critical to the overall performance of the cells and their correct determination is extraordinarily important for a detailed understanding of free charge generation mechanism. Extensive studies have been performed on the energetics of CTSs and their relation to the

www.manaraa.com

electron splitting and recombination [15–18].

The photo-current in a solar device is generated by the splitting of electron-hole pairs. In order to improve the power conversion efficiency, it is required to simultaneously increase the charge separation and minimize the recombination. The dielectric constant is an exceptionally significant parameter for reducing relaxation and recombination [19]. One of the reasons why organic solar materials have a very limited power conversion efficiency is because of their low dielectric constant ($\varepsilon_r \sim 3-4$), compared to $\varepsilon_r > 10$ for inorganic counterparts where free charge carriers can be readily created upon excitation. It has been shown that at $\varepsilon_r = 9$, the exciton binding energy is equal to $k_B T$ [19], suggesting a significant increase in charge separation. In 2016, Ma and coworkers examined the effect of dielectric screening on the CTS binding energy in MDMO-PPV: PCBM polymer-fullerene bulk heterojunction (BHJ) photovoltaic device [20]. By adding camphoric anhydride, whose relative permittivity is 24.8 in the amorphous phase and 3.2 when crystalline, they increased the film dielectric constant, reduced the CTS energy, and increased the power conversion efficiency by 75% at 20 wt % of camphoric anhydride.

Theoretical simulations can provide insightful interpretations and valuable information along with experiments [8, 21, 22]. The calculation of the OPV materials is a difficult task because of the large molecular size and the presence of the dielectric environment. In a bulk-heterojunction model, the large amount of molecules makes it impossible to calculate the properties quantum mechanically. Instead, only the optical response of a limited number of molecules can be computed. However, the number of basis functions is still large when a reasonable basis set is applied. Furthermore, the evaluation of electronic properties becomes more complicated when the solvent-solute interactions are considered. All these issues have to be examined with a detailed review of theoretical methods, which will be included in the next chapter.

The aim of this thesis is to understand the basic chemistry and physics behind the power conversion process, in particular, the exciton generation part. A model protocol will be

www.manaraa.com

provided to simulate the charge transfer state under the influence of dielectric environment, so that better optimized molecular structures for OPV applications can be proposed, simulated and tested. This will also give informative insights into the optimal design of organic solar cells. This thesis is composed of four chapters, the first one introduces OPV materials, CTSs and solvent effects; the second one gives an overview of the theoretical methods for characterizing and calculating the electronic excitations in a polarizable environment; the third part is a computational study on a typical OPV molecular system; and the last chapter summarizes and looks into the future projects. The rest of this introduction is divided into three sections. In Section 1, the development of OPV materials will be mentioned, the reasons why they are an excellent alternative to the traditional inorganic cells will be explained, and the details of the power conversion process will be examined. In Section 2, the role of CTS will be investigated. In Section 3 the solvent effect on the electronic energetic landscape will be reviewed.

1.1 Organic Solar Cells

1.1.1 Development of OPV Materials

Organic conducting polymers have evolved to the third generation since their invention. The first generation material is polyacetylene. The second generation includes more soluble and processible polymers and copolymers such as poly[paraphenylene vinylene] (PPVs). The third generation semiconducting polymers contain more complex molecular structures [23]. See Figure 1.2 for an illustration of the molecular structures of some important semiconducting polymer candidates. The most recent generation consists of the molecules which have ideal band gap for light absorption and are soluble in a variety of solvents.

www.manaraa.com

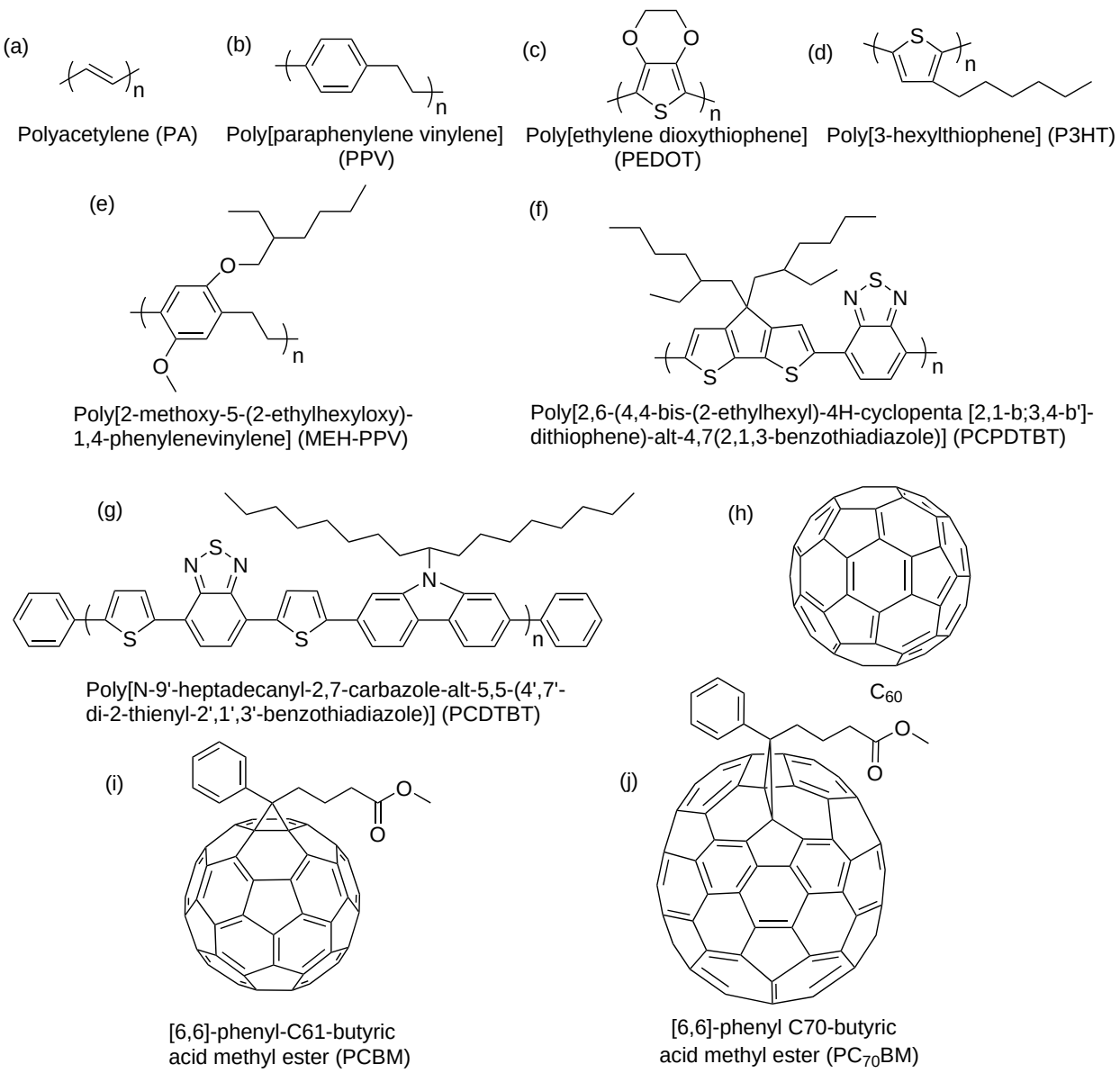

Figure 1.2: Molecular structures of some important 1^{st}, 2^{nd} and 3^{rd} Generation organic solar cell materials as donor ((a)-(g)) and acceptor ((h)-(j)). 1^{st} GEN.: (a) PA; 2^{nd} GEN.: (b) PPV, (c) PEDOT, (d) P3HT and (e) MEH-PPV; 3^{rd} GEN.: (f) PCPDTBT, (g) PCDTBT. Fullerene derivative as electron acceptors: (h) C_{60}, (i) PCBM and (j) $PC_{70}BM$.

The search for electron donor molecules which have ideal optical and electronic properties has been extensively carried out. Fullerenes are agreed as the default acceptors since they bear some excellent properties. The lowest unoccupied molecular orbitals (LUMO) of fullerenes usually have a lower energy than most polymer candidates [24], leading to a higher electron affinity than the donors [25]. In addition, they have a relatively high electron

www.manaraa.com

mobility [26], making the transport much easier after free charge carrier generation.

1.1.2 Advantages/Disadvantages of OPV Materials

Advantages

The reasons why organic solar materials are a promising alternative to the conventional inorganic semiconductors can be understood in three aspects: engineering, cost, and environmental concerns.

First, in terms of engineering, they are flexible, light-weight, and easily fabricated by simple manufacturing techniques such as vacuum evaporation/sublimation, solution cast, and roll-to-roll ink-jet printing [27]; furthermore, the electronic band gap of organic semiconductors can be optimized on the atomic level so that they can have excellent light-absorbing capabilities and the OPV layer can be extremely thin (100-200 nm) [28]. Second, they are cost-effective since the source materials are abundant in nature and manufacturing is relatively simple, enabling mass production. Lastly, they have substantial ecological and economic advantages [29].

Moreover, organic solar materials provide an excellent research tool for progressing the understanding of fundamental properties of various π-bonded molecules [9], the invention and validation of new quantum chemistry methods, and the utilization and comprehension of semiconductors.

Disadvantages

Although the organic semiconductors have so many advantages, they are still in research phase and have yet to see in commercial applications. The reasons are threefold: low PCE, stability issues, and lack of deep understanding of the structure-properties relationship.

Over nearly two decades the power conversion efficiency (PCE) of OPV devices has improved drastically, from merely $2 \sim 3\%$ to 17.3% [8]. However, the PCE is still significantly lower than inorganic-based devices. Multiple factors contribute to this limited performance, one of them is the low dielectric constant ($\sim$3) in organic components. Furthermore, the exciton binding energy in organic semiconductors is larger (1 to 2 orders of magnitude) than

www.manaraa.com

that of the silicon-based inorganic cells, making the generation of free charge carriers much more difficult. To solve this problem, a deeper understanding of the whole light-to-electricity energy conversion process is needed.

The OPV cells need to be set up in open areas, which can make them prone to incurring serious damage as the materials are susceptible to oxygen and water [30]. In order to have a consistent performance, the devices need regular maintenance, thus adding extra cost and human efforts to the whole application.

The electronic structure of organic semiconductors can be engineered on the atomic level. However, the engineering principle requires a thorough understanding of the structure-properties relationship and the basic chemistry and physics behind the power conversion process. This is not a trivial task at the current stage. Without knowledge of the connection between molecular structure and material properties, the design of novel devices can only be performed in a trial and error fashion, leading to waste of time and effort.

1.1.3 Power Conversion Process

In inorganic semiconductors, electrons and holes are free to move after the excitation happens. However, due to the low dielectric constant of organic materials, the excitons created are still strongly bound, requiring extra effort to separate. In order to improve the free charge carrier generation, a detailed understanding of the whole power conversion process in organic solar cells is necessary. OPV devices absorb energy from the sunlight, generate electron-hole pairs, create free charges by separating the electron-hole pairs, and finally produce electricity by the flow of free charges carriers. The light-to-electricity power conversion process has four fundamental steps [25, 31, 32]: (1) exciton generation; (2) exciton diffusion; (3) exciton dissociation; (4) free charge carrier transportation and collection at the electrodes. An illustration of the photoninduced electron transfer from polymer to PCBM and a schematic representation of the power conversion process are shown in Figure 1.3.

www.manaraa.com

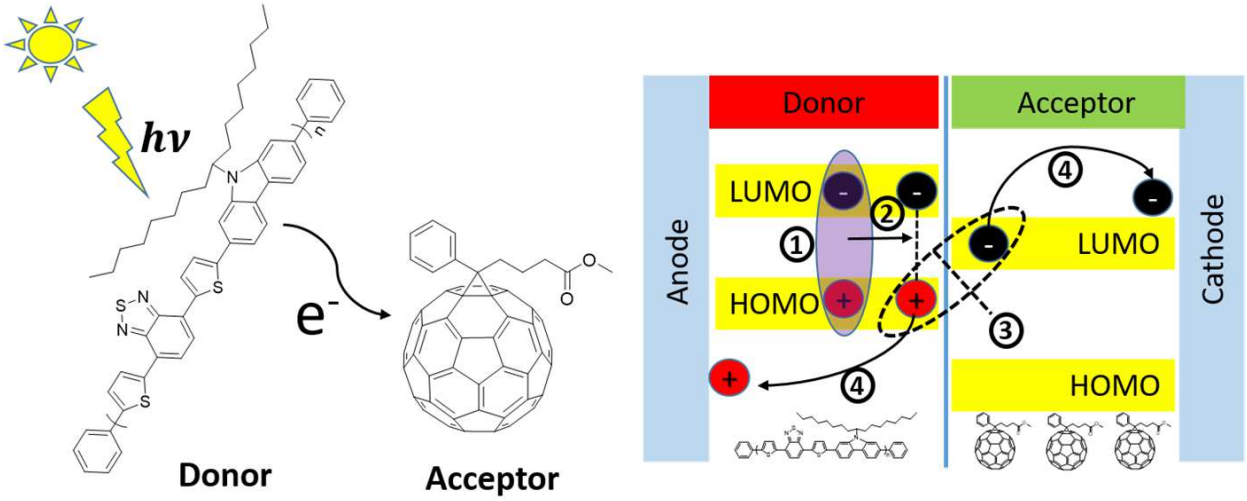

Figure 1.3: Illustration of the photoinduced charge transfer from the polymer (donor) to PCBM (acceptor) on the left, and a schematic of the power conversion process on the right.

During the exciton generation step, the donor (acceptor) absorbs photons and creates electron-hole pairs. This step involves light absorption and exciton creation on the polymer (donor) part. The electronic structure of organic semiconductor plays a crucial role. The photon flux of the AM1.5 solar spectrum peaks at around 700 nm (1.8 eV), which can be captured effectively by some low-bandgap polymers such as PCDTBT [25] in Figure 1.2(g). Massive efforts have been applied to synthesize donor candidates possessing ideal band gaps in order to effectively harness the sun's photons while keeping the polymer layers thin. After the absorption of photons whose energy is equal to or larger than the band gap, the electron-hole pairs generated are strongly bound by Coulomb attraction with a large binding energy. As a result, extra steps are needed for the dissociation of excitons to create free charge carriers, in contrast to inorganic semiconductors where weakly bound excitons are formed and free charges are obtained after excitation.

During the exciton diffusion step, electron-hole pairs diffuse within the donor (acceptor) phase. In this step, the excitons can either move to the donor/acceptor (D/A) interface and dissociate into free charges or recombine to decay. The diffusion length, which is the product of diffusion coefficient and exciton lifetime, is considerably smaller (one order of magnitude) than the thin film thickness (one order of magnitude) [33–36]. Therefore in a bilayer OPV

www.manaraa.com

model the active layer is only a small part of the overall D/A junction. In contrast to a BHJ model where the excitons can diffuse to the D/A interface easily since the polymer and fullerene molecules are mixed together, which partially explains the superior performance of BHJ devices over bilayer models.

During the exciton dissociation step, excitons move to the D/A interface and dissociate into free charges. After the competition between recombination and diffusion, some excitons survive and arrive at the interface, then dissociation can take place quite effectively with an internal quantum efficiency approaching 100% [10, 37]. The exact dissociation process is still unclear, some researchers believe that the (hot) excitons with excess electronic or vibrational energy tend to have a large dissociation probability [15, 17], whereas other studies show that cold excitons can also contribute no less to the free charge generations [10, 12]. Another concern comes from the intrinsic properties of the materials, in inorganic semiconductors, the weakly bound electron-hole pairs can be separated effortlessly because the dielectric environment has a strong screening effect on the Coulomb attraction. Whereas the organic materials usually have a small dielectric constant, making it more difficult to overcome the separation barrier.

The last step is free charge carriers transportation and collection at respective electrodes. After the separation of excitons, electrons will be in the acceptor phase and holes will be in the donor phase. Electricity can only be generated when electrons and holes are transported and collected at the corresponding electrodes as shown in Figure 1.3. During the transportation process, the free charge carriers can recombine to form an energy loss channel. The holes are more susceptible to recombination since their mobility in the polymer domain is lower than the electron mobility in fullerenes phase [38, 39]. Apart from intrinsic properties of the materials, the morphology of the overall structure is also a decisive factor in determining the transportation efficiency. An ordered (crystalline) structure can provide a much easier charge transportation route thus having higher conductivity, which affords a more efficient power conversion device [30].

www.manaraa.com

The primary focus of this thesis is on the third step, where the strongly bound excitons are called CTSs. The aim is to gain more insight into the properties of these states so that the mechanism of free charge carriers creation can be revealed and better design rules of the organic solar cells can be properly proposed. The excitons can only dissociate when the driving force (energy difference between the LUMO levels of donor and acceptor) is larger than the binding energy. One way to reduce the Coulomb interaction between the electron-hole pairs is to employ the dielectric screening. When the dielectric constant of the environment increases, the binding energy of the exciton should decrease, thus making it easier for obtaining free charge carriers. But the detailed mechanism is still unclear.

In the following sections, a brief review will be given for the role of CTSs in the performance of the OPV devices and for solvent effects on the energetics of CTSs.

1.2 Charge Transfer State

In the power conversion process, an intermediate state exists between the bound exciton and free charge carriers, it has multiple names which can be used interchangeably or to serve different purposes. These names include charge transfer state, charge transfer excitons, exciplex, polaron pairs, geminate pairs [11, 13]. In this thesis, charge transfer state will be used.

Charge transfer is one of the most important processes in a variety of photochemical, photophysical, and biological phenomena [40]. In the process of light-to-electricity conversion occurring in organic solar cells such as BHJ devices, excitons are created by absorbing photons in the electron donor domain and then diffuse to the heterojunction interface to dissociate into free charges. The existence of CTSs can be observed in experiments by using ultrafast transient absorption spectroscopy [15] or steady-state and time-resolved photoluminescence (PL) techniques [11]. Although intensive research effort has been made, the mechanism of free charge generation in BHJs is still unclear. Much research suggests that interfacial CTSs play a significant role in the generation of free photocarriers. These states are also involved in singlet fission processes, thus providing a possible way to increase the

www.manaraa.com

conversion efficiency [41]. It has been proposed that high-lying singlet states, i.e., hot excitons, could directly convert to hot interfacial CTSs which immediately yield free charge carriers [15, 42] due to the excessive energy. On the other hand, there are experimental results [10, 12] suggesting that vibrationally equilibrated or cold CTSs could also serve as precursors of free charges. In addition, the results of transient absorption spectroscopy reveal that the electric field generated by interfacial CTSs may affect the optical transitions in the surrounding molecules and cause ultrafast free charge generation [43]. There are also other works [17, 44, 45] such as the observation of polaronic signature within 100 fs but no further relaxation in the resonance Raman spectroscopy which suggests direct exciton dissociation into free charges [46]. The mechanism of resonant tunneling for delocalized excitons in the presence of strong vibronic coupling may also facilitate the ultrafast long-range charge separation [47–49]. Nevertheless, the CTS is a crucial factor in ultrafast charge separation processes in BHJ materials and deserves substantial research attention.

Electronic excitations in a multichromophoric system such as conjugated polymers are usually tightly bound excitons which are numerically difficult to characterize due to their many body nature. Compared to inorganic semiconductors, the low dimensionality (quasi-1D or 2D) and low relative permittivity ($\varepsilon = 2 - 4$) of organic conjugated molecules strengthen the electron-hole interaction and result in relatively small exciton size and large exciton binding energy (0.3-0.5 eV) that cannot be perturbatively treated. Such fact further complicates the theoretical simulation on the corresponding excited-state processes. Another difficulty in excited-state simulations comes from the interaction between the reacting molecular system and its surrounding polarizable media such as a solvent or solid state matrix. Due to the difference in electrostatic dipole between excitations such as intermolecular CTSs and intramolecular excitations, quantitative modeling of the excited-state energetic alignment is a non-trivial computational task that requires methods not only to account for the aforementioned strong excitonic effect but also to correctly model the polarizable environment with respect to the excitation.

www.manaraa.com

A thorough understanding of CTSs is crucial to obtain an optimal design for the ideal performance of organic solar cells. The expression for estimating the PCE is $\eta = \frac{J_{SC} \times V_{OC} \times FF}{P_{inc}}$, where J_{SC} is the short-circuit current density, which directly depends on the external quantum efficiency, V_{OC} is the open circuit voltage, FF is the fill factor, and P_{inc} is the power density of the incident light. The maximum open circuit voltage is determined directly by the energy of CTSs [13].

The dielectric environment of the OPV devices also has a considerable impact on the overall performance. Various studies have shown that increasing the ratio of the component with higher dielectric constant (ε) (usually fullerenes) or using polymers with larger ε, thus providing a greater spatially averaged permittivity, leads to a lower CTS energy and a more efficient charge dissociation [50–53]. In the next section, a brief overview of the role of solvent effect on the CTS energy will be given.

1.3 Solvent Effects

A major concern in the simulation of CTS comes from the interaction between the molecular system and its surroundings such as solvent or solid state. Many works have been performed in vacuo, but in order to take into account the influence of the dielectric condition on the electronic properties of the material, the solvent models must be applied in calculations. Incorporating solvent in a quantum chemistry calculation of a modestly large organic molecule is nontrivial if both solute and solvent are treated quantum mechanically. A common solution is to deal with the solvent in a continuum manner and only apply quantum mechanical treatment to the solute molecule.

The Stokes shift is used to characterize the difference between absorption and emission spectra of the same electronic transition, which is caused by the different response time of the various degrees of freedom of the solvent. The interaction between the solute molecule and the solvent system can be partitioned into to two parts, fast and slow. When a vertical excitation takes place in the solute, the solvent fast degrees of freedom readjust to the solute excited state density instantaneously, whereas the solvent slow degrees of freedom are in the

www.manaraa.com

unrelaxed configuration corresponding to the solute ground state density. This situation is called nonequilibrium solvation and is usually described by the optical dielectric constant [54]. After a certain delay, the solvent slow degrees of freedom reorganizes so that both slow and fast components are in equilibrium with the solute excited state configuration, which is named equilibrium solvation and can be represented by both the optical and the static dielectric constant [55, 56].

The environmental polarization can alter the excited-state electronic structure of the solute and vice versa [57]. In organic semiconductors, the CTSs are notably sensitive to the nearby solvent polarization because of their large electrostatic dipoles [58]. Research has shown that the electrons localized on an electron donor can be stabilized by solvent polarization [59], then as the environment becomes more polar, the energy of CTS decreases [56]. Meanwhile, the exciton binding energy and charge recombination are reduced, leading to more free charges and better device performance [19, 20, 60–64].

The CT excitations in solution can be computed by adopting basic continuum models where the solvent is a continuum dielectric hosting the solute in a cavity [65]. In such a model, the continuous dielectric medium is described by a constant referred to as dielectric constant or relative permittivity. The solvation energy can then be obtained by solving the electrostatic (Poisson) problem for the cavity surface charge induced by the solute electron density upon excitations [66]. An example of such approach is the Linear Response-Time Dependent Density Functional Theory (LR-TDDFT) method, which however, often underestimates the CT energy correction because the solvent polarization is evaluated from the transition density rather than the excited-state density [67–69]. One way to address this deficiency is to use the so-called state-specific (SS) solvation approach, in which the correction on the transition energy is computed by making the excited-state density self-consistent with the corresponding solvent polarization. As shown in previous studies [55, 69–72], the SS approach is generally reliable at determining the energy correction associated with the charge redistribution of the solute upon the electronic transition. However, the SS method

www.manaraa.com

is much more computationally demanding than the LR model because it requires external iterations to reach self-consistency between the solvent potential and the electron density of a specific excited state. This requires separate computations for each excited state of interest, whereas the LR method can calculate multiple states at once. A detailed formulation and comparison of the two solvent models, LR and SS, will be examined in the next chapter.

The aim of this thesis is to study the solvent effects on the energetics of excited states, especially CTS, in OPV devices during a light-to-electricity power conversion process computationally. In Chapter 2, the computational methods will be reviewed, a systematic analysis of the one-electron transition density matrix (TDM) will be formulated to identify excitonic and charge transfer excitations, and then two solvation models will be derived and compared. In Chapter 3, these methods will be applied to study a typical organic molecular system and investigate how the solvent polarity affects the alignment of excitation energetics. Conclusions and outlook will be given in the last Chapter.

www.manaraa.com

CHAPTER 2 COMPUTATIONAL BACKGROUND

2.1 Overview

Generally, in organic photovoltaics, the exciton binding energy and electron-hole separation lie between those of Frenkel excitons [73] and Wannier-Mott excitons [74]. Therefore both excitonic and charge transfer characters may exist simultaneously in the photoexcitation of conjugated compounds which further complicates the description of the corresponding electronic structures [75–79]. An intermolecular Charge Transfer (CT) state is formed with prominent charge displacement between neighboring molecules and is often followed by a strong Stark effect due to its large electric dipole moment. In contrast, an excitonic (EX) state is associated with limited charge movement and the electron and hole are relatively tightly bound. Therefore, one can formally distinguish a CT state from EX states by examining the static dipole moments. However, the EX and CT characters often coexist in one excitation with a varying degree of mixing. Examination of the corresponding transition density matrix (to be specified in Section 2.2.1) provides a more accurate estimate of the CT characters for a given excited state.

In the past two decades, TDDFT has become a routine technique for excited-state computation because of its favorable accuracy-to-cost ratio [80]. In the Kohn-Sham (KS) formalism the Schrödinger equation, in terms of non-interacting electron density, can be solved by the self-consistent field method with the approximate exchange-correlation (XC) functional representing molecular Hamiltonian [81]. The linear response TDDFT based on Casida's formulation has been widely used to compute electronic excitations and is programmed in a variety of electronic structure codes [82]. However, in the case of strong excitonic effect in conjugated structures, TDDFT method often fails to predict electron-hole interaction effects [83–85], the energies of CT excitations [81, 86], as well as material band gaps and chemical reaction barriers [87]. Improvements can be achieved by introducing the charge/spin constraints on the electronic density obeying chemical intuition such as constrained DFT method [59, 65, 88].

www.manaraa.com

An alternative way to eliminate the delocalization error in XC functionals is to adopt hybrid functionals that involve nonlocal exchange potential with range separation [89, 90]. CAM-B3LYP [91], ω97X [92] and screened range-separated hybrid (SRSH) [93] are examples of long-range-corrected models, where the exchange potentials at short-range and long-range are approximated separately.

The van der Waals interactions between molecules are essential in determining molecular structures and conformations for large molecules and aggregates [94, 95]. A prevalent way to account for these interactions is to add empirical dispersion corrections to the underlying functional. Popular models include Petersson-Frisch [96] and Grimme's [97–99] models which are reliable to use together with a variety of XC functionals when computing large molecular systems.

Considering all the aforementioned factors, many studies on the CT transitions in organic semiconductors have been conducted using different techniques. For example, the energetics of CT excitations at organic interfaces have been calculated based on SRSH functional [100]. This study demonstrated agreement with the experimental values for the CTS energies of the donor/acceptor complexes such as pentacene/C_{60} and poly-3-hexylthiophene (P3HT)/PCBM. Zheng and coworkers have developed several protocols to compute CT state energies for conjugated molecules in polar solvent. By employing the Baer-Neuhauser-Livshits (BNL) functional and PCM for solvent effect in the constrained DFT method, they showed that solvation can considerably affect the CTS energies [65]. This observation successfully explained the enhanced red-shift between the absorption and emission spectra of stilbene-functionalized octahedral silsesquioxanes [101]. A similar protocol also reproduces the solvated CTS energies for a series of functionalized anthracene and tetracyanoethylene dimers [65]. Nieman et al. employed TDDFT with range-corrected CAM-B3LYP functional to simulate the CTSs in P3HT: fullerenes complex separated by aligned oligothiophenes. Combined with experimental studies, their work revealed that the CT process can be improved by the dielectric environment [21]. In this Chapter, the computational methods for

www.manaraa.com

studying the characteristics of electronic excitations will be examined by means of a detailed analysis on the one-electron transition density matrix, and the formulation of solvation models for calculating excitations in a dielectric environment will be derived.

2.2 Analysis of Excitonic and Charge Transfer Interactions

In this section, a detailed analysis of the one-electron transition density matrix will be used to study the properties of electronic transitions. First, the method of how to formulate the transition density matrix will be shown, then a real space analysis on the matrices will be given, and finally, a numerical procedure to calculate the degree of charge transfer for each excited state will be proposed.

2.2.1 Transition Density Matrix

The density matrix is a powerful tool for studying the optical properties of large organic molecules since it is computationally feasible and carries the essential information on electronic excitations.

The charge density of an orbital a adopts a form

$$\bar{\rho}_{aa} = \langle g|C_a^\dagger C_a|g\rangle\,, \tag{2.1}$$

where $|g\rangle$ represents the ground-state many-electron wave function and $C_a^\dagger/C_a$ is the creation/annihilation operator.

The Hohenberg-Kohn theorems prove that the ground state density uniquely determines the properties of the system, thus the charge distribution and ground state energy can be calculated from the charge density.

The single electron density matrix can be formulated as

$$\rho_{ab}^{\nu\mu} \equiv \langle \nu|C_a^\dagger C_b|\mu\rangle\,, \tag{2.2}$$

where $|\nu\rangle$ and $|\mu\rangle$ are electronic states and a, b denote atomic orbitals. So $\rho^{\nu\nu}$ represents the reduced single-electron density matrix of state ν and $\rho^{\nu\mu}$ is the transition density matrix between states ν and μ.

For a molecular system driven by an external electric field, the time-dependent wave

www.manaraa.com

function can be written as:

$$\Psi(t) = \sum_{\nu} C_{\nu}(t) \left|\nu\right\rangle, \tag{2.3}$$

and its density matrix is given by

$$\rho_{ab}(t) \equiv \langle \Psi(t)|C_a^{\dagger}C_b|\Psi(t)\rangle = \sum_{\nu\mu} C_{\nu}^{\star}(t)C_{\mu}(t)\rho_{ab}^{\nu\mu}, \tag{2.4}$$

so the time-dependent single-electron density matrix $\rho_{ab}(t)$ can be obtained from $\rho_{ab}^{\nu\mu}$, which is density matrix of the transition between state ν and μ.

2.2.2 Real Space Representation of Transition Density Matrix

The ground state properties can be calculated from the ground state density matrix $\rho_{ab}^{gg} \equiv \langle g|C_a^{\dagger}C_b|g\rangle$. Its diagonal elements ρ_{aa}^{gg} can be used for population analysis, and the off-diagonal elements ρ_{ab}^{gg} can represent the bonding between atomic orbitals a and b. Similarly, for transition density matrix $\rho_{ab}^{g\nu}$ (transition from ground state $|g\rangle$ to excited state $|\nu\rangle$), the diagonal elements $\rho_{aa}^{g\nu}$ denote the net charge induced on atomic orbital a, whereas the off-diagonal elements $\rho_{ab}^{g\nu}$ represent the joint amplitude of an extra electron appearing on orbital a and a hole appearing on orbital b [102].

The flow of the charges induced by the optical transition can be captured with transition density matrix. The charges belong to different atomic orbitals in $\rho_{ab}^{\nu\mu}$ and need to be contracted to each atom. A procedure proposed by Tretiak and Mukamel [102] is applied for this task. Conventionally, the hydrogen atoms are ignored in this procedure since they have negligible contributions to the delocalized electronic transitions. For non-hydrogen atoms, the total induced charges on atom M are given by the sum of diagonal elements

$$(\rho^{g\nu})_M = \left|\sum_{a_M} (\rho^{g\nu})_{a_M a_M}\right| \tag{2.5}$$

and the effective electronic coherence between atom M and N is denoted by the average over

www.manaraa.com

all off-diagonal elements

$$(\rho^{g\nu})_{MN} = \sqrt{\sum_{a_M b_N} [(\rho^{g\nu})_{a_M b_N}]^2} \tag{2.6}$$

where a_M and b_N are the atomic orbitals of atom M and N, respectively.

Following this scheme, an electronic density matrix of the same dimension as the number of non-hydrogen atoms in the molecular system can be obtained. Contour charge density maps can be made from these matrices to visualize the collective electronic motions of each transition.

2.2.3 Charge Transfer Character

A procedure has been formulated to obtain and visualize the transition density matrix in both atomic orbital space and real space. Next, it is necessary to look at how to perform a quantitative analysis of the transition density matrix to get details on the character of the electronic excitations.

For a molecular system having more than one chromophore, the electronic transitions can be dominated by either EX or CT character. By visually examining the charge contour plots of the transition density matrix of certain excited state one can determine whether this transition is dominated by EX or CT character. Moreover, a detailed numerical analysis can be formulated to get a quantitative measure of the degrees of CT character for each electronic transition.

In a molecular system comprising of two parts, there are four possible types electronic excitations: local transition on each monomer and charge transfer between two parts, see Figure 2.1 for illustration. Furthermore, these four possible types of transitions can interact, creating four resonance states [103]. Following the naming conventions used by Chandra and Lim, these states are referred to as σ, γ, δ and ρ [104].

www.manaraa.com

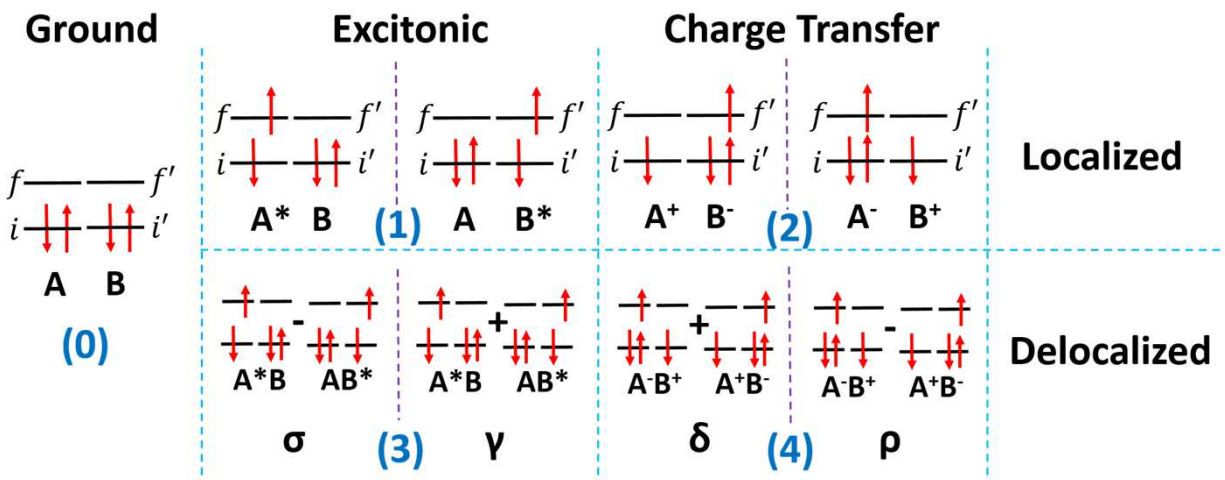

Figure 2.1: Schematic illustrations of one-electron excitation in a dimer molecular system, with two monomers A and B. (0) for ground state, (1) for local excitation (excitonic state), (2) for charge transfer state, (1) and (2) are represented with localized orbitals. The linear combinations of (1) and (2) provide the delocalized states as (3) and (4).

The molecular system in Figure 2.1 is consisted of two monomers A and B, each having two molecular orbitals: i (initial) and f (final) for monomer A; i' and f' for monomer B. If the two chromophores are considered as having weak interactions (or the separation between two monomers being at an intermediate $(6 - 150\ \mathring{A})$ to large $(> 150\ \mathring{A})$ range), then the total wave function can be given by the product of the wave functions of A and B, Ψ^A and Ψ^B, respectively.

$$\Psi^{Tot} = NM(\Psi^A \Psi^B), \tag{2.7}$$

where N is the normalization constant and M is the antisymmetrizing operator. Since A and B are weekly interacting, the interaction terms can be omitted and the Hamiltonian can be written as $H^{Tot} = H^A + H^B$ with the total energy $E^{Tot} = E^A + E^B$.

However, the main concern is in the molecular systems at the short range$(3 - 6\mathring{A})$. In particular, the aim is to study the electron transfer between the different fragments of the whole system, so the interactions have to be considered. For a pair of two-level systems, the wave function for the closed shell ground state $|g\rangle$ shown in Figure 2.1 (0) can be given as:

$$|g\rangle = |AB\rangle = 2^{-1/2} \left|(core)\ i\ \bar{i}\ i'\ \bar{i'}\right\rangle, \tag{2.8}$$

www.manaraa.com

where $(core)$ represents all the orbitals except the last four electrons. i, i' are associated with electrons of α spin and $\bar{i}$, $\bar{i}'$ for electrons of β spin.

The four localized excited states (two excitonic and two charge transfer), shown in Figure 2.1 (1) and (2), can be expressed as:

$$|A^{\star}B\rangle = 2^{-1/2}\,|(core)\; i'\; \bar{i}'\; [i\,\bar{f} + \bar{i}\,f]\rangle\,, \tag{2.9}$$

$$|AB^{\star}\rangle = 2^{-1/2}\,|(core)\; i\; \bar{i}\; [i'\,\bar{f}' + \bar{i}'\,f']\rangle\,, \tag{2.10}$$

$$|A^{+}B^{-}\rangle = 2^{-1/2}\,|(core)\; i'\; \bar{i}'\; [i\,\bar{f}' + \bar{i}\,f']\rangle\,, \tag{2.11}$$

$$|A^{-}B^{+}\rangle = 2^{-1/2}\,|(core)\; i\; \bar{i}\; [i'\,\bar{f} + \bar{i}'\,f]\rangle\,. \tag{2.12}$$

For a transition from orbital s to orbital r, the single excitation operator E_{rs} is defined as:

$$E_{rs}\,|m_1 m_2 \ldots 0_r \ldots 1_s \ldots\rangle = C_r^{\dagger} C_s\,|m_1 m_2 \ldots 0_r \ldots 1_s \ldots\rangle \tag{2.13}$$

$$= (-1)^{\theta_{(r-s)}}\,|m_1 m_2 \ldots 1_r \ldots 0_s \ldots\rangle\,, \tag{2.14}$$

where the sign factor $(-1)^{\theta_{(r-s)}}$ is determined from $\theta_{(r-s)} = \theta_r - \theta_s$, which can be considered as the number of occupied spin orbitals occurring between the locations corresponding to the spin orbital ϕ_r and ϕ_s in the wave function $|m\rangle$ [105]. With the single excitation operator and the Hartree-Fock ground state $|g\rangle$, the aforementioned four localized states can be written as:

$$|A^{\star}B\rangle = 2^{-1/2} E_{fi}\,|g\rangle\,, \tag{2.15}$$

$$|AB^{\star}\rangle = 2^{-1/2} E_{f'i'}\,|g\rangle\,, \tag{2.16}$$

$$|A^{+}B^{-}\rangle = 2^{-1/2} E_{f'i}\,|g\rangle\,, \tag{2.17}$$

$$|A^{-}B^{+}\rangle = 2^{-1/2} E_{fi'}\,|g\rangle\,. \tag{2.18}$$

At long intermolecular distances, these wave functions exist as degenerate pairs [106], and the true eigenfunctions are equal mixtures of the following delocalized states:

www.manaraa.com

$$|\sigma\rangle = 2^{-1/2}(|A^{\star}B\rangle - |AB^{\star}\rangle) \tag{2.19}$$

$$= \frac{1}{2}(E_{fi} - E_{f'i'})\,|g\rangle\,, \tag{2.20}$$

$$|\gamma\rangle = 2^{-1/2}(|A^{\star}B\rangle + |AB^{\star}\rangle) \tag{2.21}$$

$$= \frac{1}{2}(E_{fi} + E_{f'i'})\,|g\rangle\,, \tag{2.22}$$

$$|\delta\rangle = 2^{-1/2}(|A^{-}B^{+} + |A^{+}B^{-}\rangle\rangle) \tag{2.23}$$

$$= \frac{1}{2}(E_{fi'} - E_{f'i})\,|g\rangle\,, \tag{2.24}$$

$$|\rho\rangle = 2^{-1/2}(|A^{-}B^{+} - |A^{+}B^{-}\rangle\rangle) \tag{2.25}$$

$$= \frac{1}{2}(E_{fi'} - E_{f'i})\,|g\rangle\,. \tag{2.26}$$

These expressions are based on localized orbitals. They can also be given by the delocalized basis as illustrated in Figure 2.2 [106, 107]. The detailed equations are omitted here, since the aforementioned representations contain adequate information for electronic transition properties analysis.

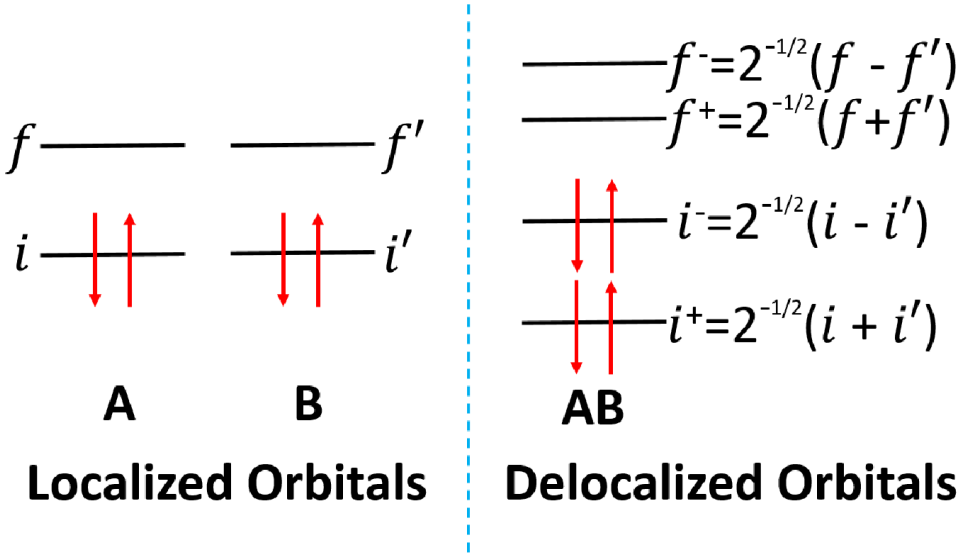

Figure 2.2: Molecular orbitals of a dimer (monomer A and B) system represented in the localized and delocalized orbital space.

To analyze these excited transitions, the one-electron transition density matrix $\rho_{ab}^{g\nu}$ formulated in the last section can be used,

www.manaraa.com

$$\rho_{ab}^{g\nu} = \langle g|C_a^\dagger C_b|\nu\rangle = \langle g|E_{ab}|\nu\rangle\,, \tag{2.27}$$

where the excitation operator E_{ab} is used to denote the transition from orbital b to orbital a.

In an orthogonal basis of localized orbitals the transition density matrix can be expressed as $\rho_{ab}^{g\nu,[LO]}$. If the orbitals a and b belong to the same monomer A or B, the transition should be considered a local excitation. If a and b are associated with different fragments, the transition is a charge transfer excitation. Following the approach developed by Luzanov [108] and Lischka [107], a concept called charge transfer number Ω_{AB}^{ν} can be defined as

$$\Omega_{AB}^{\nu} = \frac{1}{2}\sum_{\substack{a\in A\\ b\in B}}(\rho_{ab}^{g\nu,[LO]})^2, \tag{2.28}$$

where A and B represent two monomers, a and b are molecular orbitals of A and B, respectively.

To generalize the calculation of charge transfer number to the nonorthogonal basis of atomic orbitals [107], the above equation can be written as:

$$\Omega_{AB}^{\nu} = \frac{1}{2}\sum_{\substack{a\in A\\ b\in B}}(\rho^{g\nu,[AO]}S^{[AO]})_{ab}(S^{[AO]}\rho^{g\nu,[AO]})_{ab}, \tag{2.29}$$

where $\rho^{g\nu,[AO]}$ is the one-electron transition density matrix of excited state ν in AO basis and $S^{[AO]}$ is the overlap matrix.

The charge transfer character (CT) can be defined as:

$$CT = \frac{1}{\Omega}\sum_{\substack{A\\ B\neq A}}\Omega_{AB}^{\nu}, \tag{2.30}$$

where Ω is the normalization constant which is close to 1. For a completely charge transfer state, the value of CT should be 1; whereas for a completely localized or excitonic state, CT is 0.

In practice, the two monomers A and B are categorized as either donor (D) who donates electrons or acceptor (A) who accept electrons. The electronic excitations of this dimer

www.manaraa.com

system can be described by four charge transfer numbers,

$$CT(DA) = \frac{1}{\Omega} \sum_{\substack{D \\ A \neq D}} \Omega^{\nu}_{DA}, \tag{2.31}$$

$$CT(AD) = \frac{1}{\Omega} \sum_{\substack{A \\ D \neq A}} \Omega^{\nu}_{AD}, \tag{2.32}$$

$$DD = \frac{1}{\Omega} \sum_{D} \Omega^{\nu}_{DD}, \tag{2.33}$$

$$AA = \frac{1}{\Omega} \sum_{A} \Omega^{\nu}_{AA}, \tag{2.34}$$

where $CT(DA)/CT(AD)$ represents the charge transfer from (donor to acceptor)/(acceptor to donor), and DD/AA is the charge localization on donor/acceptor.

2.3 Solvation Models: Linear-Response and State-Specific Methods

There are two ways to take the solvent into account in a theoretical calculation, explicit and implicit. In an explicit formalism, the individual solvent molecules are included. The solvent-solute polarization and solvent-solvent interactions are described using empirical potentials. With an appropriate number of solvent molecules in the proper configurations, the explicit model can provide an accurate estimation of the electronic properties of the solute molecules and can be used to explore properties such as hydrogen bonding and viscosity. However, this method is too computationally demanding and prohibitively expensive for moderate size systems, let alone large organic molecules. In an implicit formalism, the solvent is treated as a polarizable continuum with a dielectric constant ε, instead of averaging over numerous configurations of individual solvent molecules. The solute is located in a cavity, surrounded by a continuous dielectric medium. The solute-solvent mutual polarization is simulated using a self-consistent reaction field (SCRF), where self-consistency should be reached between the charge density of the solute molecule and the solvent potential. The interactions can be illustrated in a three-step process using a self-consistent picture: the solute electron density polarizes the solvent by inducing charge redistribution on the cavity

www.manaraa.com

surface, then the induced charges modify the charge density of the solute, finally after a certain number of interactions a balance is achieved between the solute electron density and the induced solvent potential.

One of the most commonly used implicit models is the polarizable continuum model (PCM) [67]. The electronic properties of the solute molecule under the influence of dielectric environment can be studied by using PCM coupled with a quantum mechanical (QM) description of the solute [66]. In the solvent domain, an electrostatic problem (Poisson problem) can be formulated and solved using various approaches, such as the apparent surface charge (ASC), the multiple expansion (MPE) method, and the generalized Born approximation (GBA) [67]. In the solute domain an effective Hamiltonian can be written to include the solvent-solute interactions so that, upon applying a perturbative or a variational treatment of the QM problem, electronic excitation energies can be obtained.

Within the QM continuum solvation formalism two different schemes, LR and SS, are usually used to calculate the electronic excitation energy [55]. This section is devoted to the formulation of these two solvent approaches in the context of the basic polarizable continuum model. First, the continuum model and the electrostatic problem are presented, then the solute charge distribution is treated in a quantum regime coupled with the effects of the environment. In the second part, two solvent schemes will be formulated and compared.

2.3.1 Basic Continuum Solvation Model

According to J. Tomasi et al. [109], in a focused model, the solute-solvent system can be partitioned into two parts, one focused F, and the other remainder R. The solute is included in the focused part since it requires a more detailed description while the solvent is considered in the remainder part. For such a system, the Hamiltonian can be written as:

$$\hat{H}^{FR}(f,r) = \hat{H}^{F}(f) + \hat{H}^{R}(r) + \hat{H}^{int}(f,r), \tag{2.35}$$

where f and r stand for the degrees of freedom of F and R, respectively.

The solvent degrees of freedom are included in two terms, pure solvent $\hat{H}^{R}(r)$ and interaction $\hat{H}^{int}(f,r)$. By eliminating the solvent term and only considering the solvent in the

www.manaraa.com

interaction counterpart, a significant simplification can be made to the continuum solvation models, resulting in an effective Hamiltonian

$$\hat{H}^{FR}_{eff}(f,r) = \hat{H}^{F}(f) + \hat{H}^{int}(f,r). \tag{2.36}$$

This procedure helps to avoid a detailed consideration of the solvent and considerably simplifies the calculations. However, the solvent degrees of freedom (i.e., r) are still included in the interaction term. The model can be further simplified by bringing in the solvent response function, and then the effective Hamiltonian has a form

$$\hat{H}^{FR}_{eff}(f,r) = \hat{H}^{F}(f) + \hat{V}^{int}[f, Q(\mathbf{r},\mathbf{r}')], \tag{2.37}$$

where the solvent response function $Q(\mathbf{r},\mathbf{r}')$ is expressed as a sum of separate terms representing different contributions of the solute-solvent interaction. These include electrostatic, dispersion, repulsion and cavity formation, among which electrostatic interaction is the dominant force, thus only this term is taken into account in the basic model [109].

Electrostatic Problem

In a basic polarizable continuum model, the solute is placed in a cavity, surrounded by the solvent. The charge distribution ρ_M of the solute polarizes the solvent, which in turn modifies the solute charge density. These interactions can be seen in a self-consistent picture, requiring an iterative procedure for obtaining an explicit numerical solution. The final value of the solute charge density ρ_M, reached upon convergence of the iterative procedure, determines the interaction potential in Eq. (2.37).

An electrostatic problem as a Poisson equation is formulated to find the potential.

$$-\nabla[\epsilon(\mathbf{r})\nabla V(\mathbf{r})] = 4\pi\rho_M(\mathbf{r}), \tag{2.38}$$

$$-\nabla^2 V(\mathbf{r}) = 4\pi\rho_M(\mathbf{r}), \epsilon(\mathbf{r}) = 1 \quad \text{within cavity}, \tag{2.39}$$

$$-\epsilon\nabla^2 V(\mathbf{r}) = 0, \epsilon(\mathbf{r}) = \epsilon \quad \text{outside of cavity}. \tag{2.40}$$

V is the sum of the electrostatic potential V_M and the reaction potential V_R. V_M is generated by the solute charge distribution ρ_M. V_R is generated by the polarization of the dielectric environment. The reaction potential can be simulated by an apparent surface

www.manaraa.com

charge (ASC) distribution $\sigma(\mathbf{s})$ on the boundary between the solvent and the solute, i.e., the surface of the cavity C [66].

$$V(\mathbf{r}) = V_M(\mathbf{r}) + V_\sigma(\mathbf{r}). \tag{2.41}$$

In the ASC method, the solvent potential can be represented as:

$$V_\sigma(\mathbf{r}) = \int_\Gamma \frac{\sigma(\mathbf{s})}{\mid \mathbf{r} - \mathbf{s} \mid} \quad with \quad \Gamma = \partial C. \tag{2.42}$$

With appropriate boundary conditions, the potential V in Eq. (2.38) can be uniquely determined.

2.3.2 Electronic Excitations in QM-PCM Formulation

To calculate the solute charge distribution and how it can be affected by the dielectric medium, it is necessary to solve the Schrödinger equation with an effective Hamiltonian defined as the sum of the vacuum Hamiltonian of the solute molecule and an electrostatic interaction term describing the mutual polarization between solute and solvent, corresponding to Eq. (2.37):

$$\hat{H}_{eff} = \hat{H}^{vac} + \hat{V}^{int}. \tag{2.43}$$

In what follows two different approaches to calculating the excitation energies, namely, SS and LR methods will be examined.

State-Specific Method

The state-specific method uses perturbation theory to solve the Schrödinger equation for the states of interest and calculate the excitation energies as the differences between the corresponding values of the free energy functionals [55].

The stationary states Ψ_i of a solute can be obtained as the eigenfunctions of the time-independent Schrödinger equation:

$$H_M(\Psi_i) \left|\Psi_i\right\rangle = E_i \left|\Psi_i\right\rangle, \tag{2.44}$$

where $H_M(\Psi) = H_M^{vac} + V(\Psi_i)$. $V(\Psi_i)$ describes the interaction of the solute with the solvent. $V(\Psi_i)$ adopts a form:

www.manaraa.com

$$V(\Psi_i) = \hat{V} \langle \Psi_i | \hat{Q} | \Psi_i \rangle , \tag{2.45}$$

where $\hat{V}$ is the molecular electrostatic potential operator and $\hat{Q}$ is the apparent charge operator. The electrostatic potential generated by the solute M is described by apparent surface charges evenly distributed on the surface of the cavity containing M. $\hat{Q}$ is used to represent the polarization of the solvent under the influence of this potential.

Due to the nonlinear nature of the effective Hamiltonian, a new functional has to be defined in order to solve Eq. (2.44), which can be viewed as the free energy functional:

$$G(\Psi_i) = \langle \Psi_i | H_M(\Psi_i) | \Psi_i \rangle - \frac{1}{2} \langle \Psi_i | V(\Psi_i) | \Psi_i \rangle , \tag{2.46}$$

Hereafter the state wave function Ψ_i will be referred to as i.

The excitation energy can be calculated as the difference between the excited and the ground state (GS) value of G:

$$\Delta G_{0i} = G(i) - G(0). \tag{2.47}$$

The above definition of the excitation energy assumes instantaneous adjustment of the solvent configuration to excitation of the solute molecule, i.e., the solvent and the solute are in equilibrium. The non-equilibrium case will be examined later.

The nonlinear Schrödinger equation Eq. (2.44) can be solved perturbatively. The zero-order Hamiltonian can be written as:

$$H_M(0) = H_M^{vac} + V(0). \tag{2.48}$$

Assuming the unperturbed solutions are known:

$$H_M(0) | i^{(0)} \rangle = E_i^{(0)} | i^{(0)} \rangle , \tag{2.49}$$

where $|i^{(0)}\rangle$ represents the ith electronic state under the reaction field of the ground state $|0\rangle$.

The excitation energy corrected to first order has a form:

www.manaraa.com

$$\Delta G^I_{0i} = G^I(i) - G(0) \tag{2.50}$$

$$\begin{aligned} &= \langle i^{(0)}| H_M(0) |i^{(0)}\rangle - \langle 0| H_M(0) |0\rangle + \frac{1}{2}\langle i^{(0)}| V(i^{(0)}) |i^{(0)}\rangle \\ &\quad - \langle i^{(0)}| V(0) |i^{(0)}\rangle + \frac{1}{2}\langle 0| V(0) |0\rangle \end{aligned} \tag{2.51}$$

$$= \Delta E^{(0)}_{0i} + \frac{1}{2}[\langle i^{(0)}| V(i^{(0)}) |i^{(0)}\rangle + \langle 0| V(0) |0\rangle] - \langle i^{(0)}| V(0) |i^{(0)}\rangle\,, \tag{2.52}$$

and can be recast in terms of the solvation operators $\hat{V}$ and $\hat{Q}$:

$$\Delta G^I_{0i} = \Delta E^{(0)}_{0i} + \frac{1}{2}[\langle i^{(0)}| \hat{V} |i^{(0)}\rangle - \langle 0| \hat{V} |0\rangle] \cdot [\langle i^{(0)}| \hat{Q} |i^{(0)}\rangle - \langle 0| \hat{Q} |0\rangle], \tag{2.53}$$

where $|i^{(0)}\rangle$ is the zero-order approximation for the excited state $|i\rangle$. $\Delta E^{(0)}_{0i}$ is the zero-order excitation energy that corresponds to the electronic transition from the ground state to the unperturbed ith electronic state under $V(0)$, which is the fixed reaction field that corresponds to the ground state; the rest of the terms describe the interaction occurring from the change in reaction field from $V(0)$ to $V(i^{(0)})$, which is the reaction field created by the unperturbed excited state $|i^{(0)}\rangle$.

When non-equilibrium effects are considered, the solvent-solute interaction term V is partitioned into two parts, a dynamic (fast) part V_d and an inertial (slow) part V_{in}.

$$V(\Psi) = V_{in}(\Psi) + V_d(\Psi), \tag{2.54}$$

where $in-$ stands for inertial and $d-$ stands for dynamic.

Then a non-equilibrium free energy adapts a form:

$$G^{neq}(i,0) = \langle i| H^{vac}_M |i\rangle + \frac{1}{2}\langle i| V_d(i) |i\rangle + \langle i| V_{in}(0) |i\rangle - \frac{1}{2}\langle 0| V_{in}(0) |0\rangle \tag{2.55}$$

$$= \langle i| H^{vac}_M + V(0) |i\rangle + \frac{1}{2}\langle i| V_d(i) |i\rangle - \langle i| V_d(0) |i\rangle - \frac{1}{2}\langle 0| V_{in}(0) |0\rangle\,. \tag{2.56}$$

A non-equilibrium nonlinear Schrödinger equation can be obtained as [110, 111]:

$$[H^{vac}_m + V_{in}(0) + V_d(i)] |i\rangle = E^{neq}_i |i\rangle\,. \tag{2.57}$$

Using a similar perturbative technique:

$$\{H^{vac}_m + V(0) + \lambda[V_d(i) - V_d(0)]\} |i\rangle = E^{neq}_i |i\rangle\,, \tag{2.58}$$

with a zero-order Hamiltonian Eq. (2.48) and its solution Eq. (2.49). The perturbative non-equilibrium free energy is:

www.manaraa.com

$$G^{neq,\lambda}(i,0) = \langle i| H_m^{vac} + V(0) + \lambda[V_d(i) - V_d(0)] |i\rangle - \frac{1}{2}\lambda[\langle i| V_d(i) |i\rangle - \langle 0| V_d(0) |0\rangle] - \frac{1}{2}\langle 0| V(0) |0\rangle . \tag{2.59}$$

Substituting the energies and wave functions as a power series of λ, the non-equilibrium excitation energy, corrected to first-order has the following form:

$$\Delta G_{0i}^{neq,I} = G^{neq,I}(i,0) - G(0) \tag{2.60}$$

$$= \Delta E_{0i}^{(0)} + \frac{1}{2}[\langle i^{(0)}| \hat{V} |i^{(0)}\rangle - \langle 0| \hat{V} |0\rangle] \cdot [\langle i^{(0)}| \hat{Q}_d |i^{(0)}\rangle - \langle 0| \hat{Q}_d |0\rangle], \tag{2.61}$$

where $\hat{Q}_d$ is the apparent charge operator of the dynamic response of the solvent.

Comparing Eq. (2.53) and Eq. (2.61), it can be observed that the only difference is the apparent charge operator, i.e., only the dynamic part of the solvent-solute interaction is included in the non-equilibrium situation.

For the other solvent approach, namely linear-response, a similar excitation energy expression corresponding to $\Delta G_{0i}^{neq,I}$ in Eq. (2.61) should be derived. This will allow the differences between the two methods to be compared.

Linear-Response Method

In the linear-response approach, the excitation energies are determined directly as the singularities of the frequency-dependent linear response functions of the solute molecule in the ground state. Therefore the explicit calculation of the excited state wave functions can be avoided [55].

Contrary to the SS approach, whose states are the solutions of time-independent Schrödinger equation, the LR method starts with the nonlinear time-dependent Schrödinger equation with a time-dependent Hamiltonian and the solutions are the states of the solute under a time-dependent external field given by:

$$H_M(\Psi) |\Psi\rangle = i\frac{\partial}{\partial t} |\Psi\rangle , \tag{2.62}$$

$$H_M(\Psi) = H_M^{vac} + V(\Psi) + W(t), \tag{2.63}$$

where $H_M(\Psi)$ represents the Hamiltonian of the solute molecule M, $V(\Psi)$ is the solvent potential due to solute-solvent interaction, $W(t)$ denotes the interaction of the solute with

www.manaraa.com

the external field, and $\lim_{t\to-\infty} W(t) = 0$ since only the adiabatic case is considered.

Through a series of derivations [55], the expressions for first-order correction to the excitation energy corresponding to Eq. (2.61) is given as:

$$\omega_i^I = \Delta E_{0i}^{(0)} + \langle i^{(0)}| \hat{V} |0\rangle \langle i^{(0)}| \hat{Q}_d |0\rangle , \tag{2.64}$$

$\Delta E_{0i}^{(0)}$ has the same meaning as in Eq. (2.61), representing the zero-order transition energy of the excitation $|0\rangle \to |i^{(0)}\rangle$ under the fixed reaction field of the ground state; the rest of the terms describe the energy arising from the interaction between the excitation and the reaction field.

Comparison of State-Specific and Linear-Response Methods

Now the differences between LR and SS approaches can be examined by comparing the two excitation energy expressions, Eq. (2.61) and Eq. (2.64). The common term, $\Delta E_{0i}^{(0)}$, can be interpreted as the energy change of the solute when the molecule undergoes an excitation from the ground state $|0\rangle$ to the (unperturbed) excited state $|i^{(0)}\rangle$, under the reaction field $V(0)$. During this transition, the ground state of the solute is always in equilibrium with the solvent. The difference between the two methods comes from the second term, which describes the interaction of the solvent configuration with the solute excitation. In such a process the fast degrees of freedom of the solvent readjust to the change in the charge density of the solute excited state $|i^{(0)}\rangle$. In SS, this term is $\frac{1}{2}[\langle i^{(0)}| \hat{V} |i^{(0)}\rangle - \langle 0| \hat{V} |0\rangle] \cdot [\langle i^{(0)}| \hat{Q}_d |i^{(0)}\rangle - \langle 0| \hat{Q}_d |0\rangle]$, which includes the expectation values over both the ground and excited state of the electrostatic potential operator $\hat{V}$ as well as the dynamical apparent charge operator $\hat{Q}_d$. Whereas in LR, the corresponding term is $\langle i^{(0)}| \hat{V} |0\rangle \langle i^{(0)}| \hat{Q}_d |0\rangle$, which has expectation values over the transition matrix of the operator $\hat{V}$ and $\hat{Q}_d$. This represents a dynamical correction to the excitation energy, thus avoiding the explicit calculation of the excited state wave function.

So far, the analysis of LR and SS methods has been carried out from two different starting points. SS applies a perturbation on the time-independent Schrödinger equation whereas LR solves the time-dependent Schrödinger equation under a time-dependent external field.

www.manaraa.com

However, a unified formalism can be used to derive the excitation energy expressions for SS and LR. Bjorgaard *et al.* [56] compared these two solvent approaches by implementing conductor-like screening method (COSMO) in the time-dependent self-consistent filed (TD-SCF) framework started from a von-Neumann-type equation of motion of a single-electron density matrix.

The corresponding excitation energy expressions they obtained are

$$\Delta\Omega_{SS} = \mathrm{Tr}(TV_S(\bar{\rho}_k)) \tag{2.65}$$

for SS method, and

$$\Delta\Omega_{LR} = \mathrm{Tr}(TV_S(P)) + \mathrm{Tr}(\xi^T V_S(\xi)) \tag{2.66}$$

for LR method, where V_S is the COSMO effective solvent potential.

$$\rho_k = P + \nu_k, \tag{2.67}$$

$$\nu_k = \xi(\text{interband}) + T(\text{intraband}), \tag{2.68}$$

$$\bar{\rho}_k = P + T_k. \tag{2.69}$$

P is the ground state density matrix, ρ_k is the excited state density matrix for state k, and ν_k is the transition density matrix. ν_k can be divided into two parts in a molecular orbital picture: ξ(interband) represents hole→particle or particle→hole transitions; T(intraband) denotes hole→hole or particle→particle excitations. A simplification is made by neglecting the interband component to obtain $\bar{\rho}_k$. Note that similar to the comparison made at the beginning of this section, the SS approach requires explicit calculations of the density matrix of a specific excited state k, whereas the LR method only needs the transition density.

By employing a dipole approximation with the dipole moment defined as $\mu_\rho = \mathrm{Tr}(\hat{\mu}\rho)$ for an arbitrary density matrix ρ, where $\hat{\mu}$ is the dipole moment operator, Bjorgaard and coworkers also obtained the approximated expressions for the transition energy corresponding to Eq. (2.61) and Eq. (2.64) as:

$$\Delta\Omega_{SS} \approx \mu_T \cdot \mu_P + \mu_T \cdot \mu_{T_k}, \tag{2.70}$$

$$\Delta\Omega_{LR} \approx \mu_T \cdot \mu_P + \mu_\xi^2. \tag{2.71}$$

www.manaraa.com

It can be observed that the first term in Eq. (2.70) and Eq. (2.71), $\mu_T \cdot \mu_P$, corresponds to $\Delta E_{0i}^{(0)} = \langle i^{(0)}| H_M(0) |i^{(0)}\rangle - \langle 0| H_M(0) |0\rangle$ in Eq. (2.64) and Eq. (2.61), representing the electronic interaction energy of the ground state (P or $|0\rangle$) with the change in excited state charge density (T or $|i^{(0)}\rangle$). For the second term in Eq. (2.70) and Eq. (2.71), $\mu_T \cdot \mu_{T_k}$ is associated with $\frac{1}{2}[\langle i^{(0)}| \hat{V} |i^{(0)}\rangle - \langle 0| \hat{V} |0\rangle] \cdot [\langle i^{(0)}| \hat{Q}_d |i^{(0)}\rangle - \langle 0| \hat{Q}_d |0\rangle]$, which can be considered as the correlated readjustment of the solvent configuration with respect to the excited state electron density; μ_ξ^2 is similar to $\langle i^{(0)}| \hat{V} |0\rangle \langle i^{(0)}| \hat{Q}_d |0\rangle$, which accounts for the dispersion correction, *i.e.*, the response of the solvent due to the oscillation of the electron density of the solute molecule at the Bohr frequency [55].

www.manaraa.com

CHAPTER 3 A TDDFT STUDY ON THE PCPDTBT:PCBM LOW BAND GAP SYSTEM

This chapter is reproduced with permission from the Journal of Photonics for Energy 8(3), 032215 (21 May 2018). Kangmin Liu, Hao Li, Sergei Tretiak, Vladimir Chernyak, "Solvent effects and charge transfer states in organic photovoltaics: a time-dependent density functional theory study on the PCPDTBT:PCBM low band gap system".

3.1 Introduction

Among all the OPV devices, BHJ materials composed of polymeric electron donors and fullerene-based electron acceptors have gained enormous attention due to their high power conversion efficiency and numerous technological advantages [112, 113]. PCPDTBT: PCBM pair shown in Fig. 3.1 represents a promising BHJ family of low band gap copolymer system due to their high charge mobility, good processability, optimal band gap of PCPDTBT molecule, and the outstanding solubility of PCBM [114–116]. Although the excited-state properties of these materials have been studied by a variety of theoretical methods [15, 117, 118], detailed investigation of solvent effects on electronic transitions is still lacking. The potentially strong dipole-dipole interaction between the BHJ matter and its surrounding medium may considerably affect excited-state properties and likewise the generation of free charges. It has been reported that by adding a high permittivity additive, camphoric anhydride, to an MDMO-PPV: PCBM system, the charge-separated state energy decreases more rapidly than that of the CTS, resulting in an overall reduction of the CT exciton binding energy [19]. Loi and coworkers found that by increasing the concentration of PCBM in the PCPDTBT: PCBM bulk heterojunction system, a red shift of the CTS emission spectra was observed. This can be attributed to the reduction of Coulombic interaction between the electron and hole due to the increase in the average dielectric constant of the medium (PCBM ~ 3.9 and polymer $\sim 2.5 - 3$) [11, 119]. However, this phenomenon observed in this particular molecular system has not been reproduced in theo-

www.manaraa.com

retical calculations. Although a similar trend has been observed for smaller molecular pair anthracene: tetracyanoethylene (TCNE) using semiempirical approaches with a conductor-like screening method (COSMO) [56]. Nieman and coauthors studied the energetic ordering of excited states and the stabilization of CTSs for a P3HT/Oligomers/C_{60} system and found that the CTSs are the lowest energy states which can be further stabilized by polar environments [21]. However, the correct electronic states alignment has not been recovered in calculations of PCPDTBT: PCBM. Therefore, this molecular system is taken as a typical example to illustrate how the nearby dielectric environment affects electronic excitations and to reproduce the correct energetic alignment of excited states, especially for CTSs, using quantum-chemical simulations.

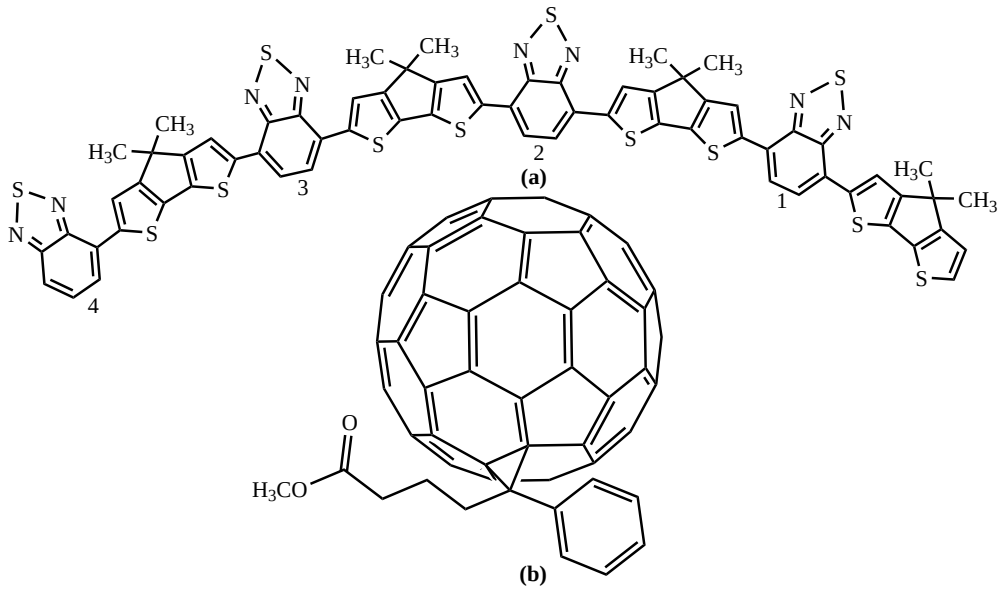

Figure 3.1: Chemical structures of (a) Poly[2,6-(4,4-dimethyl-4H-cyclopenta[2,1-b:3,4-b′]-dithiophene)-alt-4,7-(2,1,3-benzothiadiazole)] (PCPDTBT) and (b) [6,6]-Phenyl-C61-butyric acid methyl ester ($PC_{61}BM$ or PCBM)

3.2 Methods

Here the focus is on the low-lying electronic singlet states in the BHJ complex of PCPDTBT: PCBM. Detailed ab initio simulations on dynamical processes in real BHJ aggregates are currently numerically forbidden due to the large dimension of the system and the complexity arising from the configuration of the mixture. Therefore, in this work, the donor: acceptor

www.manaraa.com

interface is simplifies as a molecular model that consists of a tetramer of the donor oligomer and a single buckyball. Such a simplified model allows extensive numerical simulations by probing the effects of several density functionals, geometries and a broad range of dielectric constants, thus delivering detailed information on solvent effects on the energy level alignment. Because the optical band gap in PCPDTBT tends to saturate for oligomers with four repeat units [115, 117], PCPDTBT tetramer is selected to minimize the numerical cost and retain the essential physics of interest. Our computational model is an approximation to the experimental polymer: fullerene blend: it neglects the effects of intramolecular delocalizations beyond the oligomer length, geometrical conformations due to solid state packing, and the effects of intermolecular interactions with neighboring polymers and fullerenes that may also perturb the excited state alignment.

LC hybrid functionals CAM-B3LYP [91] and ωB97XD [120] have been employed together with the 6-31G(d) basis set for both ground-state structure optimizations and excited-state calculations. The 6-31G(d) basis was shown to be sufficient in the simulations of BHJ systems in the comparison with larger cc-pVTZ basis [65]. The Coulomb-attenuating method is used in CAM-B3LYP functional to modulate the fraction orbital exchange in the XC functional within the range of 19-65%. To describe intermolecular dispersion interactions binding the dimer, Grimme's dispersion correction has been applied together with CAM-B3LYP functional to the DFT-D2 and DFT-D3 levels [98, 99], hereafter referred to as GD2 and GD3. Compared to CAM-B3LYP, the ωB97XD functional includes more orbital exchange varying from 22% to 100%. In addition, the empirical dispersion correction is already built in ωB97XD functional.

3.2.1 Optimization of Geometries

The ground-state geometries of both PCPDTBT and PCBM monomers were optimized in vacuo using three different schemes, CAM-B3LYP/GD2, CAM-B3LYP/GD3, and ωB97XD. The optimized monomer structures were then combined together by placing the fullerene above the center of the PCPDTBT molecule. Specifically, the initial complex is oriented

www.manaraa.com

such that the center of PCBM is aligned with the second benzothiadiazole segment with the closest interatomic distance being 3.1$\mathring{A}$, whereas the side group of PCBM is placed away from PCPDTBT to minimize steric hindrance. The complex of PCPDTBT: PCBM was subject to further ground-state optimization in vacuo with the respective functionals. Different initial dimer configurations have been approached with the consideration of maximizing the $\pi - \pi$ stacking and minimizing the steric hindrance so that the global optimal structures can be found.

A tricky part of the monomer optimization is the starting geometry of PCPDTBT. The original ethylhexyl side chain on the cyclopentane ring is shortened to be a methyl group in order to avoid unnecessary complexity in the 3D dimensional structure. The original optimized geometry was obtained from Lanzani's paper [15]. After cleaning and symmetrizing using GaussView [121], it was re-optimized according to the aforementioned schemes. The results from different functionals, in Fig. 3.2, show that the general shape is planar but have a small degree of fluctuation in dihedral angles.

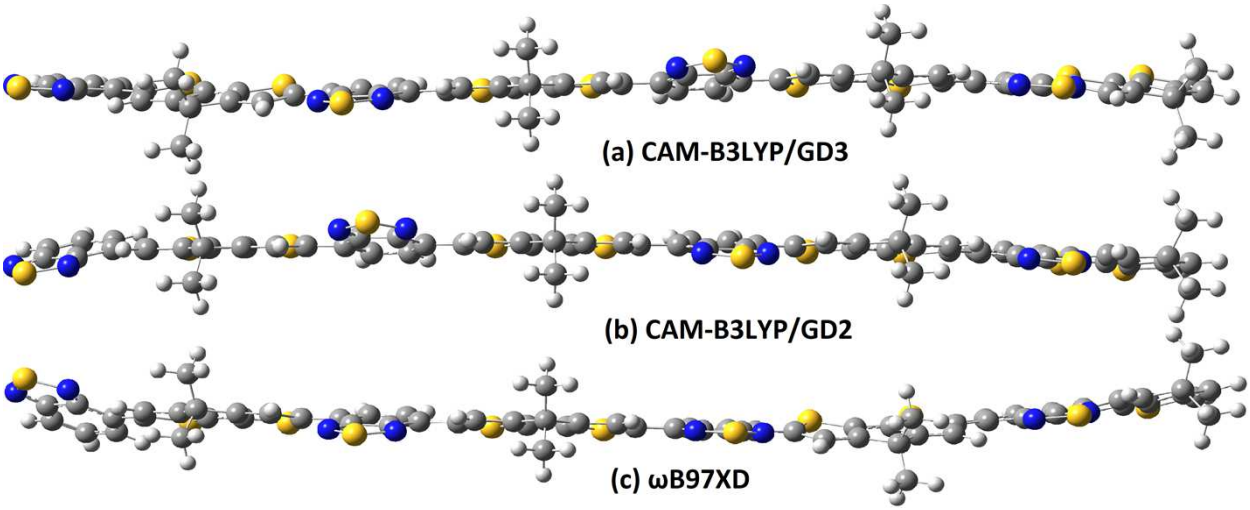

Figure 3.2: Optimized geometries of the polymer molecule PCPDTBT

3.2.2 Excited State Calculation

The lowest 20 vertical excitations of the oligomer, the buckyball, and their complex have been calculated both in vacuo and in solvent environment with varying static dielectric

www.manaraa.com

constant using DFT/TDDFT method. The density of states (DOS) of the excitonic states in the individual PCPDTBT and PCBM has been calculated respectively. The charge transfer character for the intermolecular CT excitations were evaluated from the calculation of the dimers.

3.2.3 Applying Dielectric Environment

The simulation in solution was performed using PCM [109] with varying dielectric constant. First, the solvent effect on excited states were evaluated at the LR TDDFT level [122]. Here the calculations do not require the excited-state density explicitly, thus avoiding significant numerical cost [55]. Further excited-state computations were performed based on the SS approach [72], in which the effective solvent potential directly depends on the excited state density. The energy correction due to solvation is approximated by the free energy difference between the ground and excited states. Recent studies have shown that excitations involving significant charge transfer can invoke strong solvent effects in the SS model, which is missing in the LR counterpart [56, 69].

In the case of vertical excitation, the non-equilibrium solvation procedure associated with fast solvent response requires optical dielectric constant in addition to the static counterpart. Both factors are involved in equilibrium solvation, but only the optical one is responsible for non-equilibrium states. Solvent permittivity including optical dielectric constant (ε_∞) and static dielectric constant (ε_0) can be specified for different solvents and solvation scenarios. Since the dominant solvent effect comes from the static dielectric constant of the solvent, in this work, the focus is on the solvent effect of static dielectric constant and the frequency-dependent optical one is left for future study. Specifically, in all simulations the optical dielectric constant was fixed to $\varepsilon_\infty = 2.0$ close to that of dichloromethane, whereas ε_0 was allowed to vary in the range of $3 < \varepsilon_0 < 30$. All calculations were conducted with Gaussian 09 computational package [123].

As for the optimization of the PCPDTBT: PCBM dimer geometry, it is of significant importance to sought an answer as to whether the solvent would make a significant impact.

www.manaraa.com

The geometries optimized in vacuo were subject to further optimization in solvent with various degrees of dielectric strength. The results show that the solvent stabilizes the dimer structure and the stabilization effects are stronger as the dielectric constant increases, see Fig. 3.3. And it was observed that after the permittivity of the solvent reaches a certain value, such as $\varepsilon_0 = 20$, the stabilization tends to saturate. In addition, the energy difference between ground state geometries optimized in vacuo and in solvent is substantially larger than the average thermal energy at room temperature ($1k_BT = 25meV$), so both vacuum and solvated geometries are used in the electronic excited state calculations.

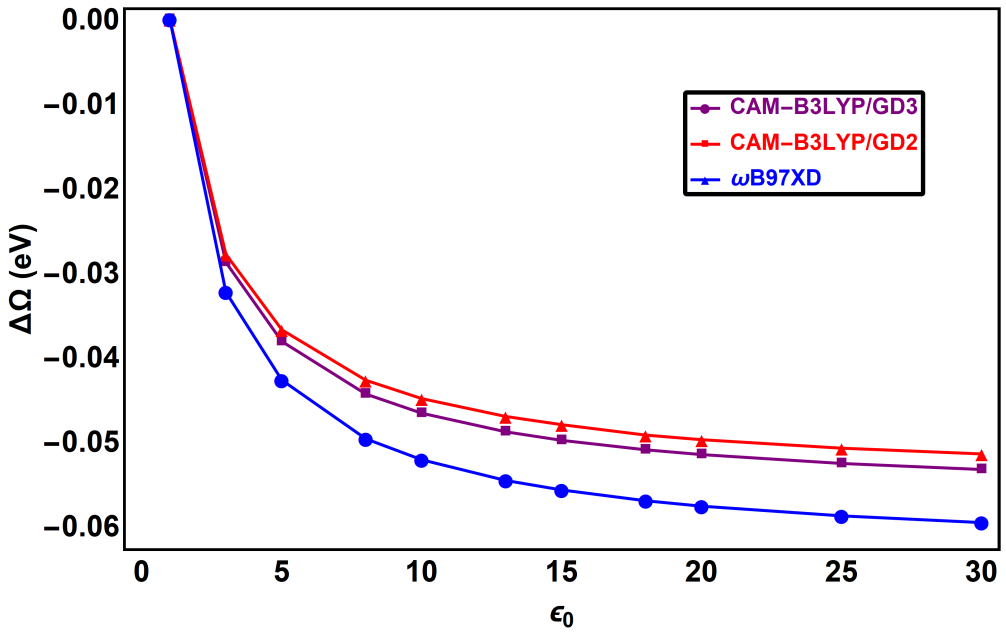

Figure 3.3: The energy of the ground state geometry optimized in vacuo and in solvent with various dielectric constant, $\varepsilon_0 = 1$ represents vacuo, $\Delta\Omega$ is the energy difference between the geometries optimized in solvent and in vacuo.

In Gaussian package, the keyword for assigning solvent environment is *SCRF=(PCM, Solvent=Generic, Read)*, where *(Generic)* enables the assignment of optical and static dielectric constant. First, a single-point TD-DFT calculation of the vertical excitation can be performed with linear response method. Then for the excited states of interest, the state-specific approach is applied using external iteration with the keyword *SCRF=(PCM, Solvent=Generic, ExternalIteration, Read)*.

www.manaraa.com

3.2.4 Calculation of Charge Transfer Character

The intermolecular CT states can be distinguished from ordinary excitonic states by employing the so-called CT character which can be obtained by averaging over the respective matrix elements of the transition density matrix [94, 107]. The CT character ranging from 0 to 1 represents completely localized excitation on a single molecule and full CT transition, respectively. In the present work, the excitations with CT character greater than 0.9 are defined as intermolecular CT states, less than 0.1 as EX states, and the transitions with $0.1 < CT < 0.9$ are referred to as hybrid states [95]. The focus of this work is on the energetics of the lowest CT state denoted by CT-1 and the lowest two EX states (EX-1 and EX-2). The solvent dielectric environment effects on the energetics and CT character are studied. The electronic excitations are visualized using the natural transition orbitals (NTOs) [124] and contour plots of the transition density matrices [102].

Extract Transition Density Matrix and Overlap Matrix from Gaussian RWF

The calculation of charge transfer character requires the extraction of transition density matrices and overlap matrices from the Gaussian read-write-file. According to the Gaussian Program Development Features, the RWF number 514 is the overlap matrix and 633 is the excited-state CI densities (transition density matrices) [125]. After extracting the matrices from the RWF, the following procedure is applied to prepare the data.

1. Determine the number of excited states n_{states} and the number of basis functions n.
2. Extract 514 and 633 from RWF using rwfdump command.
3. The raw 514 file starts from a block of header information which has no use for our analysis. Only keep the part after the line "Dump of file ...". Then the overlap matrix is obtained, which is a lower triangular matrix and needs to be converted to a full $n \times n$ matrix by copying the lower triangle elements to the corresponding positions on the upper triangle.
4. The raw 633 file also starts from a block of header information. Only the numbers after the line "Dump of file ..." should be kept. The number block can be divided into 3

www.manaraa.com

partitions. The first partition includes a random number and n_{states} zeros. The second partition is the transition density matrix needed for later calculations, it has $\frac{n(n+1)}{2} \cdot 20$ elements. The last partition is $2 \cdot n_{states}$ matrix with dimension $n \times n$, *2* stands for alpha and beta spin of the electrons.

Transition Density Matrix

In the PCPDTBT: PCBM molecular system, there are in total 218 atoms. The molecules are labeled according to the following scheme: in PCBM number 1-74 are used for non-hydrogen atoms and 163-176 are used for hydrogen atoms; in PCPDTBT number 75-162 are used for non-hydrogen atoms and 177-218 are used for hydrogen atoms. The basis set is 6-31G(d). The number of basis functions for each atom can obtained according to Table 3.1.

Table 3.1: Number of basis functions for each atom.

Element	C	N	O	S	H
Number of basis functions	15	15	15	19	2

A 4×4 matrix can be formulated to represent the structure of the transition density matrix of these two molecules. As shown in Fig. 3.4. Four terms can be used to represent the charge transfer between PCPDTBT and PCBM for each electronic excited state. These terms will be examined in details with an example later. The correspondence between the charge transfer character and the elements of the transition density matrix is shown in Table 3.2.

www.manaraa.com

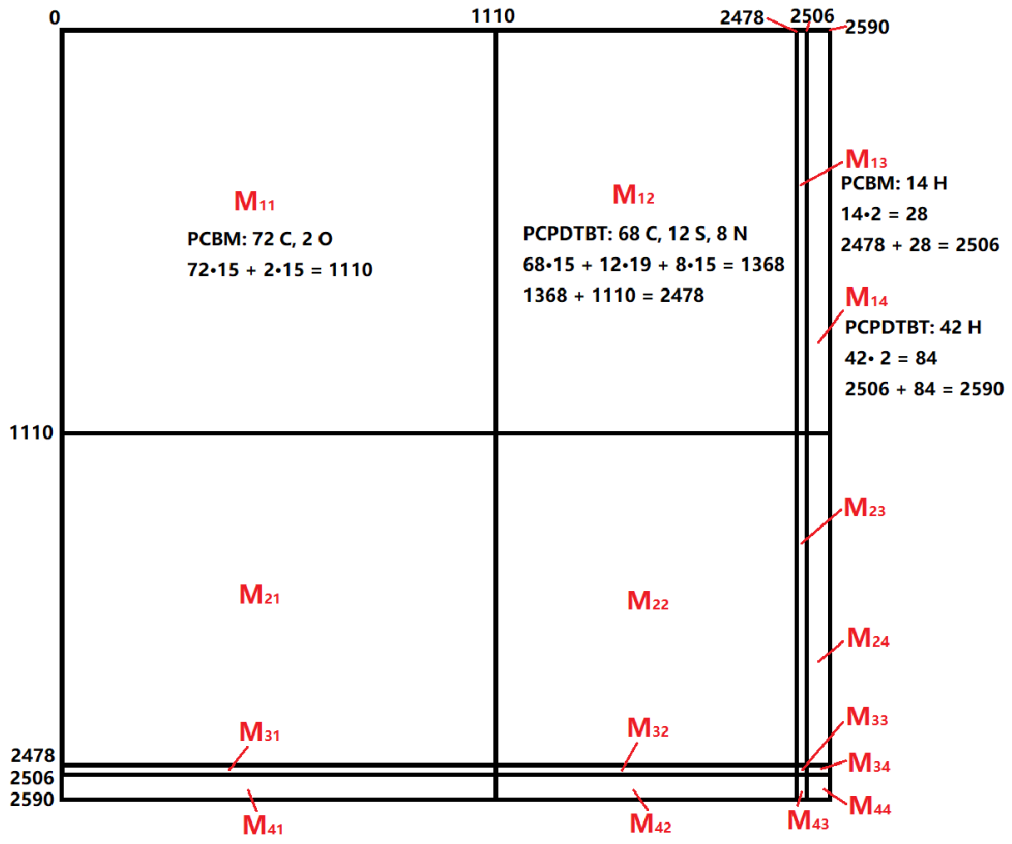

Figure 3.4: A schematic representation of the structure of the transition density matrix.

Table 3.2: Representation of Charge transfer and excitonic character by the elements of Transition Density Matrix.

Charge transfer		Excitonic	
CT(DA)	CT(AD)	DD	AA
Donor → Acceptor	Acceptor → Donor	Donor → Donor	Acceptor → Acceptor
$M_{21}+M_{23}$ $+M_{41}+M_{43}$	$M_{12}+M_{14}$ $+M_{32}+M_{34}$	$M_{22}+M_{44}$ $+M_{24}+M_{42}$	$M_{11}+M_{33}$ $+M_{13}+M_{31}$

The extracted transition density matrices are in the atomic orbital space. Using the method mentioned in Chapter 2, the matrix is contracted into atom-based real space according to the number of basis functions of each heavy (non-hydrogen) atom. Then a contour plot of the transition density matrix can be drawn for each excited state as an excellent visual aid for the determination of charge transfer and excitonic character. Fig. 3.5 includes three example contour plots of transition density matrices with different distributions of charge transfer character. There are 162 heavy atoms, 74 on the PCBM (Acceptor) part and 88 on

www.manaraa.com

the PCPDTBT (Donor) part. The contour plot can be divided into 4 blocks corresponding to the charge transfer character of Acceptor to Donor (AD), Donor to Donor (DD), Acceptor to Acceptor (AA) and Donor to Acceptor (DA). Numerical values for charge transfer character can be obtained using a scheme developed by Luzanov and Lischka [107, 108]. Note that the plots on the left and in the middle are dominated by DD. This means these two excited states have a large charge delocalization within the donor PCPDTBT molecule. Therefore they should be considered as excitonic states. Whereas in the plot on the right, the electronic transition is dominated by DA, which shows a strong charge transfer from donor PCPDTBT to acceptor PCBM. Hence this excited state should be considered as a charge transfer state. In summary, the contour plots of transition density matrices of electronic excited states provide an excellent qualitative measure of the charge transfer.

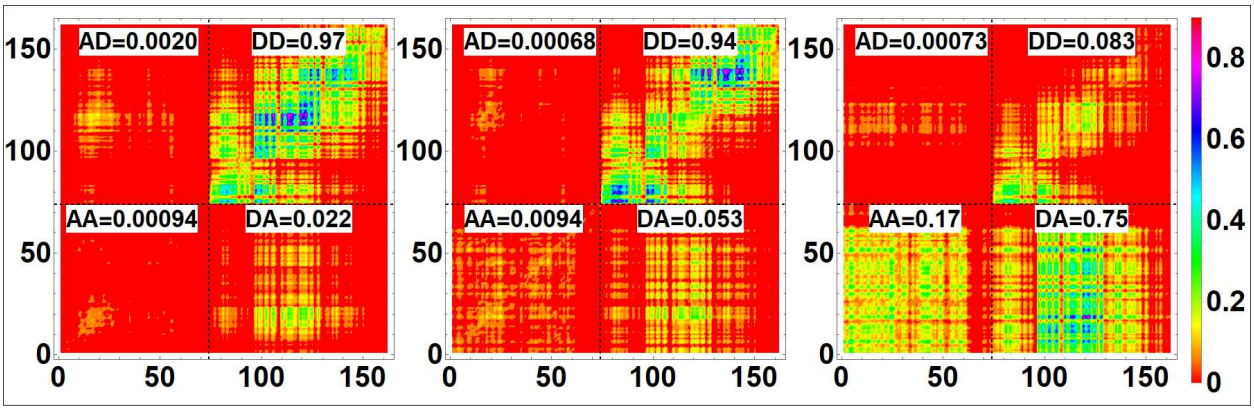

Figure 3.5: Contour plots of the transition density matrices for three excited states with one charge transfer number assigned to each block. The axis labels represent indices of non-hydrogen atoms from PCBM to PCPDTBT (PCBM: 1-74, PCPDTBT: 75-162). The inset of each plot shows the character of the electronic mode. D stands for Donor and A represents Acceptor, DA-charge transfer from Donor to Acceptor, AD-charge transfer from Acceptor to Donor, DD-charge localization within Donor, AA-charge localization in Acceptor.

3.3 Results and Discussion

Using optimal ground-state geometries for PCPDTBT, PCBM, and their complex, the lowest 20 excited states were computed in vacuo and in solvent with varied ε_0. Obtained excitation energies, oscillator strengths, transition density matrices, and NTO analysis are detailed in Appendix A Supplementary Information (SI) A. The primary focus is on the

www.manaraa.com

lowest two excitonic states (EX-1,2) and the lowest CT state (CT-1).

3.3.1 Electronic Excitations in Vacuo

The simulated stick absorption spectra for the 15 lowest states of PCPDTBT, PCBM, and the complex of PCPDTBT: PCBM computed in vacuo are shown in Fig. 3.6. The detailed numerical results can be found in SI Table A.1, A.2 and A.3.

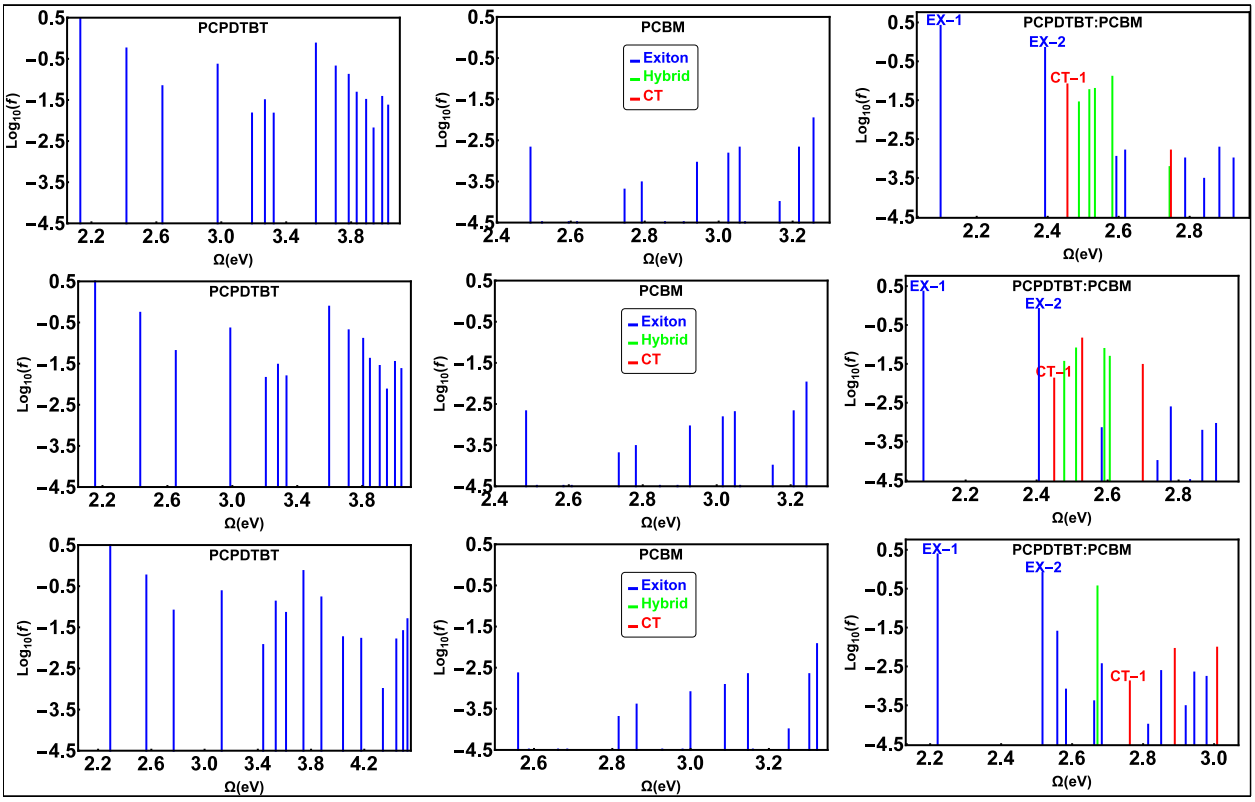

Figure 3.6: Stick absorption spectra of PCPDTBT, PCBM, and PCPDTBT: PCBM complex (from left to right) in vacuo computed at CAM-B3LYP/GD3 (top row), CAM-B3LYP/GD2 (middle row), and ωB97XD (bottom row). The x-axis denotes transition energies Ω, the y-axis denotes $\mathrm{Log}_{10}(f)$, f being unitless oscillator strength of a given transition. States are color-coded according to the CT character, i.e., blue for EX states with $CT \leq 0.1$, green for hybrid states with $0.1 < CT < 0.9$, and red for CT states with $CT \geq 0.9$.

www.manaraa.com

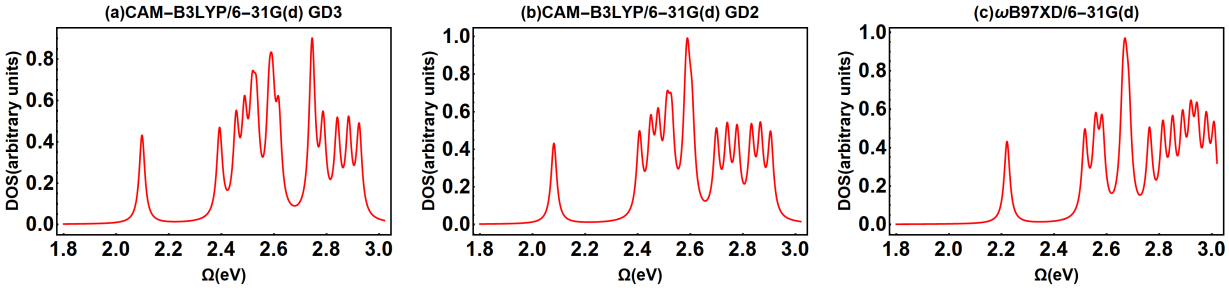

Figure 3.7: Density of states of PCPDTBT: PCBM complex in vacuo computed at (a) CAM-B3LYP/GD3, (b) CAM-B3LYP/GD2, and (c) ωB97XD. The x-axis denotes transition energies Ω; the y-axis denotes density of states with arbitrary units.

From Fig. 3.6 and 3.7, it is obvious that the distribution of the excitation energy has one common feature for all three functionals results, which is that the first excited state is far away from other states and only the first excited state has a significant oscillator strength. In addition, the DOS for CAM-B3LYP/GD3 and CAM-B3LYP/GD2 calculations are quite similar, whereas the energies predicted by ωB97XD are about 0.2 eV blue shifted.

The spectra for the monomers calculated at the three TDDFT levels agree very well with each other in terms of both excitation energy and oscillator strength. As expected, the multiple excited states in the PCPDTBT oligomer are optically allowed such as the lowest energy band-gap transition, which corresponds to the peak at 725 nm in its UV-Vis absorption spectrum associated with the $S_0 \rightarrow S_1$ transition [115]. In contrast, almost all excitations in the PCBM are optically forbidden due to the high symmetry of the molecule.

To analyze and compare the EX/CT character in the complex, the excitations of interest can be visualized using the respective NTOs and contour plots of the transition density matrices as shown in Fig. 3.8, 3.9, and Fig. A.1, A.2, A.3 in Appendix A SI. First, it can be seen that the lowest two excited states EX-1 and EX-2 in the complex are associated with the oligomer; their transition energies are only slightly perturbed by the presence of the fullerene. Indeed, the lowest excitation is limited within the PCPDTBT moiety but delocalized over the entire oligomer, whereas the second excitation can be represented by the NTOs pairs, each involving half of the oligomer chain (Fig. A.1). This observation can be interpreted by the symmetry of the exciton wave function [126]. The CT transitions in

www.manaraa.com

the complex appear at much larger energies. Namely, the lowest observed CT state from the ωB97XD calculation has slightly higher transition energy and a stronger CT character than those obtained from CAM-B3LYP levels. Specifically, the lowest CT state in the ωB97XD calculation corresponds to the eighth excited state with CT = 0.95, whereas CT-1 obtained from CAM-B3LYP is attributed to the third excitation with CT = 0.63 and 0.75 for GD2 and GD3 levels, respectively. The NTO representation in Fig. 3.8 qualitatively agrees with the CT characters evaluated from the transition densities, e.g., CT-1 in ωB97XD carries more CT character while the one determined from CAM-B3LYP/GD2 has the least. The two-dimensional contour plots (Fig. 3.9) of the transition density matrix for dimer states can be roughly interpreted as a 2×2 block matrix in which the diagonal elements represent the excitations happening within each monomer, whereas the off-diagonal blocks indicate that the excitation transfers a charge from one moiety to the other. This representation already suggests a weak hybridization of the excitonic and CT character for all states in question. Thus, both the visualized NTOs as well as the contour plots of the transition density matrices confirm that excited states EX-1,2 occur in the oligomer moiety. In contrast, in the CT-1 state electrons are driven from PCPDTBT to the fullerene moiety.

www.manaraa.com

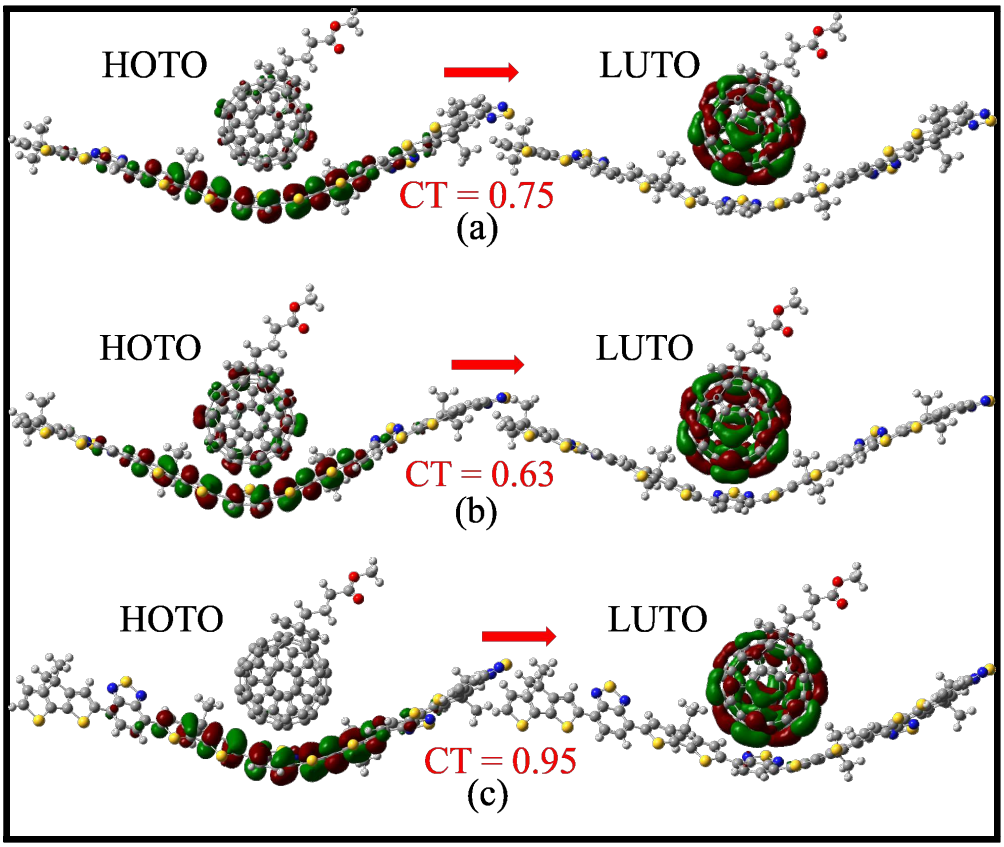

Figure 3.8: Visualization of natural transition orbitals (NTOs) of the lowest CT state with the highest occupied transition orbital (HOTO) on the left and the lowest unoccupied transition orbital (LUTO) on the right computed at (a) CAM-B3LYP/GD3, (b) CAM-B3LYP/GD2, (c) ωB97XD. The associated eigenvalues λ are 0.91, 0.92, and 0.97, respectively, which represent the weights of the particle-hole pairs contribution to the excitation.

www.manaraa.com

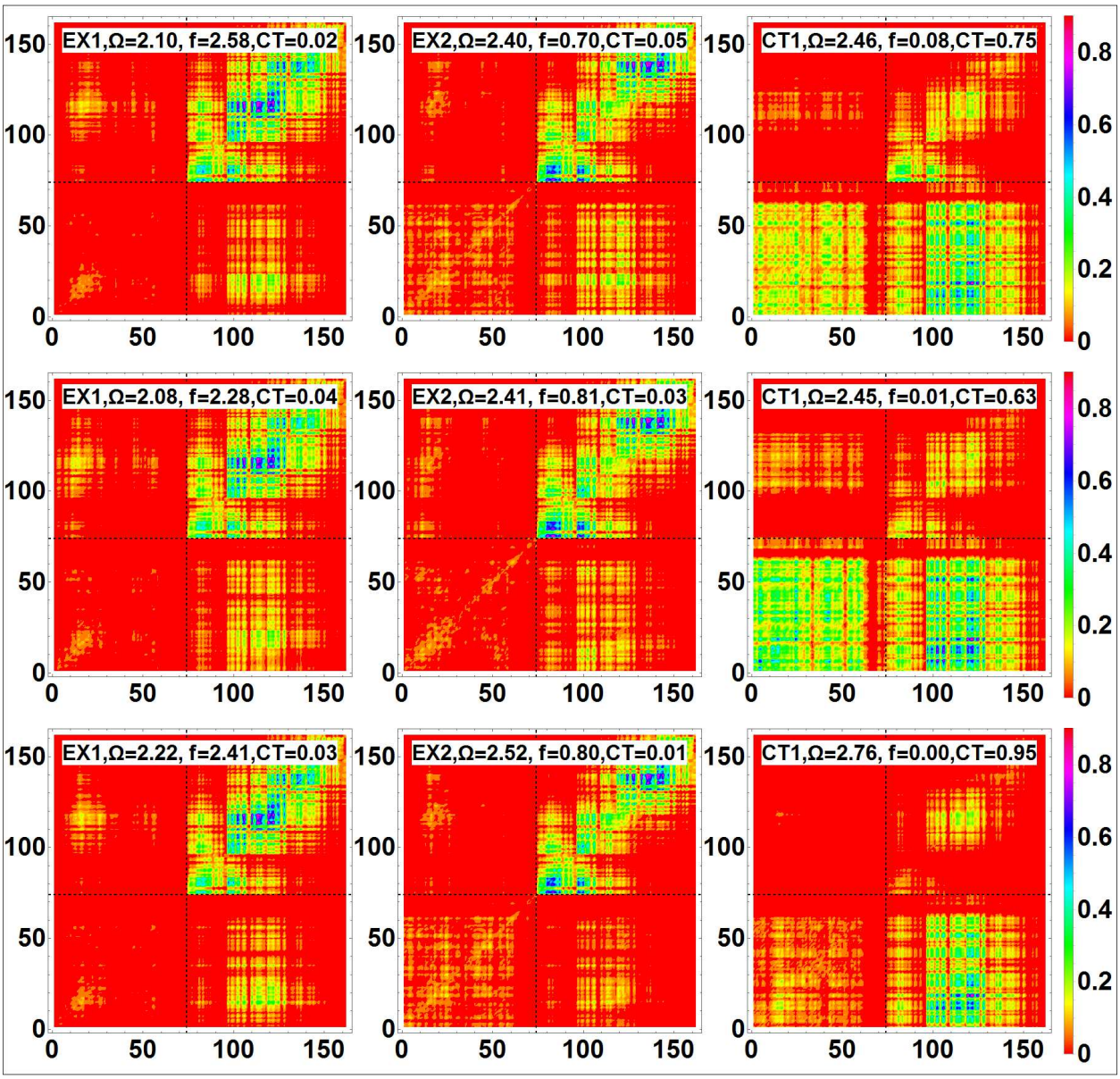

Figure 3.9: The lowest two excited states EX-1,2 and the lowest charge transfer state CT-1 of PCPDTBT: PCBM in vacuo given by contour plots of the transition density matrices from the ground state to excited states, obtained by CAM-B3LYP/GD3/6-31G(d) (top), CAM-B3LYP/GD2/6-31G(d) (middle), ωB97XD/6-31G(d) (bottom). The axis labels represent indices of non-hydrogen atoms from PCBM to PCPDTBT (PCBM: 1-74, PCPDTBT: 75-162). The inset of each plot shows the character of the electronic mode, excitation energy Ω, oscillator strength f, and the CT character.

3.3.2 Electronic Excitations in Solvent

The states of interest, EX-1,2 and CT-1 have been singled out from the simulation in vacuo by examining the excitation nature as well as evaluating the CT character. Here,

www.manaraa.com

the PCPDTBT: PCBM dimer is exposed to the polarizable solvent environment with varied static dielectric constant. In this way, the solvent effect on electronic transitions can be illustrated. Both LR and SS solvation have been performed for all simulations.

The dependence of transition energies for the states of interest of PCPDTBT: PCBM complex on the solvent polarity is shown in Fig. 3.10. Note that the respective ground-state geometries in vacuo have been directly employed in the solution simulation without further optimization in these calculations. Detailed numerical results including excitation energy, oscillator strength, and CT character can be found in Tables A.4, A.5, and A.6 in Appendix A SI. In the low-cost LR simulations, the solvatochromic shift (i.e., the excitation energy difference between gas phase and solution phase) is small, and the solvent polarity has a little to no effect on all excitations. Overall, it is observed that variation in energies due to solvent within 0.01 eV for both excitonic and CT states in all three levels of simulations. Such weak solvent effect can be attributed to the LR approach in which the solvatochromic shift is computed from transition density which tends to be small. More importantly, the CT character of CT-1 state considerably diminishes with respect to the dielectric constant in CAM-B3LYP simulations, whereas the CT character of EX-1,2 states are relatively stable (Fig. 3.12 in SI). Such observation being opposed to physical intuition motivates us to adopt the more reliable SS approach. Here, a very significant decrease in the CT-1 energy (up to 0.4 eV) has been observed in all simulations using the SS solvation approach. In the cases of CAM-B3LYP computation, the CT energy saturates when $\varepsilon_0 \geq 13$, which can be easily found in common polar solvent. In addition, the CT character of CT-1 state increases (0.95 in CAM-B3LYP) compared to the gas phase results (0.6-0.7). As expected, the solvent effects simulated by the SS approach are much less pronounced for the excitonic states EX-1,2 both in excitation energy and in the CT character. Because polar solvent affects the CT and EX states in different ways, a different alignment of energetics is observed. In CAM-B3LYP/GD3 calculation, the CT state, which in gas phase is the third excitation, becomes the second excited state in low polarity case and even becomes the lowest one when $\varepsilon_0 \geq 8$.

www.manaraa.com

In other words, strong polar solvent can stabilize polarizable excitations by much larger solvatochromic shift and can induce a more polarized character to the states. In the case of ωB97XD computations, a similar trend of energy change due to ε_0 is observed, however, the decrease in CT-1 energy (less than 0.3 eV) is less significant than those in CAM-B3LYP calculations. The CT character of both excitonic and CT state are insensitive to the change in ε_0 for both LR and SS approaches.

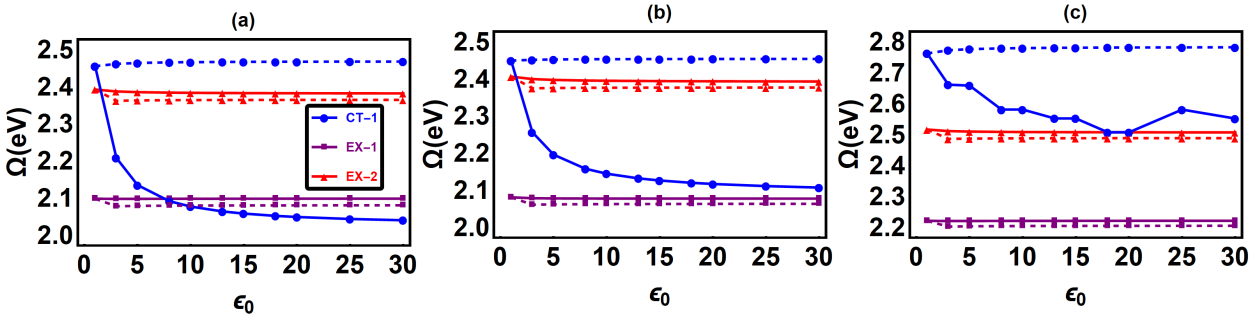

Figure 3.10: Transition energies of states with respect to the dielectric constant of the solvent. Solid and dashed curves represent SS and LR approaches, respectively. Computed at (a) CAM-B3LYP/GD3, (b) CAM-B3LYP/GD2, (c) ωB97XD based on the ground geometries optimized in vacuo.

The noticeable difference in the CTS stabilization between the three computational levels is attributed to the different range-corrected properties taken into account in the functionals. As mentioned in Section (3.2), a higher fraction of orbital exchange included in the ωB97XD functional indicates less delocalized electron effect. Therefore, less CTS stabilization due to the solvent effect is observed as a direct result of weaker CT character in ωB97XD simulation compared to CAM-B3LYP counterparts. In addition, the difference in the dispersion correction results in different dimer configurations, in particular, the distance between the two molecules. The separation between PCPDTBT and PCBM in ωB97XD simulation ($\approx$ 3.12 $\mathring{A}$) is slightly further than those in CAM-B3LYP calculations ($\approx$ 3.09 $\mathring{A}$), whereas the difference in distance between CAM-B3LYP simulations at GD2 and GD3 levels is less than 0.01 $\mathring{A}$. Such observation follows an obvious fact that the intermolecular CTSs are very sensitive to the molecular distance and are less likely to form in the case of larger separation.

www.manaraa.com

3.3.3 Comparison of Excited State Calculations in Solvent Based on *Vacuum* Geometry and *Solvated* Geometry

All results presented above are based on the calculations of geometries optimized in vacuo. Comparison with geometries optimized in solvent with the corresponding dielectric environment is also of interest. For example, the excited states are calculated in solvent ($\varepsilon_0 = 3$) using the geometries optimized in solvent ($\varepsilon_0 = 3$) at the same level of theory.

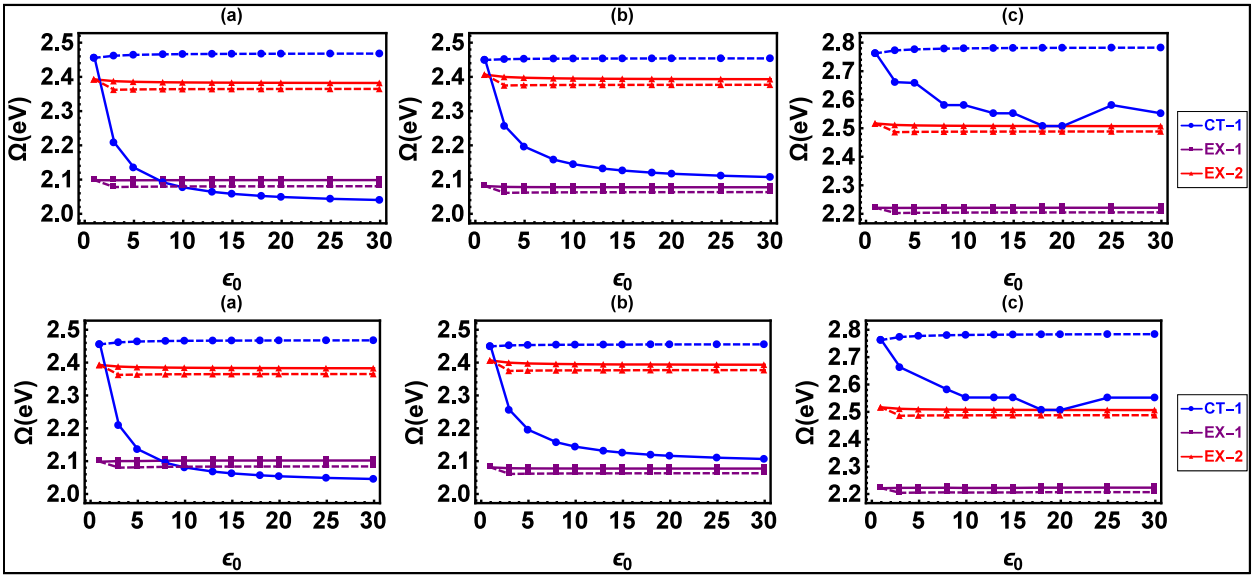

Figure 3.11: Comparison of excited state calculations in solvent based on *vacuum* geometry (1^{st} row) and *solvated* geometry (2^{nd} row). For the solvated calculations, each PCPDTBT: PCBM ground state geometry is optimized in the presence of solvent with the corresponding dielectric constant. Computed at (a) CAM-B3LYP/GD3, (b) CAM-B3LYP/GD2, (c) ωB97XD level of theory.

www.manaraa.com

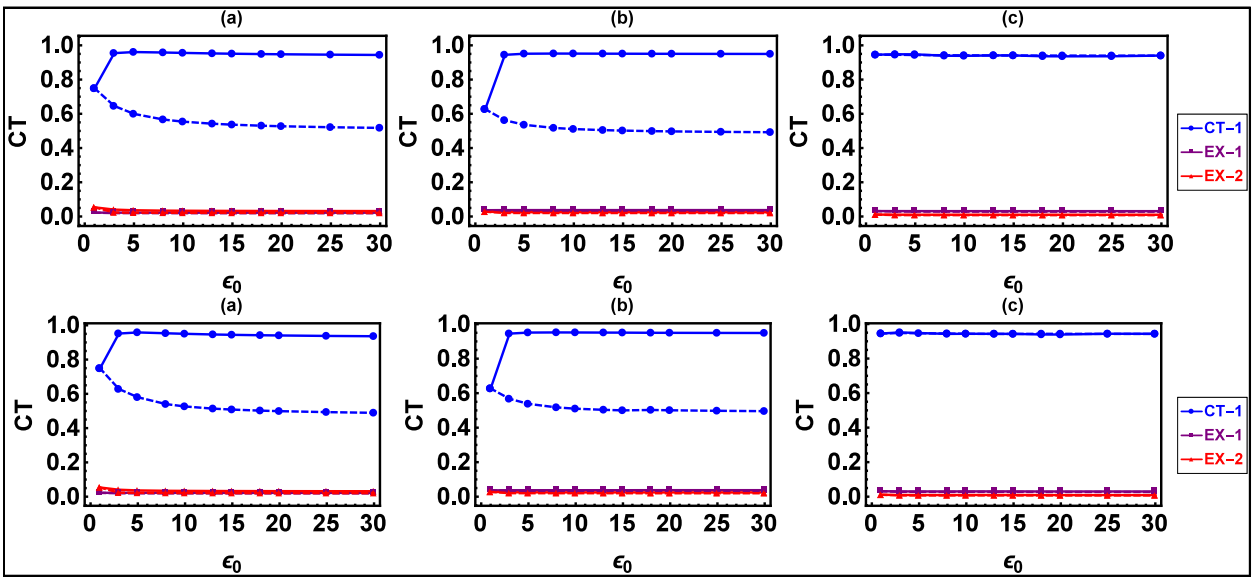

Figure 3.12: CT character of excited states with respect to the dielectric constant of the solvent. Solid and dashed curves represent SS and LR approaches, respectively. Computed at (a) CAM-B3LYP/GD3, (b) CAM-B3LYP/GD2, (c) ωB97XD based on the ground geometries optimized in vacuo (1^{st} row) and in solvent (2^{nd} row).

From Fig. 3.11 and 3.12, no significant difference between the calculation results based on vacuum geometries and solvated geometries can be observed. This phenomenon indicates that further geometrical optimization is not necessary because the molecular configuration is essentially determined by the dispersive interactions and only weakly depends on the solvent.

The high internal quantum efficiency of charge separation is routinely achieved in the devices with PCPDTBT: PCBM mixture. This suggests that CT states are generally energetically favorable compared with the excitonic counterparts. In the simulations, it is observed that CT-1 becomes lower than EX-1 only for a single modeling approach (CAM-B3LYP/GD3) for larger than the experimental value of the dielectric constant. Such observed under-stabilization of CT states is due to multiple effects. The sensitivity of CT state on the dispersion corrections and long-range-corrected model implementation in the DFT functional has been already discussed above. It has been studied that neighboring chromophores also play an important role in the CTS stabilization. The enhanced red-shift of emissive CTS in silsesquioxane derivatives can be interpreted as the strong CT character between chromophores as well as the solvent effect [101]. Such enhanced CTS stabilization

www.manaraa.com

has also been illustrated in the TDDFT simulation of P3HT: C_{60} complex with oligothiophene spacer. Significant energy drop in CTS has been obtained in the BHJ complex spaced by three π-stacking oligomers compared with the counterpart with a single oligomer spacer [21]. Generally, more chromophores result in higher degree of π-electron delocalization and hence possibly stronger CT character, which makes the state more stable in the presence of solvent effect. Considering the heterogeneous distribution of donor and acceptor in real BHJ materials, the CTS stabilization due to the solvent effect observed in the simplified molecular dimer will be enhanced when taking into account the nearby chromophores. In addition, the electric field generated by interfacial charges in BHJ mixture may act similarly as the polar solvent does to further facilitate the formation of CT state by lowering its energy and optimize the overall power conversion efficiency [43]. Finally, vibrational stabilization of polar CT state is larger than neutral EX state, which may further facilitate energetic stabilization and formation of spatially separated polarons.

3.4 Summary

In this work, a TDDFT investigation is conducted to study how the solvent polarity affects the electronic excitations in the representative organic BHJ PCPDTBT: PCBM system simplified as a molecular dimer. Range corrected hybrid functionals CAM-B3LYP and ωB97XD have been used along with the empirical Grimme's models D2 and D3 dispersion corrections to account for weak intermolecular interactions. Two prevalent solvation models, the LR and SS approaches, have been applied and compared. Little to no solvent effect on the solute energetics and CT character have been observed from the results in LR scheme. The solvent effect is more pronounced in the SS simulation which is in line with experimental observations and common physical sense. Specifically, the intermolecular CT state with large polarization is more sensitive to polar solvent than the homogeneous excitations. The excitation energy of such states can be substantially stabilized by the dielectric medium and such effects are well simulated within the SS method. The distance between donor and acceptor molecules, which is similar for CAM-B3LYP/GD3 and CAM-B3LYP/GD2 optimized

www.manaraa.com

geometries but a little longer for ωB97XD optimized structure, also has an impact on the excitation energies and charge transfer properties. Based on the analysis of the NTOs and CT characters, it can be concluded that solvent with a larger dielectric constant can lower the CT energy and aggravate the CT character but has little effect on the excitations with less charge redistribution. It has been found that the optimization of ground state geometries in vacuo can provide similar stabilization effect as the solvated geometries. This can help save a significant amount of computing time.

In summary, the TDDFT method that combines long-range-corrected hybrid functional, dispersion correction, and state-specific solvation model provides an efficient and correct approach to simulate the excited-state electronic structure of organic BHJ systems. The detailed characterization of CTS stabilization due to the polar solvent environment within the TDDFT framework has been demonstrated for the first time on the representative PCPDTBT: PCBM system. The correct electronic energetic ordering and the stabilization of CTS by polar environment are recovered in theoretical calculations. Future works include extending this protocol to study the optical properties of other BHJ systems, which is a highly active research area. These studies and proposed methods can aid in the discovery of innovative and more efficient organic photovoltaic materials.

www.manaraa.com

CHAPTER 4 CONCLUSION AND FUTURE DIRECTIONS

4.1 Conclusion

Extensive research on renewable energy materials has been carried out for decades to answer the growing demands and environmental concerns over the use of fossil fuels. One of the promising candidates is OPV devices, which have multiple advantages with respect to the traditional inorganic devices. However, the power conversion efficiency of this type of emerging solar cell still needs to be improved for it to be able to compete with other conventional energy sources. One of the reasons for the limited performance of OPV cells is the low dielectric constant ($\varepsilon \sim 3-4$). Numerous studies have shown that by increasing the device polarity, the exciton binding energy, charge transfer state energy and recombination loss can be reduced. Thus the free charge carrier generation is improved and better conversion efficiencies can be obtained [19, 20, 60–64]. However, the myth about how the dielectric constant affects the CTSs energy has not been resolved. In this thesis, a representative molecular system, PCPDTBT: PCBM, has been examined computationally.

In Chapter 3, a protocol that combines TDDFT with the polarizable continuum model (PCM) is developed. Using range corrected hybrid functionals CAM-B3LYP and ωB97XD with two solvation models, LR and SS, the electronic properties of a typical lower-band gap polymer: fullerene molecular pair under the influence of polar environment have been studied. It is observed that under the SS approach the CTS, which has characteristic large charge redistribution, could be stabilized with increasing solvent polarity, whereas the EX, which has a limited CT character, is not affected by the change in the surroundings. The calculation results from the LR model show no substantial solvent effect on excited states, regardless of the characters of the transitions. In accordance with the experimental discoveries that the polar solvent can significantly reduce the CTS energy [19, 20], it concludes that a procedure that integrates TDDFT with long-range-corrected hybrid functional CAM-B3LYP, Grimme's empirical dispersion correction D3, and state-specific solvation model can effectively predict the energetics of charge transfer states in OPV materials.

www.manaraa.com

The findings in this thesis can provide valuable insights into the optimization of OPV devices. First, the dielectric constant of the materials has a significant impact on the CTS energy and the charge dissociation efficiency. Second, the calculations of electronic properties of organic semiconductors can be performed effectively and efficiently using the geometries optimized in gas phase since the results with vacuum geometries and solvated geometries reveal negligible differences. Finally, a unified approach is provided to describe the CTS using a detailed analysis of the one-electron TDM. Three tools including CT character, contour plots of TDM in real space, and natural transition orbital can be used to effectively identify and describe the characters of electronic excitations.

4.2 Future Directions

The protocol developed in this manuscript to study the effect of polar environment on the electronic properties of PCPDTBT: PCBM molecular pair can be applied to other BHJ molecular systems as well. New polymers are being synthesized for OPV applications, and non-fullerene molecules are proposed to be effective acceptors. These various combinations of donor: acceptor systems can be studied computationally using the procedure in this thesis together with experiments to obtain a comprehensive apprehension of the material properties. There are also other methods which can be used to address the solvent effect on CTS, such as charge constraint DFT or SRSH functionals combined with PCM. These approaches can be applied and compared with the current scheme in future studies.

The findings of this work have limitations. It only examined the energetics of CTS in polar environment during vertical excitation, but charge dissociation is a dynamic picture, which requires a dynamic simulation. The calculation of energetics of relevant states is only a preliminary step for simulating the charge separation dynamics at the donor: acceptor interface. A real-time (RT) view of the dissociation process can only be obtained by time-domain simulations. Some candidate approaches include QM/MM simulation [17], RT-TDDFT coupled with RT-TDPCM [127–129], and Monte Carlo method [130].

This work studied a polymer with four repeating units coupled with a fullerene molecule

www.manaraa.com

PCBM. However, in real BHJ devices the polymers are not limited to a certain length and the number of molecules cannot be controlled macroscopically, only the ratio of polymer/fullerene can be adjusted. In the active layer of a working OPV cell, the molecular shape, length, relative positions/orientations of the consisting donor and acceptor compounds can all influence the overall performance. Thus a study including more polymer and fullerene molecules, as well as different combinations of the structural configurations is necessary to pursue a thorough understanding of the power conversion process.

Two solvation methods, LR and SS, were applied to account for the dielectric medium in electronic excitation calculations. In the estimation of effective solvent potential, LR only considers the ground-state and transition electron density, whereas SS takes both ground-state and excited-state density into account. There is another intermediate approach referred to as the vertical excitation model (VE). In such a model, the effective solvent potential for the ground-state is determined by ground-state density only, but the electronic transition is described by excited-state density [56]. VE is expected to be more efficient than SS while providing a substantially correct description for the CTS. In future studies, VE should also be employed and compared with LR and SS methods.

The dielectric constant can be divided into static and optical depending on the frequency. The fast partition of the solvent response is determined by the dielectric constant at optical frequency, whereas the slow component depends on both static and optical dielectric constant. The electronic structure was computed in polar medium with varying static dielectric constant while keeping the optical one at $\varepsilon_\infty = 2$. Although the optical relative permittivity can only change in a small range, it is necessary to know how different values of ε_∞ could affect the solvent relaxation time, the equilibrium, and nonequilibrium solvation. However, the current existing quantum chemistry packages might not be able to evaluate these effects. Therefore new methods need to be developed for a thorough research on this area.

Theoretical and computational research acts as a supporting role in the discovery and optimization of novel materials. Theoreticians rely on experimental studies to build the

www.manaraa.com

real devices and verify the calculation results. A collaboration between theoreticians and experimentalists is not only necessary but also beneficial to all parties and the development for better OPV applications. Researchers shall apply the calculation protocol developed in this thesis to more molecular systems, work with experimental groups to obtain the optimal combinations, and push the limit of power conversion efficiency to a higher degree.

www.manaraa.com

APPENDIX A SUPPLEMENTARY INFORMATION

Excited electronic structure calculations are performed with three functional models. In Sec. A.1, the results of the calculations in vacuo are provided. The NTOs for EX-1, 2 are shown in Fig. A.1, A.2, and A.3, the excitation energies and oscillator strengths for the first 15 excited states of PCPDTBT, PCBM, and PCPDTBT: PCBM are included in Table A.1, A.2, and A.3, which correspond to the results calculated with the functional CAM-B3LYP/GD3/6-31G(d), CAM-B3LYP/GD2/6-31G(d), and B97XD/6-31G(d), respectively.

In Sec. A.2, the results of the calculations in solvent based on the geometries optimized in vacuo are provided. Table A.4, A.5, and A.6 correspond to functional CAM-B3LYP/6-31G(d)+GD3, CAMB3LYP/6-31G(d)+GD2, and B97XD/6-31G(d), respectively. In each table, the excitation energy, oscillator strength, and CT character of EX-1, 2, as well as CT-1 in solvent with different polarity are shown with two solvent approaches, namely, LR and SS.

The previous section examines the electronic properties based on vacuum geometries. In Sec. A.3, the results of the calculations in solvent based on solvated geometries are provided. Table A.7, A.8, and A.9 correspond to functional CAM-B3LYP/6-31G(d)+GD3, CAM-B3LYP/6-31G(d)+GD2, and B97XD/6-31G(d), respectively. In each table, the excitation energy, oscillator strength, and CT character of EX-1, 2, as well as CT-1 in solvent with different polarity are shown with two solvent approaches, namely, LR and SS.

www.manaraa.com

A.1 Excited State Calculations in Vacuo

A.1.1 CAM-B3LYP/6-31G(d) with Grimmes D3 Dispersion

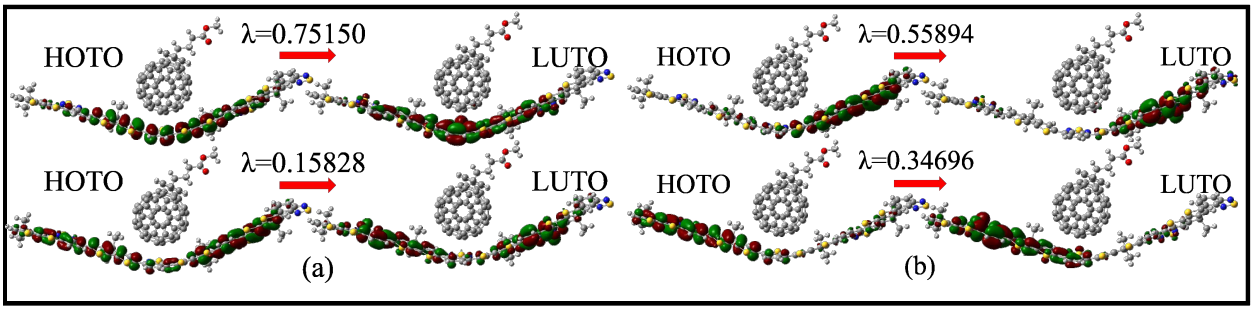

Figure A.1: Natural transition orbitals of (a) EX-1 and (b) EX-2 states, both have two major contributing pairs, λ is the associated eigenvalue which represents the weight of the particle-hole pair contribution to the excitation. The highest occupied transition orbital (HOTO) and the lowest unoccupied transition orbital (LUTO) are labeled.

Table A.1: Excitation energies Ω and oscillator strengths f of PCPDTBT, PCBM, and PCPDTBT: PCBM in vacuo. Charge transfer characters for PCPDTBT: PCBM are listed. D stands for Donor and A for Acceptor, DA-charge transfer from Donor to Acceptor, AD-charge transfer from Acceptor to Donor, DD-charge localization within Donor, AA-charge localization in Acceptor. Computed by CAM-B3LYP/6-31G(d) on the ground state geometry optimized by the same functional with the empirical dispersion correction GD3.

CAM-B3LYP-GD3/6-31G(d) geometry in vacuo										
	PCPDTBT		PCBM		PCPDTBT: PCBM					
mode	$\Omega(eV)$	f	$\Omega(eV)$	f	$\Omega(eV)$	f	DA	AD	DD	AA
1	2.13	3.38	2.49	0.00	2.10	2.58	0.02	0.00	0.97	0.00
2	2.42	0.56	2.52	0.00	2.39	0.70	0.05	0.00	0.94	0.01
3	2.64	0.07	2.59	0.00	2.46	0.08	0.75	0.00	0.08	0.17
4	2.98	0.23	2.62	0.00	2.49	0.03	0.29	0.00	0.03	0.68
5	3.19	0.01	2.75	0.00	2.52	0.06	0.33	0.00	0.11	0.55
6	3.27	0.03	2.79	0.00	2.53	0.06	0.28	0.00	0.14	0.58
7	3.32	0.01	2.85	0.00	2.58	0.13	0.46	0.00	0.48	0.06
8	3.58	0.74	2.91	0.00	2.59	0.00	0.00	0.00	0.00	0.99
9	3.71	0.21	2.94	0.00	2.62	0.00	0.04	0.00	0.01	0.95
10	3.79	0.13	3.03	0.00	2.74	0.00	0.15	0.00	0.06	0.79
11	3.83	0.05	3.06	0.00	2.75	0.00	0.56	0.00	0.20	0.24
12	3.89	0.03	3.07	0.00	2.79	0.00	0.03	0.01	0.00	0.96
13	3.94	0.01	3.16	0.00	2.84	0.00	0.01	0.01	0.00	0.99
14	3.99	0.04	3.22	0.00	2.88	0.00	0.02	0.01	0.01	0.97
15	4.03	0.02	3.26	0.01	2.92	0.00	0.01	0.01	0.00	0.98

www.manaraa.com

A.1.2 CAM-B3LYP/6-31G(d) with Grimmes D2 Dispersion

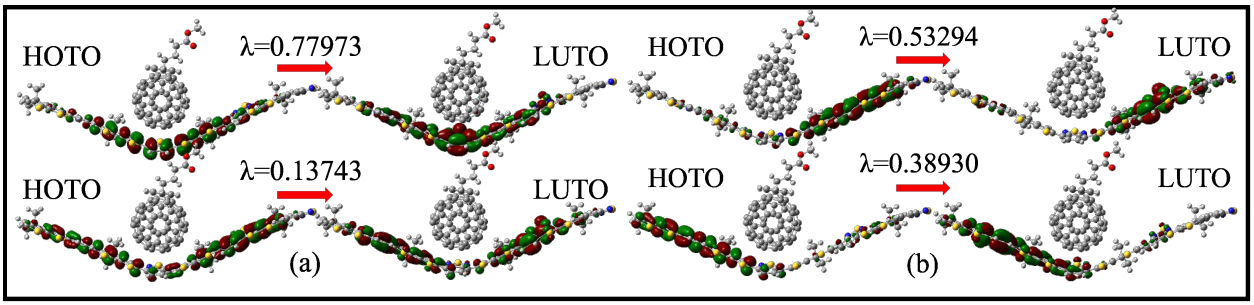

Figure A.2: Natural transition orbitals of (a) EX-1 and (b) EX-2 states, both have two major contributing pairs, λ is the associated eigenvalue which represents the weight of the particle-hole pair contribution to the excitation. The highest occupied transition orbital (HOTO) and the lowest unoccupied transition orbital (LUTO) are labeled.

Table A.2: Excitation energies Ω and oscillator strengths f of PCPDTBT, PCBM, and PCPDTBT: PCBM in vacuo. Charge transfer characters for PCPDTBT: PCBM are listed. Computed by CAM-B3LYP/6-31G(d) on the ground state geometry optimized by the same functional with the empirical dispersion correction GD2.

CAM-B3LYP-GD2/6-31G(d) in vacuo										
	PCPDTBT		PCBM		PCPDTBT: PCBM					
mode	$\Omega(eV)$	f	$\Omega(eV)$	f	$\Omega(eV)$	f	DA	AD	DD	AA
1	2.15	3.39	2.48	0.00	2.08	2.28	0.037	0.00	0.96	0.00
2	2.43	0.54	2.51	0.00	2.41	0.81	0.028	0.00	0.97	0.00
3	2.65	0.06	2.59	0.00	2.45	0.013	0.63	0.00	0.02	0.35
4	2.99	0.23	2.61	0.00	2.48	0.04	0.23	0.01	0.03	0.74
5	3.21	0.01	2.74	0.00	2.51	0.08	0.17	0.00	0.09	0.74
6	3.28	0.03	2.78	0.00	2.53	0.14	0.60	0.00	0.20	0.19
7	3.33	0.02	2.85	0.00	2.58	0.00	0.01	0.01	0.00	0.99
8	3.60	0.77	2.89	0.00	2.59	0.08	0.15	0.00	0.30	0.55
9	3.72	0.20	2.93	0.00	2.61	0.05	0.29	0.00	0.26	0.44
10	3.81	0.13	3.02	0.00	2.70	0.03	0.74	0.00	0.20	0.06
11	3.85	0.04	3.05	0.00	2.74	0.00	0.01	0.01	0.00	0.98
12	3.91	0.03	3.06	0.00	2.78	0.00	0.03	0.01	0.00	0.95
13	3.95	0.01	3.15	0.00	2.83	0.00	0.02	0.01	0.00	0.97
14	4.00	0.03	3.21	0.00	2.87	0.00	0.02	0.01	0.01	0.96
15	4.04	0.02	3.24	0.01	2.91	0.00	0.02	0.01	0.00	0.97

www.manaraa.com

A.1.3 ωB97XD/6-31G(d)

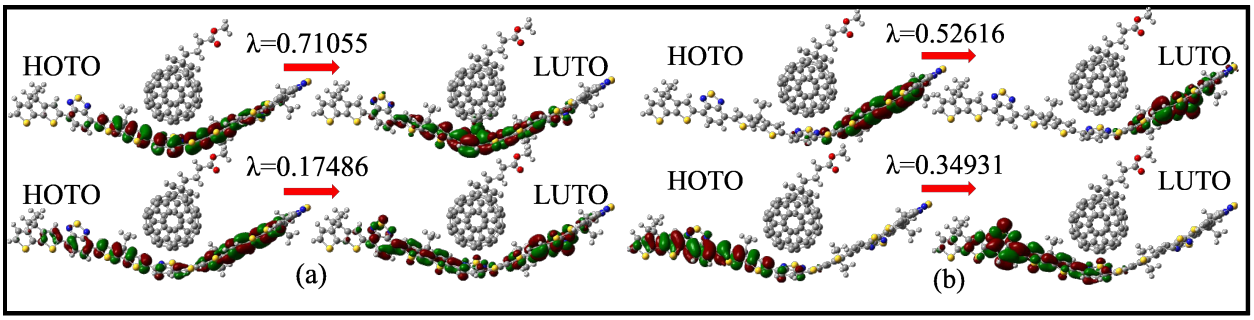

Figure A.3: Natural transition orbitals of (a) EX-1 and (b) EX-2 states, both have two major contributing pairs, λ is the associated eigenvalue which represents the weight of the particle-hole pair contribution to the excitation. The highest occupied transition orbital (HOTO) and the lowest unoccupied transition orbital (LUTO) are labeled.

Table A.3: Excitation energies Ω and oscillator strengths f of PCPDTBT, PCBM, and PCPDTBT: PCBM in vacuo. Charge transfer characters for PCPDTBT: PCBM are listed. Computed by ωB97XD/6-31G(d) on the ground state geometry optimized by the same functional.

ωB97XD/6-31G(d) in vacuo										
	PCPDTBT		PCBM		PCPDTBT: PCBM					
mode	$\Omega(eV)$	f	$\Omega(eV)$	f	$\Omega(eV)$	f	DA	AD	DD	AA
1	2.29	3.38	2.56	0.00	2.22	2.41	0.03	0.00	0.97	0.00
2	2.56	0.57	2.59	0.00	2.52	0.80	0.01	0.00	0.98	0.01
3	2.77	0.08	2.66	0.00	2.56	0.02	0.01	0.00	0.01	0.98
4	3.13	0.24	2.69	0.00	2.58	0.00	0.01	0.00	0.00	0.99
5	3.44	0.01	2.82	0.00	2.66	0.00	0.00	0.00	0.00	0.99
6	3.53	0.13	2.86	0.00	2.67	0.36	0.16	0.00	0.81	0.02
7	3.61	0.07	2.93	0.00	2.68	0.00	0.00	0.00	0.01	0.98
8	3.74	0.74	2.98	0.00	2.76	0.00	0.95	0.00	0.02	0.03
9	3.88	0.17	3.00	0.00	2.81	0.00	0.01	0.01	0.00	0.99
10	4.04	0.02	3.09	0.00	2.85	0.00	0.05	0.01	0.01	0.94
11	4.18	0.02	3.15	0.00	2.89	0.01	0.79	0.00	0.11	0.11
12	4.34	0.00	3.16	0.00	2.92	0.00	0.01	0.01	0.00	0.98
13	4.44	0.02	3.25	0.00	2.94	0.00	0.07	0.01	0.00	0.92
14	4.49	0.03	3.30	0.00	2.98	0.00	0.08	0.01	0.01	0.90
15	4.52	0.05	3.32	0.01	3.01	0.01	0.77	0.00	0.11	0.12

www.manaraa.com

A.2 Excited State Calculations in Solvent Based on *Vacuum* Geometries

A.2.1 CAM-B3LYP/6-31G(d) with Grimmes D3 Dispersion

Table A.4: Excitation energies Ω, oscillator strengths f, and CT characters of the molecular pair of PCPDTBT: PCBM in solvent with varying static dielectric constant, ε. Three modes are of the main concern, including the first two excitonic states (EX-1,2) and the charge transfer state (CT-1). Computed by CAM-B3LYP/6-31G(d) using the LR and the SS approaches on the *vacuum* geometry optimized by the same functional with the empirical dispersion correction GD3.

CAM-B3LYP-GD3/6-31G(d) PCPDTBT: PCBM in solvent with *vacuum* geometry													
		LR						SS					
ε_0	mode	$\Omega(eV)$	f	DA	AD	DD	AA	$\Omega(eV)$	f	DA	AD	DD	AA
1	EX-1	2.10	2.58	0.02	0.00	0.97	0.00	2.10	2.58	0.02	0.00	0.97	0.00
	EX-2	2.39	0.70	0.05	0.00	0.94	0.01	2.39	0.70	0.05	0.00	0.94	0.01
	CT-1	2.46	0.08	0.75	0.00	0.08	0.17	2.46	0.08	0.75	0.00	0.08	0.17
3	EX-1	2.08	2.72	0.02	0.00	0.98	0.00	2.10	2.57	0.02	0.00	0.97	0.00
	EX-2	2.36	0.81	0.02	0.00	0.97	0.00	2.39	0.70	0.04	0.00	0.95	0.01
	CT-1	2.46	0.08	0.65	0.00	0.08	0.28	2.21	0.05	0.95	0.00	0.03	0.01
5	EX-1	2.08	2.73	0.02	0.00	0.98	0.00	2.10	2.57	0.02	0.00	0.97	0.00
	EX-2	2.36	0.81	0.02	0.00	0.97	0.00	2.39	0.70	0.04	0.00	0.96	0.01
	CT-1	2.46	0.08	0.60	0.00	0.08	0.32	2.14	0.07	0.96	0.00	0.03	0.01
8	EX-1	2.08	2.73	0.02	0.00	0.98	0.00	2.10	2.56	0.02	0.00	0.97	0.00
	EX-2	2.36	0.81	0.02	0.00	0.97	0.00	2.38	0.70	0.03	0.00	0.96	0.01
	CT-1	2.47	0.08	0.57	0.00	0.08	0.36	2.09	0.09	0.96	0.00	0.03	0.01
10	EX-1	2.08	2.73	0.02	0.00	0.98	0.00	2.10	2.56	0.02	0.00	0.97	0.00
	EX-2	2.36	0.81	0.02	0.00	0.97	0.00	2.38	0.70	0.03	0.00	0.96	0.01
	CT-1	2.47	0.08	0.55	0.00	0.08	0.37	2.08	0.10	0.96	0.00	0.04	0.01
13	EX-1	2.08	2.73	0.02	0.00	0.98	0.00	2.10	2.56	0.02	0.00	0.97	0.00
	EX-2	2.36	0.81	0.02	0.00	0.97	0.00	2.38	0.70	0.03	0.00	0.96	0.01
	CT-1	2.47	0.08	0.54	0.00	0.08	0.38	2.06	0.11	0.95	0.00	0.04	0.01
15	EX-1	2.08	2.73	0.02	0.00	0.98	0.00	2.10	2.56	0.02	0.00	0.97	0.00
	EX-2	2.36	0.81	0.02	0.00	0.97	0.00	2.38	0.70	0.03	0.00	0.96	0.01
	CT-1	2.47	0.08	0.54	0.00	0.08	0.39	2.06	0.12	0.95	0.00	0.04	0.01
18	EX-1	2.08	2.73	0.02	0.00	0.98	0.00	2.10	2.56	0.02	0.00	0.97	0.00
	EX-2	2.36	0.81	0.02	0.00	0.97	0.00	2.38	0.70	0.03	0.00	0.96	0.01
	CT-1	2.47	0.08	0.53	0.00	0.08	0.39	2.05	0.12	0.95	0.00	0.04	0.01
20	EX-1	2.08	2.73	0.02	0.00	0.00	0.00	2.10	2.56	0.02	0.00	0.97	0.00
	EX-2	2.36	0.81	0.02	0.00	0.00	0.00	2.38	0.70	0.03	0.00	0.96	0.01
	CT-1	2.47	0.08	0.53	0.00	0.00	0.40	2.05	0.13	0.95	0.00	0.04	0.01
25	EX-1	2.08	2.73	0.02	0.00	0.98	0.00	2.10	2.56	0.02	0.00	0.97	0.00
	EX-2	2.36	0.81	0.02	0.00	0.97	0.00	2.38	0.70	0.03	0.00	0.96	0.01
	CT-1	2.47	0.08	0.52	0.00	0.08	0.40	2.04	0.14	0.95	0.00	0.05	0.01
30	EX-1	2.08	2.73	0.02	0.00	0.98	0.00	2.10	2.56	0.02	0.00	0.97	0.00
	EX-2	2.36	0.81	0.02	0.00	0.97	0.00	2.38	0.70	0.03	0.00	0.96	0.01
	CT-1	2.47	0.08	0.52	0.00	0.08	0.41	2.04	0.14	0.94	0.00	0.05	0.01

www.manaraa.com

A.2.2 CAM-B3LYP/6-31G(d) with Grimmes D2 Dispersion

Table A.5: Excitation energies Ω, oscillator strengths f, and CT characters of the molecular pair of PCPDTBT: PCBM in solvent with varying static dielectric constant, ε. Computed by CAM-B3LYP/6-31G(d) using the LR and the SS approaches on the *vacuum* geometry optimized by the same functional with the empirical dispersion correction GD2.

CAM-B3LYP-GD2/6-31G(d) PCPDTBT: PCBM in solvent with *vacuum* geometry													
		LR						SS					
ε_0	mode	$\Omega(eV)$	f	DA	AD	DD	AA	$\Omega(eV)$	f	DA	AD	DD	AA
1	EX-1	2.08	2.28	0.04	0.00	0.96	0.00	2.08	2.28	0.04	0.00	0.96	0.00
	EX-2	2.41	0.81	0.03	0.00	0.97	0.00	2.41	0.81	0.03	0.00	0.97	0.00
	CT-1	2.45	0.01	0.63	0.00	0.02	0.35	2.45	0.01	0.63	0.00	0.02	0.35
3	EX-1	2.06	2.41	0.03	0.00	0.96	0.00	2.08	2.26	0.04	0.00	0.96	0.00
	EX-2	2.37	0.91	0.02	0.00	0.98	0.00	2.40	0.81	0.03	0.00	0.97	0.00
	CT-1	2.45	0.01	0.56	0.00	0.02	0.42	2.26	0.04	0.94	0.00	0.02	0.03
5	EX-1	2.06	2.41	0.03	0.00	0.96	0.00	2.08	2.26	0.04	0.00	0.96	0.00
	EX-2	2.38	0.91	0.02	0.00	0.98	0.00	2.40	0.80	0.03	0.00	0.97	0.00
	CT-1	2.45	0.01	0.54	0.00	0.01	0.45	2.20	0.05	0.95	0.00	0.02	0.03
8	EX-1	2.06	2.42	0.03	0.00	0.96	0.00	2.08	2.25	0.04	0.00	0.96	0.00
	EX-2	2.38	0.92	0.02	0.00	0.98	0.00	2.40	0.80	0.02	0.00	0.97	0.00
	CT-1	2.45	0.01	0.52	0.00	0.01	0.47	2.16	0.06	0.95	0.00	0.03	0.02
10	EX-1	2.06	2.42	0.03	0.00	0.96	0.00	2.08	2.25	0.04	0.00	0.96	0.00
	EX-2	2.38	0.92	0.02	0.00	0.98	0.00	2.40	0.80	0.02	0.00	0.97	0.00
	CT-1	2.45	0.01	0.51	0.00	0.01	0.47	2.14	0.07	0.95	0.00	0.03	0.02
13	EX-1	2.06	2.42	0.03	0.00	0.96	0.00	2.08	2.25	0.04	0.00	0.96	0.00
	EX-2	2.38	0.92	0.02	0.00	0.98	0.00	2.39	0.80	0.02	0.00	0.97	0.00
	CT-1	2.45	0.01	0.50	0.00	0.01	0.48	2.13	0.07	0.95	0.00	0.03	0.02
15	EX-1	2.06	2.42	0.03	0.00	0.96	0.00	2.08	2.25	0.04	0.00	0.96	0.00
	EX-2	2.38	0.92	0.02	0.00	0.98	0.00	2.39	0.80	0.02	0.00	0.97	0.00
	CT-1	2.45	0.01	0.50	0.00	0.01	0.48	2.13	0.07	0.95	0.00	0.03	0.02
18	EX-1	2.06	2.42	0.03	0.00	0.96	0.00	2.08	2.25	0.04	0.00	0.96	0.00
	EX-2	2.38	0.92	0.02	0.00	0.98	0.00	2.39	0.80	0.02	0.00	0.97	0.00
	CT-1	2.45	0.01	0.50	0.00	0.01	0.49	2.12	0.08	0.95	0.00	0.03	0.02
20	EX-1	2.06	2.42	0.03	0.00	0.96	0.00	2.08	2.25	0.04	0.00	0.96	0.00
	EX-2	2.38	0.92	0.02	0.00	0.98	0.00	2.39	0.80	0.02	0.00	0.97	0.00
	CT-1	2.45	0.01	0.50	0.00	0.01	0.49	2.12	0.08	0.95	0.00	0.03	0.02
25	EX-1	2.06	2.42	0.03	0.00	0.96	0.00	2.08	2.25	0.04	0.00	0.96	0.00
	EX-2	2.38	0.92	0.02	0.00	0.98	0.00	2.39	0.80	0.02	0.00	0.97	0.00
	CT-1	2.45	0.01	0.49	0.00	0.01	0.49	2.11	0.08	0.95	0.00	0.03	0.02
30	EX-1	2.06	2.42	0.03	0.00	0.96	0.00	2.08	2.25	0.04	0.00	0.96	0.00
	EX-2	2.38	0.92	0.02	0.00	0.98	0.00	2.39	0.80	0.02	0.00	0.97	0.00
	CT-1	2.45	0.01	0.49	0.00	0.01	0.49	2.11	0.08	0.95	0.00	0.03	0.02

www.manaraa.com

A.2.3 ωB97XD/6-31G(d)

Table A.6: Excitation energies Ω, oscillator strengths f, and CT characters of the molecular pair of PCPDTBT: PCBM in solvent with varying static dielectric constant, ε. Computed by ωB97XD/6-31G(d) using the LR and the SS approaches on the *vacuum* geometry optimized by the same functional.

ωB97XD/6-31G(d) PCPDTBT: PCBM in solvent with *vacuum* geometry													
		LR						SS					
ε_0	mode	$\Omega(eV)$	f	DA	AD	DD	AA	$\Omega(eV)$	f	DA	AD	DD	AA
1	EX-1	2.22	2.41	0.03	0.00	0.97	0.00	2.22	2.41	0.03	0.00	0.97	0.00
	EX-2	2.52	0.80	0.01	0.00	0.98	0.01	2.52	0.80	0.01	0.00	0.98	0.01
	CT-1	2.76	0.00	0.95	0.00	0.02	0.03	2.76	0.00	0.95	0.00	0.02	0.03
3	EX-1	2.20	2.55	0.03	0.00	0.97	0.00	2.22	2.40	0.03	0.00	0.97	0.00
	EX-2	2.49	0.90	0.01	0.00	0.99	0.00	2.51	0.79	0.01	0.00	0.98	0.01
	CT-1	2.77	0.00	0.94	0.00	0.02	0.03	2.66	0.00	0.95	0.00	0.02	0.03
5	EX-1	2.20	2.55	0.03	0.00	0.97	0.00	2.22	2.40	0.03	0.00	0.97	0.00
	EX-2	2.49	0.90	0.01	0.00	0.99	0.00	2.51	0.79	0.01	0.00	0.98	0.01
	CT-1	2.78	0.00	0.94	0.00	0.02	0.04	2.66	0.00	0.95	0.00	0.03	0.03
8	EX-1	2.20	2.56	0.03	0.00	0.97	0.00	2.22	2.40	0.03	0.00	0.97	0.00
	EX-2	2.49	0.90	0.01	0.00	0.99	0.00	2.51	0.79	0.01	0.00	0.98	0.01
	CT-1	2.78	0.00	0.94	0.00	0.02	0.04	2.58	0.00	0.94	0.00	0.02	0.04
10	EX-1	2.20	2.56	0.03	0.00	0.97	0.00	2.22	2.40	0.03	0.00	0.97	0.00
	EX-2	2.49	0.90	0.01	0.00	0.99	0.00	2.51	0.79	0.01	0.00	0.98	0.01
	CT-1	2.78	0.00	0.94	0.00	0.02	0.04	2.58	0.00	0.94	0.00	0.02	0.04
13	EX-1	2.20	2.56	0.03	0.00	0.97	0.00	2.22	2.40	0.03	0.00	0.97	0.00
	EX-2	2.49	0.90	0.01	0.00	0.99	0.00	2.51	0.79	0.01	0.00	0.98	0.01
	CT-1	2.78	0.00	0.94	0.00	0.02	0.04	2.55	0.00	0.94	0.00	0.02	0.04
15	EX-1	2.20	2.56	0.03	0.00	0.97	0.00	2.22	2.40	0.03	0.00	0.97	0.00
	EX-2	2.49	0.90	0.01	0.00	0.99	0.00	2.51	0.79	0.01	0.00	0.98	0.01
	CT-1	2.78	0.00	0.94	0.00	0.02	0.04	2.55	0.00	0.94	0.00	0.02	0.04
18	EX-1	2.20	2.56	0.03	0.00	0.97	0.00	2.22	2.40	0.03	0.00	0.97	0.00
	EX-2	2.49	0.90	0.01	0.00	0.99	0.00	2.50	0.79	0.01	0.00	0.98	0.01
	CT-1	2.78	0.00	0.94	0.00	0.02	0.04	2.50	0.00	0.94	0.00	0.02	0.04
20	EX-1	2.20	2.56	0.03	0.00	0.97	0.00	2.22	2.40	0.03	0.00	0.97	0.00
	EX-2	2.49	0.90	0.01	0.00	0.99	0.00	2.50	0.79	0.01	0.00	0.98	0.01
	CT-1	2.78	0.00	0.94	0.00	0.02	0.04	2.50	0.00	0.94	0.00	0.02	0.04
25	EX-1	2.21	2.56	0.03	0.00	0.97	0.00	2.22	2.40	0.03	0.00	0.97	0.00
	EX-2	2.49	0.90	0.01	0.00	0.99	0.00	2.50	0.79	0.01	0.00	0.98	0.01
	CT-1	2.78	0.00	0.94	0.00	0.02	0.04	2.58	0.00	0.94	0.00	0.02	0.04
30	EX-1	2.21	2.56	0.03	0.00	0.97	0.00	2.22	2.40	0.03	0.00	0.97	0.00
	EX-2	2.49	0.90	0.01	0.00	0.99	0.00	2.50	0.79	0.01	0.00	0.98	0.01
	CT-1	2.78	0.00	0.94	0.00	0.02	0.04	2.55	0.00	0.94	0.00	0.02	0.04

www.manaraa.com

A.3 Excited State Calculations in Solvent Based on *Solvated* Geometries

A.3.1 CAM-B3LYP/6-31G(d) with Grimmes D3 Dispersion

Table A.7: Excitation energies Ω, oscillator strengths f, and CT characters of PCPDTBT:PCBM in solvent with varying dielectric constant, ε. The first two excitonic states (EX-1,2) and the charge transfer state (CT-1) are of the main concern. Computed by CAM-B3LYP/6-31G(d) using the LR and the SS approaches on the *solvated* geometry optimized by the same functional with the empirical dispersion correction GD3.

CAM-B3LYP-GD3/6-31G(d) PCPDTBT: PCBM in solvent with *solvated* geometry													
		LR						SS					
ε_0	mode	$\Omega(eV)$	f	DA	AD	DD	AA	$\Omega(eV)$	f	DA	AD	DD	AA
1	EX-1	2.10	2.58	0.02	0.00	0.97	0.00	2.10	2.58	0.02	0.00	0.97	0.00
	EX-2	2.39	0.70	0.05	0.00	0.94	0.01	2.39	0.70	0.05	0.00	0.94	0.01
	CT-1	2.46	0.08	0.75	0.00	0.08	0.17	2.46	0.08	0.75	0.00	0.08	0.17
3	EX-1	2.08	2.72	0.02	0.00	0.98	0.00	2.10	2.58	0.02	0.00	0.97	0.00
	EX-2	2.36	0.81	0.02	0.00	0.97	0.00	2.39	0.69	0.04	0.00	0.95	0.01
	CT-1	2.46	0.08	0.63	0.00	0.08	0.29	2.21	0.06	0.95	0.00	0.03	0.01
5	EX-1	2.08	2.73	0.02	0.00	0.98	0.00	2.10	2.58	0.02	0.00	0.97	0.00
	EX-2	2.36	0.81	0.02	0.00	0.97	0.00	2.39	0.69	0.04	0.00	0.96	0.01
	CT-1	2.46	0.08	0.58	0.00	0.08	0.34	2.14	0.08	0.96	0.00	0.03	0.01
8	EX-1	2.08	2.73	0.02	0.00	0.98	0.00	2.10	2.59	0.02	0.00	0.97	0.00
	EX-2	2.36	0.81	0.02	0.00	0.97	0.00	2.38	0.68	0.03	0.00	0.96	0.01
	CT-1	2.47	0.08	0.54	0.00	0.08	0.38	2.09	0.10	0.95	0.00	0.04	0.01
10	EX-1	2.08	2.73	0.02	0.00	0.98	0.00	2.10	2.59	0.02	0.00	0.97	0.00
	EX-2	2.36	0.81	0.02	0.00	0.97	0.00	2.38	0.68	0.03	0.00	0.96	0.01
	CT-1	2.47	0.08	0.53	0.00	0.08	0.39	2.08	0.12	0.95	0.00	0.04	0.01
13	EX-1	2.08	2.73	0.02	0.00	0.98	0.00	2.10	2.59	0.02	0.00	0.97	0.00
	EX-2	2.36	0.81	0.02	0.00	0.97	0.00	2.38	0.68	0.03	0.00	0.96	0.01
	CT-1	2.47	0.08	0.51	0.00	0.08	0.41	2.07	0.13	0.95	0.00	0.05	0.01
15	EX-1	2.08	2.73	0.02	0.00	0.98	0.00	2.10	2.59	0.02	0.00	0.97	0.00
	EX-2	2.36	0.81	0.02	0.00	0.97	0.00	2.38	0.68	0.03	0.00	0.96	0.01
	CT-1	2.47	0.08	0.51	0.00	0.08	0.41	2.06	0.14	0.94	0.00	0.05	0.01
18	EX-1	2.08	2.73	0.02	0.00	0.98	0.00	2.10	2.59	0.02	0.00	0.97	0.00
	EX-2	2.37	0.81	0.02	0.00	0.97	0.00	2.38	0.68	0.03	0.00	0.96	0.01
	CT-1	2.47	0.08	0.50	0.00	0.08	0.42	2.06	0.15	0.94	0.00	0.05	0.01
20	EX-1	2.08	2.73	0.02	0.00	0.98	0.00	2.10	2.59	0.02	0.00	0.97	0.00
	EX-2	2.37	0.81	0.02	0.00	0.97	0.00	2.38	0.68	0.03	0.00	0.96	0.01
	CT-1	2.47	0.08	0.50	0.00	0.08	0.42	2.05	0.15	0.94	0.00	0.05	0.01
25	EX-1	2.08	2.73	0.02	0.00	0.98	0.00	2.10	2.59	0.02	0.00	0.97	0.00
	EX-2	2.37	0.81	0.02	0.00	0.97	0.00	2.38	0.68	0.03	0.00	0.96	0.01
	CT-1	2.47	0.08	0.49	0.00	0.08	0.43	2.05	0.16	0.94	0.00	0.05	0.01
30	EX-1	2.08	2.73	0.02	0.00	0.98	0.00	2.10	2.59	0.02	0.00	0.97	0.00
	EX-2	2.37	0.81	0.02	0.00	0.97	0.00	2.38	0.68	0.03	0.00	0.96	0.01
	CT-1	2.47	0.08	0.49	0.00	0.08	0.43	2.05	0.17	0.94	0.00	0.06	0.01

www.manaraa.com

A.3.2 CAM-B3LYP/6-31G(d) with Grimmes D2 Dispersion

Table A.8: Excitation energies Ω, oscillator strengths f, and CT characters of the molecular pair of PCPDTBT: PCBM in solvent with varying static dielectric constant, ε. Computed by CAM-B3LYP/6-31G(d) using the LR and the SS approaches on the *solvated* geometry optimized by the same functional with the empirical dispersion correction GD2.

CAM-B3LYP-GD2/6-31G(d) PCPDTBT: PCBM in solvent with *solvated* geometry													
		LR						SS					
ε_0	mode	$\Omega(eV)$	f	DA	AD	DD	AA	$\Omega(eV)$	f	DA	AD	DD	AA
1	EX-1	2.08	2.28	0.04	0.00	0.96	0.00	2.08	2.28	0.04	0.00	0.96	0.00
	EX-2	2.41	0.81	0.03	0.00	0.97	0.00	2.41	0.81	0.03	0.00	0.97	0.00
	CT-1	2.45	0.01	0.63	0.00	0.02	0.35	2.45	0.01	0.63	0.00	0.02	0.35
3	EX-1	2.06	2.42	0.03	0.00	0.96	0.00	2.08	2.27	0.04	0.00	0.96	0.00
	EX-2	2.37	0.91	0.02	0.00	0.98	0.00	2.40	0.80	0.03	0.00	0.97	0.00
	CT-1	2.45	0.01	0.57	0.00	0.02	0.41	2.26	0.05	0.95	0.00	0.02	0.03
5	EX-1	2.06	2.42	0.03	0.00	0.96	0.00	2.08	2.27	0.04	0.00	0.96	0.00
	EX-2	2.38	0.91	0.02	0.00	0.98	0.00	2.40	0.80	0.03	0.00	0.97	0.00
	CT-1	2.45	0.01	0.54	0.00	0.02	0.44	2.20	0.06	0.95	0.00	0.02	0.02
8	EX-1	2.06	2.43	0.03	0.00	0.96	0.00	2.08	2.26	0.04	0.00	0.96	0.00
	EX-2	2.38	0.91	0.02	0.00	0.98	0.00	2.40	0.79	0.02	0.00	0.97	0.00
	CT-1	2.45	0.01	0.52	0.00	0.01	0.47	2.16	0.07	0.95	0.00	0.03	0.02
10	EX-1	2.06	2.43	0.03	0.00	0.96	0.00	2.08	2.26	0.04	0.00	0.96	0.00
	EX-2	2.38	0.91	0.02	0.00	0.98	0.00	2.40	0.79	0.02	0.00	0.97	0.00
	CT-1	2.45	0.01	0.51	0.00	0.01	0.47	2.14	0.07	0.95	0.00	0.03	0.02
13	EX-1	2.06	2.43	0.03	0.00	0.96	0.00	2.08	2.26	0.04	0.00	0.96	0.00
	EX-2	2.38	0.91	0.02	0.00	0.98	0.00	2.39	0.79	0.02	0.00	0.97	0.00
	CT-1	2.45	0.01	0.50	0.00	0.01	0.48	2.13	0.07	0.95	0.00	0.03	0.02
15	EX-1	2.06	2.43	0.03	0.00	0.96	0.00	2.08	2.26	0.04	0.00	0.96	0.00
	EX-2	2.38	0.91	0.02	0.00	0.98	0.00	2.39	0.79	0.02	0.00	0.97	0.00
	CT-1	2.45	0.01	0.50	0.00	0.01	0.48	2.13	0.08	0.95	0.00	0.03	0.02
18	EX-1	2.06	2.43	0.03	0.00	0.96	0.00	2.08	2.26	0.04	0.00	0.96	0.00
	EX-2	2.38	0.90	0.02	0.00	0.98	0.00	2.39	0.79	0.02	0.00	0.97	0.00
	CT-1	2.46	0.01	0.50	0.00	0.01	0.48	2.12	0.08	0.95	0.00	0.03	0.02
20	EX-1	2.06	2.43	0.03	0.00	0.96	0.00	2.08	2.26	0.04	0.00	0.96	0.00
	EX-2	2.38	0.90	0.02	0.00	0.98	0.00	2.39	0.79	0.02	0.00	0.97	0.00
	CT-1	2.46	0.01	0.50	0.00	0.01	0.48	2.12	0.08	0.95	0.00	0.03	0.02
25	EX-1	2.06	2.43	0.03	0.00	0.96	0.00	2.08	2.26	0.04	0.00	0.96	0.00
	EX-2	2.38	0.90	0.02	0.00	0.98	0.00	2.39	0.79	0.02	0.00	0.97	0.00
	CT-1	2.46	0.01	0.50	0.00	0.01	0.49	2.11	0.09	0.95	0.00	0.03	0.02
30	EX-1	2.06	2.43	0.03	0.00	0.96	0.00	2.08	2.26	0.04	0.00	0.96	0.00
	EX-2	2.38	0.90	0.02	0.00	0.98	0.00	2.39	0.79	0.02	0.00	0.97	0.00
	CT-1	2.46	0.01	0.50	0.00	0.01	0.49	2.11	0.09	0.95	0.00	0.03	0.02

www.manaraa.com

A.3.3 ωB97XD/6-31G(d)

Table A.9: Excitation energies Ω, oscillator strengths f, and CT characters of the molecular pair of PCPDTBT: PCBM in solvent with varying static dielectric constant, ε. Computed by ωB97XD/6-31G(d) using the LR and the SS approaches on the *solvated* geometry optimized by the same functional.

ωB97XD/6-31G(d) PCPDTBT: PCBM in solvent with *solvated* geometry													
		LR						SS					
ε_0	mode	$\Omega(eV)$	f	DA	AD	DD	AA	$\Omega(eV)$	f	DA	AD	DD	AA
1	EX-1	2.22	2.41	0.03	0.00	0.97	0.00	2.22	2.41	0.03	0.00	0.97	0.00
	EX-2	2.52	0.80	0.01	0.00	0.98	0.01	2.52	0.80	0.01	0.00	0.98	0.01
	CT-1	2.76	0.00	0.95	0.00	0.02	0.03	2.76	0.00	0.95	0.00	0.02	0.03
3	EX-1	2.20	2.57	0.03	0.00	0.97	0.00	2.22	2.42	0.03	0.00	0.97	0.00
	EX-2	2.49	0.90	0.01	0.00	0.99	0.00	2.51	0.79	0.01	0.00	0.98	0.01
	CT-1	2.77	0.00	0.95	0.00	0.02	0.03	2.66	0.00	0.95	0.00	0.02	0.03
5	EX-1	2.21	2.57	0.03	0.00	0.97	0.00	2.22	2.41	0.03	0.00	0.97	0.00
	EX-2	2.49	0.90	0.01	0.00	0.99	0.00	2.51	0.79	0.01	0.00	0.98	0.01
	CT-1	2.78	0.00	0.95	0.00	0.02	0.04						
8	EX-1	2.21	2.57	0.03	0.00	0.97	0.00	2.22	2.41	0.03	0.00	0.97	0.00
	EX-2	2.49	0.90	0.01	0.00	0.99	0.00	2.51	0.79	0.01	0.00	0.98	0.01
	CT-1	2.78	0.00	0.95	0.00	0.02	0.04	2.58	0.00	0.94	0.00	0.02	0.04
10	EX-1	2.21	2.57	0.03	0.00	0.97	0.00	2.22	2.41	0.03	0.00	0.97	0.00
	EX-2	2.49	0.90	0.01	0.00	0.99	0.00	2.51	0.78	0.01	0.00	0.98	0.01
	CT-1	2.78	0.00	0.94	0.00	0.02	0.04	2.55	0.00	0.94	0.00	0.02	0.04
13	EX-1	2.21	2.57	0.03	0.00	0.97	0.00	2.22	2.41	0.03	0.00	0.97	0.00
	EX-2	2.49	0.90	0.01	0.00	0.99	0.00	2.51	0.78	0.01	0.00	0.98	0.01
	CT-1	2.78	0.00	0.94	0.00	0.02	0.04	2.55	0.00	0.94	0.00	0.02	0.04
15	EX-1	2.21	2.57	0.03	0.00	0.97	0.00	2.22	2.41	0.03	0.00	0.97	0.00
	EX-2	2.49	0.90	0.01	0.00	0.99	0.00	2.51	0.78	0.01	0.00	0.98	0.01
	CT-1	2.78	0.00	0.94	0.00	0.02	0.04	2.55	0.00	0.94	0.00	0.02	0.04
18	EX-1	2.21	2.58	0.03	0.00	0.97	0.00	2.22	2.41	0.03	0.00	0.97	0.00
	EX-2	2.49	0.90	0.01	0.00	0.99	0.00	2.51	0.78	0.01	0.00	0.98	0.01
	CT-1	2.78	0.00	0.94	0.00	0.02	0.04	2.51	0.00	0.94	0.00	0.02	0.04
20	EX-1	2.21	2.58	0.03	0.00	0.97	0.00	2.22	2.41	0.03	0.00	0.97	0.00
	EX-2	2.49	0.90	0.01	0.00	0.99	0.00	2.51	0.78	0.01	0.00	0.98	0.01
	CT-1	2.78	0.00	0.94	0.00	0.02	0.04	2.51	0.00	0.94	0.00	0.02	0.04
25	EX-1	2.21	2.58	0.03	0.00	0.97	0.00	2.22	2.41	0.03	0.00	0.97	0.00
	EX-2	2.49	0.90	0.01	0.00	0.99	0.00	2.51	0.78	0.01	0.00	0.98	0.01
	CT-1	2.78	0.00	0.94	0.00	0.02	0.04	2.55	0.00	0.94	0.00	0.02	0.04
30	EX-1	2.21	2.58	0.03	0.00	0.97	0.00	2.22	2.41	0.03	0.00	0.97	0.00
	EX-2	2.49	0.90	0.01	0.00	0.99	0.00	2.51	0.78	0.01	0.00	0.98	0.01
	CT-1	2.78	0.00	0.94	0.00	0.02	0.04	2.55	0.00	0.94	0.00	0.02	0.04

www.manaraa.com

BIBLIOGRAPHY

[1] Edmund Hosker and Robert Priddle, editors. *World Energy Outlook 2017*, 2017.

[2] Market report series: Renewables 2018. *International Energy Agency*, 2018.

[3] Renewables 2018 global status report. *REN21*, 2018.

[4] $1/w photovoltaic systems - white paper to explore a grand challenge for electricity from solar. *U.S. Department of Energy*, 2010.

[5] Wesley J. Cole, Bethany A. Frew, Pieter J. Gagnon, James Richards, Yinong Sun, Robert M. Margolis, and Michael A. Woodhouse. Sunshot 2030 for photovoltaics (PV): Envisioning a low-cost PV future. *National Renewable Energy Laboratory*, 9 2017.

[6] Solar research spotlight: Photovoltaics. *Solar Energy Technologies Office*, 2018.

[7] Dean Levi. Best research-cell efficiencies. `https://commons.wikimedia.org/wiki/File:PVeff(rev181211)x.png`, Dec 2018. Accessed: 2018-12-17.

[8] Lingxian Meng, Yamin Zhang, Xiangjian Wan, Chenxi Li, Xin Zhang, Yanbo Wang, Xin Ke, Zuo Xiao, Liming Ding, Ruoxi Xia, Hin-Lap Yip, Yong Cao, and Yongsheng Chen. Organic and solution-processed tandem solar cells with 17.3% efficiency. *Science*, 2018.

[9] Alan J. Heeger. Semiconducting and metallic polymers: The fourth generation of polymeric materials. *The Journal of Physical Chemistry B*, 105(36):8475–8491, 2001.

[10] Koen Vandewal, Steve Albrecht, Eric T. Hoke, Kenneth R. Graham, Johannes Widmer, Jessica D. Douglas, Marcel Schubert, William R. Mateker, Jason T. Bloking, George F. Burkhard, Alan Sellinger, Jean M. J. Fréchet, Aram Amassian, Moritz K. Riede, Michael D. McGehee, Dieter Neher, and Alberto Salleo. Efficient charge generation by relaxed charge-transfer states at organic interfaces. *Nature Materials*, 13:63–68, 2014.

[11] Claudia Piliego and Maria Antonietta Loi. Charge transfer state in highly efficient polymerfullerene bulk heterojunction solar cells. *J. Mater. Chem.*, 22:4141–4150, 2012.

www.manaraa.com

[12] Jiye Lee, Koen Vandewal, Shane R. Yost, Matthias E. Bahlke, Ludwig Goris, Marc A. Baldo, Jean V. Manca, and Troy Van Voorhis. Charge transfer state versus hot exciton dissociation in polymerfullerene blended solar cells. *Journal of the American Chemical Society*, 132(34):11878–11880, 2010.

[13] Carsten Deibel, Thomas Strobel, and Vladimir Dyakonov. Role of the charge transfer state in organic donoracceptor solar cells. *Advanced Materials*, 22(37):4097–4111, 2010.

[14] Jona Kurpiers, Thomas Ferron, Steffen Roland, Marius Jakoby, Tobias Thiede, Frank Jaiser, Steve Albrecht, Silvia Janietz, Brian A. Collins, Ian A. Howard, and Dieter Neher. Probing the pathways of free charge generation in organic bulk heterojunction solar cells. *Nature Communications*, 9(2038), 2018.

[15] G. Grancini, M. Maiuri, D. Fazzi, A. Petrozza, H-J. Egelhaaf, D. Brida, G. Cerullo, and G. Lanzani. Hot exciton dissociation in polymer solar cells. *Nature Mateirals*, 12:29–33, 2013.

[16] Ya-shih Huang, Sebastian Westenhoff, Igor Avilov, Paiboon Sreearunothai, Justin M. Hodgkiss, Caroline Deleener, Richard H. Friend, and David Beljonne. Electronic structures of interfacial states formed at polymeric semiconductor heterojunctions. *Nature Materials*, 7(6):483–489, 2008.

[17] Askat E. Jailaubekov, Adam P. Willard, John R. Tritsch, Wai-Lun Chan, Na Sai, Raluca Gearba, Loren G. Kaake, Kenrick J. Williams, Kevin Leung, Peter J. Rossky, and X-Y. Zhu. Hot charge-transfer excitons set the time limit for charge separation at donor/acceptor interfaces in organic photovoltaics. *Nature Materials*, 12(1):66–73, 2013.

[18] Kakali Sen, Rachel Crespo-Otero, Oliver Weingart, Walter Thiel, and Mario Barbatti. Interfacial states in donoracceptor organic heterojunctions: Computational insights into thiophene-oligomer/fullerene junctions. *Journal of Chemical Theory and Computation*, 9(1):533–542, 2013. PMID: 26589052.

[19] L. Jan Anton Koster, Sean E. Shaheen, and Jan C. Hummelen. Pathways to a new

www.manaraa.com

efficiency regime for organic solar cells. *Advanced Energy Materials*, 2(10):1246–1253, 2012.

[20] Sibel Leblebici, Jiye Lee, Alexander Weber-Bargioni, and Biwu Ma. Dielectric screening to reduce charge transfer state binding energy in organic bulk heterojunction photovoltaics. *The Journal of Physical Chemistry C*, 121(6):3279–3285, 2017.

[21] Reed Nieman, Hsinhan Tsai, Wanyi Nie, Adelia J. A. Aquino, Aditya D. Mohite, Sergei Tretiak, Hao Li, and Hans Lischka. The crucial role of a spacer material on the efficiency of charge transfer processes in organic donor-acceptor junction solar cells. *Nanoscale*, 10:451–459, 2018.

[22] Tatiana S. Kolesnikova, Margarita S. Chernovyants, Mikhail E. Kletskii, Oleg N. Burov, Gennady I. Bondarenko, and Pavel A. Knyazev. Charge transfer complexes formed by heterocyclic thioamides and tetracyanoethylene: Experimental and theoretical study. *The Journal of Physical Chemistry A*, 121(37):7000–7008, 2017. PMID: 28849931.

[23] Alan J. Heeger. Semiconducting polymers: The third generation. *Chemical Society Reviews*, 39:2354–2371, 2010.

[24] P. M. Allemand, A. Koch, Fred Wudl, Y. Rubin, F. Diederich, M. M. Alvarez, S. J. Anz, and R. L. Whetten. Two different fullerenes have the same cyclic voltammetry. *Journal of the American Chemical Society*, 113(3):1050–1051, 1991.

[25] Patrick G. Nicholson and Fernando A. Castro. Organic photovoltaics: Principles and techniques for nanometre scale characterization. *Nanotechnology*, 21(49):492001, 2010.

[26] Th. B. Singh, N. Marjanović, G.J. Matt, S. Gnes, N.S. Sariciftci, A. Montaigne Ramil, A. Andreev, H. Sitter, R. Schwödiauer, and S. Bauer. High-mobility n-channel organic field-effect transistors based on epitaxially grown C60 films. *Organic Electronics*, 6(3):105–110, 2005.

[27] Serap Gü nes, Helmut Neugebauer, and Niyazi Serdar Sariciftci. Conjugated polymer-based organic solar cells. *Chemical Reviews*, 107(4):1324–1338, 2007.

www.manaraa.com

[28] Andriy Zhugayevych, Olena Postupna, Ronald C. Bakus II, Gregory C. Welch, Guillermo C. Bazan, and Sergei Tretiak. Ab initio study of a molecular crystal for photovoltaics: Light absorption, exciton and charge carrier transport. *The Journal of Physical Chemistry C*, 117(10):4920–4930, 2013.

[29] Christoph J. Brabec. Organic photovoltaics: technology and market. *Solar Energy Materials and Solar Cells*, 83(2):273–292, 2004. The development of organic and polymer photovoltaics.

[30] G. Chidichimo and L. Filippelli. Organic solar cells: Problems and perspectives. *International Journal of Photoenergy*, 2010(123534):1–11, 2010.

[31] C. J. Brabec, N. S. Sariciftci, and J. C. Hummelen. Plastic solar cells. *Advanced Functional Materials*, 11(1):15–26, 2001.

[32] Barry C. Thompson and Jean M. J. Fréchet. Polymerfullerene composite solar cells. *Angewandte Chemie International Edition*, 47(1):58–77, 2008.

[33] D. E. Markov, C. Tanase, P. W. M. Blom, and J. Wildeman. Simultaneous enhancement of charge transport and exciton diffusion in poly(*p*-phenylene vinylene) derivatives. *Phys. Rev. B*, 72:045217, Jul 2005.

[34] J. J. M. Halls, K. Pichler, R. H. Friend, S. C. Moratti, and A. B. Holmes. Exciton diffusion and dissociation in a poly(*p*-phenylenevinylene)/C60 heterojunction photovoltaic cell. *Applied Physics Letters*, 68(22):3120–3122, 1996.

[35] Denis E. Markov, Emiel Amsterdam, Paul W. M. Blom, Alexander B. Sieval, and Jan C. Hummelen. Accurate measurement of the exciton diffusion length in a conjugated polymer using a heterostructure with a side-chain cross-linked fullerene layer. *The Journal of Physical Chemistry A*, 109(24):5266–5274, 2005.

[36] J.J.M. Halls and R.H. Friend. The photovoltaic effect in a poly(*p*-phenylenevinylene)/perylene heterojunction. *Synthetic Metals*, 85(1):1307–1308, 1997.

[37] Pavel Schilinsky, Christoph Waldauf, and Christoph J. Brabec. Recombination and loss analysis in polythiophene based bulk heterojunction photodetectors. *Applied Physics*

www.manaraa.com

Letters, 81(20):3885–3887, 2002.

[38] Roberto Pacios, Jenny Nelson, Donal D. C. Bradley, and Christoph J. Brabec. Composition dependence of electron and hole transport in polyfluorene:[6,6]-phenyl C61-butyric acid methyl ester blend films. *Applied Physics Letters*, 83(23):4764–4766, 2003.

[39] S. A. Choulis, J. Nelson, Y. Kim, D. Poplavskyy, T. Kreouzis, J. R. Durrant, and D. D. C. Bradley. Investigation of transport properties in polymer/fullerene blends using time-of-flight photocurrent measurements. *Applied Physics Letters*, 83(18):3812–3814, 2003.

[40] Kurt V. Mikkelsen and Mark A. Ratner. Electron tunneling in solid-state electron-transfer reactions. *Chemical Reviews*, 87(1):113–153, 1987.

[41] Eric A. Margulies, Jenna L. Logsdon, Claire E. Miller, Lin Ma, Ethan Simonoff, Ryan M. Young, George C. Schatz, and Michael R. Wasielewski. Direct observation of a charge-transfer state preceding high-yield singlet fission in terrylenediimide thin films. *Journal of the American Chemical Society*, 139(2):663–671, 2017.

[42] Riccardo Volpi, Racine Nassau, Morten Steen Nørby, and Mathieu Linares. Theoretical study of the charge-transfer state separation within marcus theory: The C60-anthracene case study. *ACS Applied Materials & Interfaces*, 8(37):24722–24736, 2016.

[43] Simon Gélinas, Akshay Rao, Abhishek Kumar, Samuel L. Smith, Alex W. Chin, Jenny Clark, Tom S. van der Poll, Guillermo C. Bazan, and Richard H. Friend. Ultrafast long-range charge separation in organic semiconductor photovoltaic diodes. *Science*, 343(6170):512–516, 2014.

[44] Minghong Tong, Nelson E. Coates, Daniel Moses, Alan J. Heeger, Serge Beaupré, and Mario Leclerc. Charge carrier photogeneration and decay dynamics in the poly(2,7-carbazole) copolymer pcdtbt and in bulk heterojunction composites with $pc_{70}BM$. *Phys. Rev. B*, 81:125210, Mar 2010.

[45] Arne C. Morteani, Paiboon Sreearunothai, Laura M. Herz, Richard H. Friend, and Carlos Silva. Exciton regeneration at polymeric semiconductor heterojunctions. *Phys.*

www.manaraa.com

Rev. Lett., 92:247402, Jun 2004.

[46] Françoise Provencher, Nicolas Bérubé, Anthony W. Parker, Gregory M. Greetham, Michael Towrie, Christoph Hellmann, Michel Côté, Natalie Stingelin, Carlos Silva, and Sophia C. Hayes. Direct observation of ultrafast long-range charge separation at polymerfullerene heterojunctions. *Nature Communications*, 5:4288, 2014.

[47] Carlo Andrea Rozzi, Sarah Maria Falke, Nicola Spallanzani, Angel Rubio, Elisa Molinari, Daniele Brida, Margherita Maiuri, Giulio Cerullo, Heiko Schramm, Jens Christoffers, and Christoph Lienau. Quantum coherence controls the charge separation in a prototypical artificial light-harvesting system. *Nature Communications*, 4:1602, Mar 2013.

[48] Sarah Maria Falke, Carlo Andrea Rozzi, Daniele Brida, Margherita Maiuri, Michele Amato, Ephraim Sommer, Antonietta De Sio, Angel Rubio, Giulio Cerullo, Elisa Molinari, and Christoph Lienau. Coherent ultrafast charge transfer in an organic photovoltaic blend. *Science*, 344(6187):1001–1005, 2014.

[49] Eric R. Bittner and Carlos Silva. Noise-induced quantum coherence drives photo-carrier generation dynamics at polymeric semiconductor heterojunctions. *Nature Communications*, 5:3119, 2014.

[50] M. Lenes, F. B. Kooistra, J. C. Hummelen, I. Van Severen, L. Lutsen, D. Vanderzande, T. J. Cleij, and P. W. M. Blom. Charge dissociation in polymer:fullerene bulk heterojunction solar cells with enhanced permittivity. *Journal of Applied Physics*, 104(11):114517, 2008.

[51] V.D. Mihailetchi, L. J. A. Koster, P. W. M. Blom, C. Melzer, B. de Boer, J. K. J. van Duren, and R. A. J. Janssen. Compositional dependence of the performance of poly(*p*-phenylene vinylene):methanofullerene bulk-heterojunction solar cells. *Advanced Functional Materials*, 15(5):795–801, 2005.

[52] Dirk Veldman, Özlem İpek, Stefan C. J. Meskers, Jörgen Sweelssen, Marc M. Koetse, Sjoerd C. Veenstra, Jan M. Kroon, Svetlana S. van Bavel, Joachim Loos, and René

www.manaraa.com

A. J. Janssen. Compositional and electric field dependence of the dissociation of charge transfer excitons in alternating polyfluorene copolymer/fullerene blends. *Journal of the American Chemical Society*, 130(24):7721–7735, 2008.

[53] J. J. Benson-Smith, L. Goris, K. Vandewal, K. Haenen, J. V. Manca, D. Vanderzande, D. D. C. Bradley, and J. Nelson. Formation of a ground-state charge-transfer complex in polyfluorene//[6,6]-phenyl-C61 butyric acid methyl ester (PCBM) blend films and its role in the function of polymer/PCBM solar cells. *Advanced Functional Materials*, 17(3):451–457, 2007.

[54] M. A. Aguilar. Separation of the electric polarization into fast and slow components: a comparison of two partition schemes. *The Journal of Physical Chemistry A*, 105(45):10393–10396, 2001.

[55] R. Cammi, S. Corni, B. Mennucci, and J. Tomasi. Electronic excitation energies of molecules in solution: State specific and linear response methods for nonequilibrium continuum solvation models. *The Journal of Chemical Physics*, 122(10):104513–104524, 2005.

[56] J. A. Bjorgaard, V. Kuzmenko, K. A. Velizhanin, and S. Tretiak. Solvent effects in time-dependent self-consistent field methods. I. optical response calculations. *The Journal of Chemical Physics*, 142(4):044103–044112, 2015.

[57] Young Il Park, Cheng-Yu Kuo, Jennifer S. Martinez, Young-Shin Park, Olena Postupna, Andriy Zhugayevych, Seungho Kim, Jongwook Park, Sergei Tretiak, and Hsing-Lin Wang. Tailored electronic structure and optical properties of conjugated systems through aggregates and dipoledipole interactions. *ACS Applied Materials & Interfaces*, 5(11):4685–4695, 2013.

[58] Benedetta Mennucci, Chiara Cappelli, Ciro Achille Guido, Roberto Cammi, and Jacopo Tomasi. Structures and properties of electronically excited chromophores in solution from the polarizable continuum model coupled to the time-dependent density functional theory. *The Journal of Physical Chemistry A*, 113(13):3009–3020, 2009.

www.manaraa.com

[59] Benjamin Kaduk, Tim Kowalczyk, and Troy Van Voorhis. Constrained density functional theory. *Chemical Reviews*, 112(1):321–370, 2012.

[60] Xi Liu, Boming Xie, Chunhui Duan, Zhaojing Wang, Baobing Fan, Kai Zhang, Baojun Lin, Fallon J. M. Colberts, Wei Ma, Ren A. J. Janssen, Fei Huang, and Yong Cao. A high dielectric constant non-fullerene acceptor for efficient bulk-heterojunction organic solar cells. *J. Mater. Chem. A*, 6:395–403, 2018.

[61] Solmaz Torabi, Fatemeh Jahani, Ineke Van Severen, Catherine Kanimozhi, Satish Patil, Remco W. A. Havenith, Ryan C. Chiechi, Laurence Lutsen, Dirk J. M. Vanderzande, Thomas J. Cleij, Jan C. Hummelen, and L. Jan Anton Koster. Strategy for enhancing the dielectric constant of organic semiconductors without sacrificing charge carrier mobility and solubility. *Advanced Functional Materials*, 25(1):150–157, 2014.

[62] Jeroen Brebels, Evgenia Douvogianni, Dries Devisscher, Raghavendran Thiruvallur Eachambadi, Jean Manca, Laurence Lutsen, Dirk Vanderzande, Jan C. Hummelen, and Wouter Maes. An effective strategy to enhance the dielectric constant of organic semiconductors CPDTTPD-based low bandgap polymers bearing oligo(ethylene glycol) side chains. *J. Mater. Chem. C*, 6:500–511, 2018.

[63] Ardalan Armin, Dani M. Stoltzfus, Jenny E. Donaghey, Andrew J. Clulow, Ravi Chandra Raju Nagiri, Paul L. Burn, Ian R. Gentle, and Paul Meredith. Engineering dielectric constants in organic semiconductors. *J. Mater. Chem. C*, 5:3736–3747, 2017.

[64] Jeroen Brebels, Jean V. Manca, Laurence Lutsen, Dirk Vanderzande, and Wouter Maes. High dielectric constant conjugated materials for organic photovoltaics. *J. Mater. Chem. A*, 5:24037–24050, 2017.

[65] Shaohui Zheng, Eitan Geva, and Barry D. Dunietz. Solvated charge transfer states of functionalized anthracene and tetracyanoethylene dimers: A computational study based on a range separated hybrid functional and charge constrained self-consistent field with switching gaussian polarized continuum models. *Journal of Chemical Theory and Computation*, 9(2):1125–1131, 2013.

www.manaraa.com

[66] Benedetta Mennucci. Polarizable continuum model. *Wiley Interdisciplinary Reviews: Computational Molecular Science*, 2(3):386–404, 2012.

[67] Jacopo Tomasi, Benedetta Mennucci, and Roberto Cammi. Quantum mechanical continuum solvation models. *Chemical Reviews*, 105(8):2999–3094, 2005.

[68] Benedetta Mennucci. Polarizable continuum model. *Wiley Interdisciplinary Reviews: Computational Molecular Science*, 2(3):386–404, 2012.

[69] Ciro A. Guido, Denis Jacquemin, Carlo Adamo, and Benedetta Mennucci. Electronic excitations in solution: The interplay between state specific approaches and a time-dependent density functional theory description. *Journal of Chemical Theory and Computation*, 11(12):5782–5790, 2015.

[70] S. Corni, R. Cammi, B. Mennucci, and J. Tomasi. Electronic excitation energies of molecules in solution within continuum solvation models: Investigating the discrepancy between state-specific and linear-response methods. *The Journal of Chemical Physics*, 123(13):134512, 2005.

[71] Roberto Improta, Vincenzo Barone, Giovanni Scalmani, and Michael J. Frisch. A state-specific polarizable continuum model time dependent density functional theory method for excited state calculations in solution. *The Journal of Chemical Physics*, 125:054103, 2006.

[72] Roberto Improta, Giovanni Scalmani, Michael J. Frisch, and Vincenzo Barone. Toward effective and reliable fluorescence energies in solution by a new state specific polarizable continuum model time dependent density functional theory approach. *The Journal of Chemical Physics*, 127:074504, 2007.

[73] J. Frenkel. On the transformation of light into heat in solids. I. *Phys. Rev.*, 37:17–44, Jan 1931.

[74] Gregory H. Wannier. The structure of electronic excitation levels in insulating crystals. *Phys. Rev.*, 52:191–197, Aug 1937.

[75] Carlos E. Crespo-Hernández, Boiko Cohen, and Bern Kohler. Base stacking controls

www.manaraa.com

excited-state dynamics in A·T DNA. *Nature*, 436:1141–1144, 2005.

[76] Dimitra Markovitsi, Francis Talbot, Thomas Gustavsson, Delphine Onidas, Elodie Lazzarotto, and Sylvie Marguet. Molecular spectroscopy: Complexity of excited-state dynamics in DNA. *Nature*, 441:E7, 2006.

[77] Ivan Buchvarov, Qiang Wang, Milen Raytchev, Anton Trifonov, and Torsten Fiebig. Electronic energy delocalization and dissipation in single- and double-stranded DNA. *Proceedings of the National Academy of Sciences*, 104(12):4794–4797, 2007.

[78] Tomohisa Takaya, Charlene Su, Kimberly de La Harpe, Carlos E. Crespo-Hernández, and Bern Kohler. Uv excitation of single DNA and RNA strands produces high yields of exciplex states between two stacked bases. *Proceedings of the National Academy of Sciences*, 105(30):10285–10290, 2008.

[79] Ignacio Vayá, Thomas Gustavsson, Franois-Alexandre Miannay, Thierry Douki, and Dimitra Markovitsi. Fluorescence of natural DNA: From the femtosecond to the nanosecond time scales. *Journal of the American Chemical Society*, 132(34):11834–11835, 2010.

[80] Axel D. Becke. Perspective: Fifty years of density-functional theory in chemical physics. *The Journal of Chemical Physics*, 140(18):18A301, 2014.

[81] Andreas Dreuw and Martin Head-Gordon. Single-reference ab initio methods for the calculation of excited states of large molecules. *Chemical Reviews*, 105(11):4009–4037, 2005.

[82] Mark E. Casida. *Time-Dependent Density Functional Response Theory for Molecules*, volume 1 of *Recent Advances in Computational Chemistry*, pages 155–192. WORLD SCIENTIFIC, November 1995.

[83] Sergei Tretiak, Kirill Igumenshchev, and Vladimir Chernyak. Exciton sizes of conducting polymers predicted by time-dependent density functional theory. *Phys. Rev. B*, 71:033201, Jan 2005.

[84] Kirill I. Igumenshchev, Sergei Tretiak, and Vladimir Y. Chernyak. Excitonic effects

www.manaraa.com

in a time-dependent density functional theory. *The Journal of Chemical Physics*, 127(11):114902, 2007.

[85] Lucia Reining, Valerio Olevano, Angel Rubio, and Giovanni Onida. Excitonic effects in solids described by time-dependent density-functional theory. *Phys. Rev. Lett.*, 88:066404, Jan 2002.

[86] R. J. Magyar and S. Tretiak. Dependence of spurious charge-transfer excited states on orbital exchange in TDDFT: Large molecules and clusters. *Journal of Chemical Theory and Computation*, 3(3):976–987, 2007.

[87] Aron J. Cohen, Paula Mori-Sánchez, and Weitao Yang. Insights into current limitations of density functional theory. *Science*, 321(5890):792–794, 2008.

[88] Tom Ziegler and Mykhaylo Krykunov. On the calculation of charge transfer transitions with standard density functionals using constrained variational density functional theory. *The Journal of Chemical Physics*, 133(7):074104, 2010.

[89] Andreas Dreuw and Martin Head-Gordon. Failure of time-dependent density functional theory for long-range charge-transfer excited states: The Zincbacteriochlorinbacteriochlorin and bacteriochlorophyllspheroidene complexes. *Journal of the American Chemical Society*, 126(12):4007–4016, 2004.

[90] Roi Baer and Daniel Neuhauser. Density functional theory with correct long-range asymptotic behavior. *Phys. Rev. Lett.*, 94:043002, Feb 2005.

[91] David P. Tew Takeshi Yanai and Nicholas C. Handy. A new hybrid exchangecorrelation functional using the coulomb-attenuating method (CAM-B3LYP). *Chemical Physics Letters*, 393:51–57, 2004.

[92] Jeng-Da Chai and Martin Head-Gordon. Systematic optimization of long-range corrected hybrid density functionals. *The Journal of Chemical Physics*, 128:084106, 2008.

[93] Sivan Refaely-Abramson, Sahar Sharifzadeh, Manish Jain, Roi Baer, Jeffrey B. Neaton, and Leeor Kronik. Gap renormalization of molecular crystals from density-functional theory. *Phys. Rev. B*, 88:081204, Aug 2013.

www.manaraa.com

[94] Hao Li, Reed Nieman, Adélia J. A. Aquino, Hans Lischka, and Sergei Tretiak. Comparison of LC-TDDFT and ADC(2) methods in computations of bright and charge transfer states in stacked oligothiophenes. *Journal of Chemical Theory and Computation*, 10(8):3280–3289, 2014.

[95] Myeong H. Lee, Eitan Geva, and Barry D. Dunietz. The effect of interfacial geometry on charge-transfer states in the phthalocyanine/fullerene organic photovoltaic system. *The Journal of Physical Chemistry A*, 120(19):2970–2975, 2016.

[96] Amy Austin, George A. Petersson, Michael J. Frisch, Frank J. Dobek, Giovanni Scalmani, and Kyle Throssell. A density functional with spherical atom dispersion terms. *Journal of Chemical Theory and Computation*, 8(12):4989–5007, 2012.

[97] Stefan Grimme. Accurate description of van der Waals complexes by density functional theory including empirical corrections. *Journal of Computational Chemistry*, 25(12):1463–1473, 2004.

[98] Stefan Grimme. Semiempirical GGA-type density functional constructed with a long-range dispersion correction. *Journal of Computational Chemistry*, 27:1787–1799, 2006.

[99] Stefan Grimme, Jens Antony, Stephan Ehrlich, and Helge Krieg. A consistent and accurate ab initio parametrization of density functional dispersion correction (DFT-D) for the 94 elements H-Pu. *The Journal of Chemical Physics*, 130:154104, 2010.

[100] Zilong Zheng, David A. Egger, Jean-Luc Brédas, Leeor Kronik, and Veaceslav Coropceanu. Effect of solid-state polarization on charge-transfer excitations and transport levels at organic interfaces from a screened range-separated hybrid functional. *The Journal of Physical Chemistry Letters*, 8(14):3277–3283, 2017.

[101] Shaohui Zheng, Heidi Phillips, Eitan Geva, and Barry D. Dunietz. Ab initio study of the emissive charge-transfer states of solvated chromophore-functionalized silsesquioxanes. *Journal of the American Chemical Society*, 134(16):6944–6947, 2012.

[102] Sergei Tretiak and Shaul Mukamel. Density matrix analysis and simulation of electronic excitations in conjugated and aggregated molecules. *Chemical Reviews*, 102(9):3171–

www.manaraa.com

3212, 2002.

[103] Gregory D. Scholes and Kenneth P. Ghiggino. Electronic interactions and interchromophore excitation transfer. *The Journal of Physical Chemistry*, 98(17):4580–4590, 1994.

[104] A. K. Chandra and E. C. Lim. Semiempirical theory of excimer luminescence. *The Journal of Chemical Physics*, 48(6):2589–2595, 1968.

[105] Ron Shepard. The multiconfiguration self-consistent field method. *Ab Initio Methods in Quantum Chemistry II*, 69:63–200, 1987.

[106] Allan L. L. East and Edward C. Lim. Naphthalene dimer: Electronic states, excimers, and triplet decay. *The Journal of Chemical Physics*, 113(20):8981–8994, 2000.

[107] Felix Plasser and Hans Lischka. Analysis of excitonic and charge transfer interactions from quantum chemical calculations. *Journal of Chemical Theory and Computation*, 8(8):2777–2789, 2012.

[108] A. V. Luzanov and O. V. Prezhdo. Irreducible charge density matrices for analysis of many-electron wave functions. *International Journal of Quantum Chemistry*, 102(5):582–601, 2005.

[109] Jacopo Tomasi, Benedetta Mennucci, and Roberto Cammi. Quantum mechanical continuum solvation models. *Chemical Reviews*, 105(8):2999–3094, 2005.

[110] J. E. Sanhueza, O. Tapia, W. G. Laidlaw, and M. Trsic. On the application of the variational principle to a type of nonlinear "Schrödinger equation". *The Journal of Chemical Physics*, 70(6):3096–3098, 1979.

[111] R. Cammi and J. Tomasi. Time-dependent variational principle for nonlinear hamiltonians and its application to molecules in the liquid phase. *International Journal of Quantum Chemistry*, 60(1):297–306, 1996.

[112] Hongkyu Kang, Geunjin Kim, Junghwan Kim, Sooncheol Kwon, Heejoo Kim, and Kwanghee Lee. Bulk-heterojunction organic solar cells: Five core technologies for

www.manaraa.com

their commercialization. *Advanced Materials*, 28(36):7821–7861, 2016.

[113] Ram Prakash Singh and Omkar Singh Kushwaha. Polymer solar cells: An overview. *Macromolecular Symposia*, 327(1):128–149, 2013.

[114] J. Peet, J. Y. Kim, N. E. Coates, W. L. Ma, D. Moses, A. J. Heeger, and G. C. Bazan. Efficiency enhancement in low-bandgap polymer solar cells by processing with alkane dithiols. *Nature Materials*, 6:497–500, 2007.

[115] Daniele Fazzi, Giulia Grancini, Margherita Maiuri, Daniele Brida, Giulio Cerullo, and Guglielmo Lanzani. Ultrafast internal conversion in a low band gap polymer for photovoltaics: experimental and theoretical study. *Phys. Chem. Chem. Phys.*, 14:6367–6374, 2012.

[116] Giulia Grancini, Nicola Martino, Maria Rosa Antognazza, Michele Celebrano, Hans-Joachim Egelhaaf, and Guglielmo Lanzani. Influence of blend composition on ultrafast charge generation and recombination dynamics in low band gap polymer-based organic photovoltaics. *The Journal of Physical Chemistry C*, 116(17):9838–9844, 2012.

[117] Chad Risko, Michael D. McGehee, and Jean-Luc Brédas. A quantum-chemical perspective into low optical-gap polymers for highly-efficient organic solar cells. *Chem. Sci.*, 2:1200–1218, 2011.

[118] Patrick Boland, Keejoo Lee, and Gon Namkoong. Device optimization in PCPDTBT:PCBM plastic solar cells. *Solar Energy Materials and Solar Cells*, 94(5):915–920, 2010.

[119] M. A. Loi, S. Toffanin, M. Muccini, M. Forster, U. Scherf, and M. Scharber. Charge transfer excitons in bulk heterojunctions of a polyfluorene copolymer and a fullerene derivative. *Advanced Functional Materials*, 17(13):2111–2116, 2006.

[120] Jeng-Da Chai and Martin Head-Gordon. Long-range corrected hybrid density functionals with damped atomatom dispersion corrections. *Physical Chemistry Chemical Physics*, 10:6615, 2008.

[121] Roy Dennington, Todd A. Keith, and John M. Millam. Gaussview Version 5, 2009.

www.manaraa.com

Semichem Inc. Shawnee Mission KS.

[122] Maurizio Cossi and Vincenzo Barone. Time-dependent density functional theory for molecules in liquid solutions. *The Journal of Chemical Physics*, 115(10):4708–4717, 2001.

[123] M. J. Frisch, G. W. Trucks, H. B. Schlegel, G. E. Scuseria, M. A. Robb, J. R. Cheeseman, G. Scalmani, V. Barone, B. Mennucci, G. A. Petersson, H. Nakatsuji, M. Caricato, X. Li, H. P. Hratchian, A. F. Izmaylov, J. Bloino, G. Zheng, J. L. Sonnenberg, M. Hada, M. Ehara, K. Toyota, R. Fukuda, J. Hasegawa, M. Ishida, T. Nakajima, Y. Honda, O. Kitao, H. Nakai, T. Vreven, J. A. Montgomery Jr., J. E. Peralta, F. Ogliaro, M. Bearpark, J. J. Heyd, E. Brothers, K. N. Kudin, V. N. Staroverov, T. Keith, R. Kobayashi, J. Normand, K. Raghavachari, A. Rendell, J. C. Burant, S. S. Iyengar, J. Tomasi, M. Cossi, N. Rega, J. M. Millam, M. Klene, J. E. Knox, J. B. Cross, V. Bakken, C. Adamo, J. Jaramillo, R. Gomperts, R. E. Stratmann, O. Yazyev, A. J. Austin, R. Cammi, C. Pomelli, J. W. Ochterski, R. L. Martin, K. Morokuma, V. G. Zakrzewski, G. A. Voth, P. Salvador, J. J. Dannenberg, S. Dapprich, A. D. Daniels, O. Farkas, J. B. Foresman, J. V. Ortiz, J. Cioslowski, and D. J. Fox. Gaussian 09, Revision D.01, 2013. Gaussian Inc. Wallingford CT.

[124] Richard L. Martin. Natural transition orbitals. *The Journal of Chemical Physics*, 118(11):4775–4777, 2003.

[125] Program development features | Gaussian.com. `http://gaussian.com/progdev/`. Accessed: 2018-09-30.

[126] Hao Li, Chao Wu, Sergey V. Malinin, Sergei Tretiak, and Vladimir Y. Chernyak. Exciton scattering approach for optical spectra calculations in branched conjugated macromolecules. *Chemical Physics*, 481(Supplement C):124–132, 2016. Quantum Dynamics and Femtosecond Spectroscopy dedicated to Prof. Vladimir Y. Chernyak on the occasion of his 60th birthday.

[127] Wenkel Liang, Craig T. Chapman, Feizhi Ding, and Xiaosong Li. Modeling ultrafast

www.manaraa.com

solvated electronic dynamics using time-dependent density functional theory and polarizable continuum model. *The Journal of Physical Chemistry A*, 116(8):1884–1890, 2012. PMID: 22277083.

[128] Craig T. Chapman, Wenkel Liang, and Xiaosong Li. Solvent effects on intramolecular charge transfer dynamics in a fullerene derivative. *The Journal of Physical Chemistry A*, 117(13):2687–2691, 2013.

[129] Phu D. Nguyen, Feizhi Ding, Sean A. Fischer, Wenkel Liang, and Xiaosong Li. Solvated first-principles excited-state charge-transfer dynamics with time-dependent polarizable continuum model and solvent dielectric relaxation. *The Journal of Physical Chemistry Letters*, 3(19):2898–2904, 2012.

[130] Carsten Deibel, Thomas Strobel, and Vladimir Dyakonov. Origin of the efficient polaron-pair dissociation in polymer-fullerene blends. *Phys. Rev. Lett.*, 103:036402, Jul 2009.

www.manaraa.com

ABSTRACT

SOLVENT EFFECTS AND CHARGE TRANSFER STATES IN ORGANIC PHOTOVOLTAICS

by

KANGMIN LIU

May 2019

Advisor: Dr. Vladimir Y. Chernyak

Major: Chemistry (Physical)

Degree: Doctor of Philosophy

Due to their various advantages, including lightweight, flexible, and cheap manufacturing, organic photovoltaic materials have gained enormous research interest. Over nearly two decades, the power conversion efficiency of organic solar devices has increased dramatically. However, it is still low compared to traditional inorganic semiconductors. In order to improve efficiency, a better understanding of the basic thermodynamic properties of the light-to-electricity power conversion process is needed. One nontrivial aspect of organic solar cells is the low dielectric constant, which leads to tightly-bound excitons upon vertical excitations. The separation of electron-hole pairs requires a larger driving force to overcome the Coulombic binding energy in organic semiconductors compared to their inorganic counterpart. A particular state called charge transfer state appears during the dissociation process of the bound excitons. The exact role of this particular type of state, whether a precursor to efficient charge separation or a detrimental process which hinders the generation of free charges, is still under debate. Extensive research has been performed to elucidate the mechanism of free charge carrier creation. Some studies show that the dielectric environment plays a significant role during the charge dissociation process by affecting the energetics of excited states. For example, MDMO-PPV: PCBM device becomes more efficient when the dielectric constant reaches a certain value ($\varepsilon_r = 9$). The aim of this work is to map out the alignment of excited states of a typical polymer: fullerene device, taking PCPDTBT: PCBM

www.manaraa.com

as a specific example system, and find out the characteristics of the charge transfer state under the influence of polar solvent.

Long-range corrected time-dependent density functional theory combined with the polarizable continuum model has been used to study the solvent effect on excited state properties of PCPDTBT: PCBM molecular system. Solvation model has been applied using the linear-response and state-specific approaches to account for the dielectric environment. Electronic transitions are characterized by their intrinsic properties based on a detailed analysis of the one-electron transition density matrices. The tools include a numerical value termed charge transfer character, contour plots of the transition density matrix, and natural transition orbital of each excited state. The results show that the influence of the solvent depends on the nature of the excitations. For excitonic states, which have a characteristic of local excitations, the solvent has little to no effects on the excitation energies according to both solvent schemes. In contrast, a different trend is observed for states with a significant amount of charge transfer. State-specific predicts a sufficient decline in the excitation energy as the dielectric constant increases such that the charge transfer state can be stabilized to the lowest excited state, whereas linear-response shows almost no change. The comparison of two solvent approaches is discussed.

It concludes that a protocol that combines TDDFT with long-range-corrected hybrid functional, CAM-B3LYP, Grimme's empirical dispersion correction D3, and state-specific solvation model can effectively and efficiently predict the energetics of charge transfer state in organic photovoltaic materials. Future directions are also provided, including extension of the current calculation scheme to more polymer: fullerene molecular systems, application of other methods such as charge constraint density functional theory and range-separated hybrid functionals combined with polarizable continuum model, simulation of the charge dissociation process in a dynamic picture, and investigation of the solvent effect under the variation of optical dielectric constant instead of focusing only on the static permittivity.

www.manaraa.com

AUTOBIOGRAPHICAL STATEMENT

KANGMIN LIU

Education

12/2018 Ph.D., Chemistry (Physical), Wayne State University.
06/2012 B.S., Chemistry, Nankai University

Awards and Honors

April 27th, 2015 Honor Citation for Teaching Service in Chemistry, Wayne State University, Department of Chemistry

Publications

1. Kangmin Liu, Hao Li, Sergei Tretiak, Vladimir Chernyak, "Solvent effects and charge transfer states in organic photovoltaics: a time-dependent density functional theory study on the PCPDTBT:PCBM low band gap system," Journal of Photonics for Energy 8(3), 032215 (21 May 2018).

Presentations

1. *"Solvent effects and charge transfer states in organic photovoltaics: a time-dependent density functional theory study on the PCPDTBT:PCBM low band gap system"*, seminar, 9th Annual Midwest Graduate Research Symposium, University of Toledo, Toledo OH, April 7th, 2018.

Experience

1. *Graduate Student Assistant*, WSU. Barcoding chemicals project, September 2017 - May 2018.
2. *Graduate Teaching Assistant*, WSU. Lab instructor for Physical Chemistry, General Chemistry, September 2012 - May 2014, September 2014 - August 2017.
3. *Graduate Student*, Summer Intern at Los Alamos National Laboratory. May 2014 - August 2014.

www.manaraa.com